# Transient Stability Enhancement of a Power System Using STATCOM Based on Particle Swarm Optimization

Case Study: IEEE 30-bus test system integrated into Adama II Wind Farm

Merera Taresa Edesa

A Thesis Submitted to the Department of Electrical Power and Control Engineering

School of Electrical Engineering and Computing

Presented in Partial Fulfillment of the Requirement for the Degree of Master's in Power System Engineering

Office of Graduate Studies

Adama Science and Technology University

June, 2024

Adama, Ethiopia

# Transient Stability Enhancement of a Power System Using STATCOM Based on Particle Swarm Optimization

Case Study: IEEE 30-bus test system integrated into Adama II Wind Farm

Merera Taresa Edesa

Major Advisor: Dr. Tefera T.Y

Co-Advisor: Mesfin Megra (MSc)

A Thesis Submitted to the Department of Electrical Power and Control Engineering

School of Electrical Engineering and Computing

Presented in Partial Fulfillment of the Requirement for the Degree of Master's in Power System Engineering

Office of Graduate Studies

Adama Science and Technology University

June, 2024

Adama, Ethiopia

# DECLARATION

I hereby declare that this Master Thesis entitled **"Transient stability enhancement of a Power System using STATCOM based on particle swarm optimization"** is my original work. That is, it has not been submitted for the award of any academic degree, diploma or certificate in any other university. All sources of materials that are used for this thesis have been duly acknowledged through citation.

| Merera Taresa Edesa | ____________________ | ____________________ |
|---|---|---|
| Name of Student | Signature | Date |

# RECOMMENDATION

We, the advisors of this thesis, hereby certify that we have read the revised version of the thesis entitled **"Transient stability enhancement of a Power System using STATCOM based on particle swarm optimization"** prepared under our guidance by **Merera Taresa** submitted in partial fulfillment of the requirements for the degree of Mater's of Science in Power System Engineering. Therefore, we recommend the submission of revised version of the thesis to the department following the applicable procedures.

| | | |
|---|---|---|
| Dr. Tefera T.Y | ______________________ | ______________________ |
| Major Advisor | Signature | Date |
| Mesfin Megra (MSc.) | ______________________ | ______________________ |
| Co-Advisor | Signature | Date |

# APPROVAL PAGE

We, the advisors of the thesis entitled **"Transient stability enhancement of a Power System using STATCOM based on particle swarm optimization"** and developed by **Merera Taresa**, hereby certify that the recommendation and suggestions made by the board of examiners are appropriately incorporated into the final version of the thesis.

| | | |
|---|---|---|
| Dr. Tefera T.Y | ____________________ | ____________________ |
| Major Advisor | Signature | Date |
| Mesfin Megra (MSc.) | ____________________ | ____________________ |
| Co-Advisor | Signature | Date |

We, the undersigned, members of the Board of Examiners of the thesis by **Merera Taresa** have read and evaluated the thesis entitled **"Transient stability enhancement of a Power System using STATCOM based on particle swarm optimization"** and examined the candidate during open defense. This is, therefore, to certify that the thesis is accepted for partial fulfillment of the requirement of the degree of Master of Science in Power System Engineering.

| | | |
|---|---|---|
| ____________________ | ____________________ | ____________________ |
| Chairperson | Signature | Date |
| ____________________ | ____________________ | ____________________ |
| Internal Examiner | Signature | Date |
| ____________________ | ____________________ | ____________________ |
| External Examiner | Signature | Date |

Final approval and acceptance of the thesis is contingent upon submission of its final copy to the Office of Postgraduate Studies (OPGS) through the Department Graduate Council (DGC) and School Graduate Committee (SGC).

| | | |
|---|---|---|
| ____________________ | ____________________ | ____________________ |
| Department Head | Signature | Date |
| ____________________ | ____________________ | ____________________ |
| School Dean | Signature | Date |
| ____________________ | ____________________ | ____________________ |
| Office of Postgraduate Studies, Dean | Signature | Date |

# ACKNOWLEDGMENT

First and foremost, I would like to express my sincere gratitude to Almighty God, the creator of life, the source of all knowledge for granting me the wisdom and perseverance to complete this research paper. I am thankful for the gift of life itself, and for the strength He provided me to conduct this research. His blessings and guidance throughout this journey have been instrumental in making this research a reality.

I would like to express my deepest gratitude to my advisor, **Dr. Tefera T.Y**, for his invaluable guidance, constant encouragement, patience, insightful feedback and support throughout this research journey. From the very beginning, **Dr. Tefera T.Y** has provided me with the direction and encouragement I needed to navigate the challenges of research. He has always been available to answer my questions and offer advice, and confidence to follow my dreams has been fueled by an everlasting belief in my talents.

I would also like to extend my sincere appreciation to my co-advisor, **Mr. Mesfin Megra (Msc)**. His expertise and constructive criticism have been immensely helpful in refining my research and ensuring its clarity. **Mr. Mesfin Megra's (Msc)** dedication to his students is truly remarkable. He has invested countless hours in helping me to develop my skills and refine my ideas, and his commitment to excellence has inspired me to strive for the highest standards in my work. His passion for his field and his dedication to advancing knowledge are truly inspiring, and I feel honored to have had the opportunity to learn from him.

I am deeply indebted to **Dr. Endalew Ayenew** for his invaluable support and mentorship. His constant encouragement, insightful feedback, and meticulous guidance have been instrumental in shaping this research project. I am grateful for his patience and willingness to share his knowledge, which has significantly improved the quality of this work.

# TABLE OF CONTENTS

**CONTENTS** **PAGE**

**DECLARATION** . . . . . . . . . . **i**

**RECOMMENDATION** . . . . . . . . . . **ii**

**APPROVAL PAGE** . . . . . . . . . . **iii**

**ACKNOWLEDGEMENT** . . . . . . . . . . **iv**

**TABLE OF CONTENTS** . . . . . . . . . . **v**

**LIST OF TABLES** . . . . . . . . . . **ix**

**LIST OF FIGURES** . . . . . . . . . . **x**

**LIST OF ACRONYMS AND ABBREVIATIONS** . . . . . . . . . . **xii**

**ABSTRACT** . . . . . . . . . . **xiv**

**CHAPTER ONE** . . . . . . . . . . **1**

**1 INTRODUCTION** . . . . . . . . . . **1**

1.1 Background . . . . . . . . . . 1

1.2 Statement of the Problem . . . . . . . . . . 3

1.3 Objective . . . . . . . . . . 4

1.3.1 General Objective . . . . . . . . . . 4

1.3.2 Specific Objective . . . . . . . . . . 4

1.4 Significance of the Study . . . . . . . . . . 4

1.5 Scope of the Study . . . . . . . . . . 5

1.6 Limitation of the Study . . . . . . . . . . 5

1.7 Thesis Organization . . . . . . . . . . 6

**CHAPTER TWO** . . . . . . . . . . **7**

**2 LITERATURE REVIEW** . . . . . . . . . . **7**
2.1 Basic Theories and Overview . . . . . . . . . . 7
2.2 Utilization of FACTS devices Benefits . . . . . . . . . . 8
2.2.1 Static Synchronous Compensator (STATCOM) . . . . . . . . . . 10
2.3 Classification and Definition of Stability in Power System . . . . . . . . . . 12
2.3.1 Rotor Angle Stability . . . . . . . . . . 13
2.3.2 Voltage Stability . . . . . . . . . . 13
2.3.3 Frequency Stability . . . . . . . . . . 14
2.4 Classification of Buses in Power System . . . . . . . . . . 14
2.4.1 Load Bus . . . . . . . . . . 14
2.4.2 Generator Bus . . . . . . . . . . 15
2.4.3 Slack Bus . . . . . . . . . . 15
2.5 Wind Turbine Modeling . . . . . . . . . . 15
2.5.1 Induction Machine Wind Turbines . . . . . . . . . . 16
2.5.2 Doubly Fed Induction Generator . . . . . . . . . . 18
2.5.3 Aggregation of Wind Farm . . . . . . . . . . 20
2.5.4 General Assumptions for the Modeling of Wind Farms . . . . . . . . . . 23
2.5.5 Steps for Aggregating Wind Farms . . . . . . . . . . 23
2.6 Techniques for Time Domain Simulation . . . . . . . . . . 27
2.7 Literature Review on Previous Works . . . . . . . . . . 28
2.8 Research Gaps . . . . . . . . . . 30
2.9 Summary . . . . . . . . . . 30

**CHAPTER THREE** . . . . . . . . . . **31**

**3 MATERIALS AND METHODS** . . . . . . . . . . **31**
3.1 Methodology . . . . . . . . . . 31
3.2 Case Study Test System Selections . . . . . . . . . . 31
3.3 Data Collection . . . . . . . . . . 33
3.4 Data Analysis . . . . . . . . . . 34
3.5 Adama II Wind Farm Model . . . . . . . . . . 34

3.5.1 An integrated model of wind farm Adama II with IEEE 30 bus modified test systems . . . 43
3.6 Load Flow Analysis . . . 44
3.7 Particle Swarm Optimization . . . 45
3.7.1 PSO Parameters . . . 47
3.7.2 PSO Implementation Procedures . . . 48
3.8 Optimal Allocation and Size of STATCOM . . . 51
3.9 Problem Formulation . . . 51
3.9.1 Power Loss Minimization . . . 51
3.9.2 Voltage Deviation Minimization . . . 52
3.9.3 Power System Constraints . . . 53

**CHAPTER FOUR . . . 56**

**4 RESULTS AND DISCUSSIONS . . . 56**
4.1 Integration of STATCOM Controller into IEEE 30-Bus System . . . 56
4.1.1 Bus Voltage Profiles . . . 57
4.1.2 Active Power Loss Minimization . . . 58
4.1.3 Minimization of Reactive Power Loss . . . 59
4.2 Enhancement of Transient Stability Using Case Study Analysis . . . 61
4.2.1 Scenario 1: Base Case Condition . . . 63
4.2.2 Scenario 2: Under fault condition without STATCOM devices . . . 68
4.2.3 Scenario 3: Under Faulty Conditions With PSO-Determined STATCOM Placement . . . 69

**CHAPTER FIVE . . . 78**

**5 CONCLUSIONS AND RECOMMENDATIONS . . . 78**
5.1 CONCLUSIONS . . . 78
5.2 RECOMMENDATIONS . . . 79
5.3 FUTURE WORKS . . . 79

**REFERENCES** . . . . . . . . . . . . . . . . . . . . . . . . . . . . . . . . . . . **80**

**APPENDICES** . . . . . . . . . . . . . . . . . . . . . . . . . . . . . . . . . . . **84**

A. 1 IEEE 30-Bus System Single Line Diagram . . . . . . . . . . . . . . . . . . . . 84

A. 2 IEEE 30-Bus Test System Bus Data . . . . . . . . . . . . . . . . . . . . . . . 85

A. 3 IEEE 30-Bus System Line Data . . . . . . . . . . . . . . . . . . . . . . . . . 86

A. 4 Double-fed induction generator data with variable speed wind turbine data . . . 87

A. 5 Static Synchronous Compensator (STATCOM) Data . . . . . . . . . . . . . . . 88

A. 6 IEEE 30-Bus Modified Test System Compensator Data . . . . . . . . . . . . . 88

A. 7 Turbine Governor Data for the IEEE 30-Bus Modified Test System . . . . . . . 88

A. 8 Synchronous Machine Data for the IEEE 30-Bus Modified Test System . . . . 89

A. 9 Automatic Voltage Regulator Data for IEEE 30-Bus Modified Test System . . . 89

A. 10 Results of Power Flow for IEEE 30 bus system for faulty condition in PSAT . . 90

A. 11 Results of Power Flow for IEEE 30 bus system for faulty with PSO-placed STATCOM in PSAT . . . . . . . . . . . . . . . . . . . . . . . . . . . . 91

A. 12 Results of Line Flow for IEEE 30 bus system for Faulty condition in PSAT . . 92

A. 13 Results of Line Flow for IEEE 30 bus system for Faulty With PSO-placed STATCOM in PSAT . . . . . . . . . . . . . . . . . . . . . . . . . . . . . . . 93

A. 14 Branch impedance of cluster A and distance between each tower . . . . . . . . 95

A. 15 MATLAB Code for Particle Swarm Optimization Algorithm . . . . . . . . . . 95

# LIST OF TABLES


**TABLE** **PAGE**

Table 2.1 Different FACTS controller comparison . . . . . . . . . . . . . . . . . . . . . 8

Table 3.1 Data input for power flow modeling of wind farm Adama II (Source: Adama II WF) . . . . . . . . . . . . . . . . . . . . . . . . . . . . . . . . . . . . . . . 36

Table 3.2 An overview of the unit transformer's equivalent impedance for each cluster . 42

Table 3.3 An overview of each cluster's equivalent impedances across all collector circuits 42

Table 3.4 Control Variables Boundaries . . . . . . . . . . . . . . . . . . . . . . . . . 53

Table 3.5 Particle swarm optimization algorithm parameters and constraint of the decision variables of the objective function . . . . . . . . . . . . . . . . . . . . . . . 55

Table 4.1 Results of the test network's total active and reactive power losses . . . . . . 61

Table 4.2 Results of Power Flow for IEEE 30 bus system for base case condition in PSAT 65

Table 4.3 Results of Line Flow for IEEE 30 bus system for base case condition in PSAT 67

# LIST OF FIGURES


| FIGURE | | PAGE |
|---|---|---|
| Figure 2.1 | FACTS devices classification | 9 |
| Figure 2.2 | Basic STATCOM configuration | 10 |
| Figure 2.3 | V-I and V-Q STATCOM characteristics | 12 |
| Figure 2.4 | Classification of power system stability (Kundur et al., 2004) | 13 |
| Figure 2.5 | Typical wind turbine generators | 18 |
| Figure 2.6 | Schematic illustration of a wind turbine with DFIG (Tavoosi et al., 2022) | 20 |
| Figure 2.7 | A generic wind power plant's topology | 22 |
| Figure 2.8 | Combining several wind farms into one WTG | 22 |
| Figure 2.9 | (a) A system with three turbines, and (b) A representation with single turbine | 24 |
| Figure 2.10 | Representing the wind farm's line capacitance | 25 |
| Figure 2.11 | A Daisy-chained string of wind turbines connected to an equivalent circuit. | 26 |
| Figure 3.1 | Flow chart of the methods | 32 |
| Figure 3.2 | The structure of the Adama II wind farm | 35 |
| Figure 3.3 | Cluster A represented with a single turbine in the Adama II WPP | 41 |
| Figure 3.4 | Dynamic IEEE 30-bus modified test systems with integration of wind farm Adama II in MATLAB/PSAT | 44 |
| Figure 3.5 | Flow chart of particle swarm optimization algorithm | 50 |
| Figure 4.1 | Bus voltage profile for each of the two test scenarios | 57 |
| Figure 4.2 | Minimization of active power loss in both scenarios | 58 |
| Figure 4.3 | Total active power loss minimization in both scenarios | 59 |
| Figure 4.4 | Reduction of reactive power loss in the two scenarios | 60 |
| Figure 4.5 | Reduction of total reactive power loss in both scenarios | 60 |
| Figure 4.6 | IEEE 30−bus dynamic test systems with Wind farm Adama II under base case condition | 64 |
| Figure 4.7 | Magnitude of voltage profile for base case condition of IEEE 30 bus in PSAT | 66 |
| Figure 4.8 | Dynamic IEEE 30-bus modified test systems with integration of wind farm Adama II in MATLAB/PSAT under faulty condition | 69 |

Figure 4.9 IEEE 30−bus modified dynamic test systems interlinked with wind farm Adama II under faulty with PSO−placed STATCOM . . . . . . . . . . . . . . . . . 70
Figure 4.10 Rotor angle responses of the generator 1 . . . . . . . . . . . . . . . . . . . . 71
Figure 4.11 Rotor speed responses of the generator 1 . . . . . . . . . . . . . . . . . . . . 71
Figure 4.12 Rotor angle responses of the generator 2 . . . . . . . . . . . . . . . . . . . . 72
Figure 4.13 Rotor speed responses of the generator 2 . . . . . . . . . . . . . . . . . . . . 72
Figure 4.14 Rotor angle responses of the generator 3 . . . . . . . . . . . . . . . . . . . . 73
Figure 4.15 Rotor speed responses of the generator 3 . . . . . . . . . . . . . . . . . . . . 73
Figure 4.16 Real power responses of the generator 1 . . . . . . . . . . . . . . . . . . . . 74
Figure 4.17 Reactive power responses of the generator 1 . . . . . . . . . . . . . . . . . . 75
Figure 4.18 Real power responses of the generator 2 . . . . . . . . . . . . . . . . . . . . 76
Figure 4.19 Reactive power responses of the generator 2 . . . . . . . . . . . . . . . . . . 76
Figure 4.20 Real power responses of the generator 3 . . . . . . . . . . . . . . . . . . . . 77
Figure 4.21 Reactive power responses of the generator 3 . . . . . . . . . . . . . . . . . . 77

# LIST OF ACRONYMS

| | |
|---|---|
| **AC** | Alternating Current |
| **AVR** | Automatic Voltage Regulator |
| **DC** | Direct Current |
| **DFIG** | Doubly Fed Induction Generator |
| **FACTS** | Flexible Alternating Current Transmission System |
| **GSA** | Gravitational Search Algorithms |
| **GTO** | Gate Turn Off Thyristor |
| **IEEE** | International Electronics and Electrical Engineers |
| **IGBT** | Insulated Gate Bipolar Thyristors |
| **IPFC** | Interline Power Flow |
| **OC** | Open Circuit |
| **PI** | Proportional Integral |
| **PSAT** | Power System Analysis Toolbox |
| **PSO** | Particle Swarm Optimization |
| **PSS** | Power System Stabilizer |
| **SCIG** | Squirrel Cage Induction Generator |
| **SSSC** | Static Synchronous Series Compensator |
| **STATCOM** | Static Compensator |
| **STR** | Single Turbine Representation |
| **SVC** | Static Var Compensator |
| **SVS** | Static Var System |

| | |
|---|---|
| **TCPAR** | Thyristor Controlled Phase Angle Regulator |
| **TCPST** | Thyristor Controlled Phase Shift Transformer |
| **TCSC** | Thyristor Controlled Series Capacitor |
| **TDS** | Time Domain Simulation |
| **UPFC** | Unified Power Flow Controller |
| **VSC** | Voltage Source Converter |
| **WT** | Wind Turbine |
| **WTG** | Wind Turbine Generator |

# ABSTRACT

*A transmission system is a network of inter-connected lines that makes it possible to transport large amounts of electricity from a generation station to a substation. Power system transient stability is a critical aspect in ensuring reliable and secure power system operation. FACTS devices, such as STATCOM, have proven to be effective in enhancing power system transient stability. These devices have the capability to control power flow in the network, resulting in increased system load capacity, reduced flow in heavily loaded lines, lower system losses, and improved system security. STATCOM controllers are integrated into existing approaches to address these issues, but they are sized and placed incorrectly, which could result in a negligible reduction in magnitude of voltage deviations and transmission network losses. Hence, the purpose of this research is to minimize transmission network losses, transient instability and voltage magnitude variation in the transmission network by appropriately allocating the STATCOM controller through the use of PSO. After optimization, the results indicated that bus 05 with the injection of 39.93 MVAr of shunt reactive power with PSO had the best STATCOM controller positions in the test system. At steady state, the network under consideration's total active power loss was 9.003 MW, while the STATCOM controller optimized using PSO was 8.4173 MW, correspond to 6.5% total active power loss reduction. In accordance, the total reactive power loss was 32.6309 MVAr and 30.2954 MVAr, respectively, correspond to 7.157% total reactive power loss reduction. Further analysis is done on the impact of the compensation device STATCOM in the areas of transient stability improvement, loss reduction, damped oscillation in power system, and voltage profile support of a case study involving the incorporation of wind farm Adama II into IEEE 30-bus modified test systems using MATLAB/PSAT has been implemented. The results are compared to the impact in the absence of STATCOM under faulty conditions. The overall test systems with STATCOM placement have significantly improved transient stability, damped the multiple-machine system oscillations, and shortened the transient period of the oscillations.*
***Keywords:*** *FACTS, MATLAB/PSAT, PSO, STATCOM, Transient Stability*

# CHAPTER ONE

# 1 INTRODUCTION

## 1.1 Background

Power system is an electrical network comprising components designed for the generation, transmission, and utilization of power. Modern power systems are intricate networks characterized by multiple generation plants and load centers that are interconnected by power transmission lines and form an integrated electrical system. The electric power system encompasses generators, transmission and distribution facilities, and interconnected electrical loads. Due to the extensive system size, various disturbances can occur, potentially leading to adverse effects such as blackouts or the loss of synchronism in generators. Resolving transient stability issues is important because it dictates the behavior of electrical system for several seconds following a power disturbance. With the escalating demand for energy, there exists a shortage of primary energy sources, particularly fossil fuels, within the integrated power generation system. This shortage becomes more pronounced as demand continues to rise without a corresponding increase in alternative generation resources and transmission line capacity. These factors have put a strain on the power system, pushing it beyond its originally intended capability (Khan et al., 2017). Here, power system transient stability improvement is the main area of concern. Significant disturbances might arise from transient stability problems when load centers are distant from the generation. These disturbances not only pose risks to the security of the power supply but also make daily power system operations challenging. The power system ability to maintain synchronism and steady operation after a significant disturbance, like loss of generation via transmission lines or a failure, is known as transient stability. This holds true even in the face of substantial and sudden variations in the power system environment, such as three phase $(3-\phi)$ faults or abrupt damage to significant load or generation units. An overloaded power system may exhibit nonlinear behavior, and the abnormal interaction among different power system units can result in various modes of oscillations. If timely measures are not taken to dampen these oscillations, they can disrupt power flow and potentially lead to the un-synchronization of generators, culminating in either partial or total system shutdown.

FACTS devices provide a solution to mitigate these challenges without the limitations associated with electromechanical equipment, such deterioration and slow response. Maintaining transient stability is necessary to guaranteeing the secure and dependable functioning of power systems. These devices have capability to improve network stability, encompassing both transient and small signal stability. They achieve this by regulating parameters like series and shunt impedance, current, phase angle and voltage. Increased system load capacity, decreased system losses, improved system security, and decreased flow in severely loaded lines are all outcomes of controlling power flows in the network. This demonstrates effectiveness of FACTS devices in optimizing power system performance while avoiding the drawbacks often linked to traditional electromechanical solutions (Latt, 2019). The utilization of FACTS devices allows for an increase in both the maximum capacity of carrying power and flow of power in the transmission lines (Siddula et al., 2020). A conceptualization of the power system would be an extensive interconnected nonlinear system featuring numerous lightly damped electromechanical oscillation modes. When dampening these modes diminishes or becomes negative, it poses a significant constraint on the power system operation. Therefore, it is essential to describe these oscillation modes, pinpoint stability bounds, and, in many cases, put safeguards in place to prevent instability. As power industry shifts towards deregulation, there is a growing trend of long-distance power transfers that surpass the addition of new transmission facilities. Consequently, inter-area oscillations are becoming more lightly damped. Synchronous machines in a steady power system will either return to their initial condition in the absence of a net power change or attain a new condition while maintaining synchronism in the presence of a net change in power; synchronism is abandoned if stability is compromised

One approach to improving power system transient stability involves utilizing advanced FACTS controller devices, such as STATCOM optimized through optimization of particle swarms for optimal sizing and allocation. STATCOM belongs to category of FACTS devices, offering the ability to control power flow and enhance voltage stability. These devices function by supplying the electrical grid with reactive power, aiding in regulation of voltage levels and overall system stability. Particle Swarm Optimization serves as a method for sizing and siting advanced FACTS devices, allowing them to adapt to changing operating conditions and enhance power system performance. Employing optimization of particle swarms for the sizing and optimal allocation of

STATCOM facilitates fast and adaptive control of power flow and voltage stability within power systems. This, in turn, helps prevent loss of synchronism and improves the overall reliability and security of power systems.

## 1.2 Statement of the Problem

The wind promises a cleaner future, its energy pulses with the potential to power our lives without the harmful emissions of fossil fuels. Grid integration has become an issue in recent years with wind energy's penetration increasing in a number of countries such as Ethiopia, which could hinder the widespread adoption of wind energy systems.

Maintaining grid stability during transient events in wind farms is a major challenge. Transient instability can lead to cascading outages that cause widespread power outages, impacting entire communities and causing significant economic and social disruption. Grid instability can damage equipment such as transformers and generators, resulting in the need for costly repairs and replacements. Voltage and frequency fluctuations can affect the quality of energy delivered to consumers, damage sensitive electronic equipment and disrupt industrial processes.

Wind energy is intermittent and stochastic by nature, making it difficult to predict and control its contribution to grid stability. In addition to the challenges of transient stability, grid-connected wind farms can also experience voltage sags and swells, which can further affect grid performance and power quality. Voltage sags are Short-term voltage dips, often caused by faults or sudden load changes, can disrupt sensitive equipment and processes. Voltage swells are Short-term voltage surges, often caused by switching operations or load disconnections, can stress electrical components and potentially damage equipment.

By addressing the challenges of transient stability and power quality through smart grid technologies such as STATCOMs and optimization algorithms such as PSO, we can realize the full potential of wind energy while ensuring a resilient, reliable and sustainable energy future. STATCOMs can quickly inject or use reactive power absorption to control voltage levels during disturbances, reducing the severity and duration of voltage dips and surges. STATCOMs can provide continuous voltage support at the point of interconnection, increasing the resilience of the grid to voltage fluctuations. The problem addressed in this thesis, conducting investigation on the impact of integrating wind farm Adama II into the grid on transient stability.

## 1.3 Objective

### 1.3.1 General Objective

The general objective of this study is to enhance the transient stability of the power system by using STATCOM optimized through Particle Swarm Optimization (PSO) techniques, specifically focusing on the IEEE 30-bus test system integrated into the Adama II Wind Farm.

### 1.3.2 Specific Objective

- Development of aggregated wind farm Adama II.
- Formulation of PSO for optimal allocation and sizing of STATCOM.
- Development of test network in PSAT with STATCOM to maintain the transient stability.
- Perform time-domain simulations (under baseline conditions, under three-phase fault condition without and with STATCOM to show the improvement in system stability).

## 1.4 Significance of the Study

Transient stability is crucial for ensuring system security. This implies that the occurrence of a fault should not result in the shutdown of a generating unit due to a loss of synchronism, and it should not create the risk of a cascaded outage and system blackout. Enhancing transient stability, therefore, should be instantaneous, and FACTS devices can accomplish this task. Using FACTS for transient instability prevention mechanisms is advantageous in minimizing equipment failure due to disturbances in power systems, decreasing total interruption time, and decreasing maintenance costs for power system equipment. The following describes the study's significance:

- To incorporate FACTS devices STATCOM into a multiple-machine power system network so as to improve transient stability.
- To efficiently determine optimal allocation and size of STATCOM.

This accomplished by identifying most line loss and least robust bus in the combined study of integrating wind farm Adama II into IEEE 30-bus modified test system. STATCOM positioned near the weak bus and the line with the highest active power loss. Subsequently, transient stability enhancement analyzed for the integrated case study that connect wind farm Adama II into IEEE 30-bus modified system of the synchronous generator. The importance of this research lies in its capacity to advance our comprehension of how FACTS devices STATCOM can enhance power system transient stability. By incorporating these advanced control techniques into a multiple-machine power network system, this research has potential to improve significantly ability to maintain reliable and secure operation of power systems. Additionally, by using PSO to optimally locate and size these devices can be achieved, further enhancing power system performance.

## 1.5 Scope of the Study

The scope of the research involves evaluating efficiency of STATCOM based on PSO in a multiple-machine network of power system for enhancing transient stability. This assessment focused on the integrated study of connecting wind farm Adama II into IEEE 30-bus modified test system model, utilizing the PSAT in MATLAB/simulink.

## 1.6 Limitation of the Study

Limitations of the study on transient stability enhancement using STATCOM based on PSO, focusing on the IEEE 30-bus test system integrated with the Adama II wind farm, include the reliance on simulation-based analysis, which may not fully capture the complexities and dynamics of real-world power systems. The study may also be limited by the simplifications and assumptions made in the modeling of the power system, wind farm, and control algorithms, potentially leading to discrepancies between simulation results and actual operating conditions. Additionally, the scalability and applicability of the proposed methodology to larger and more complex power systems remain to be fully evaluated. Furthermore, the study may lack empirical validation through field experiments, which are crucial for verifying the effectiveness and robustness of the proposed approach under practical conditions.

## 1.7 Thesis Organization

This thesis is organized into five chapters, each playing a significant role in presenting research:

**Chapter 1: Introduction** – This opening chapter sets the stage by providing a brief background on the growing use of wind farms and the challenges it presents for power system stability. It then clearly defines the problem of maintaining stability with wind farm integration. Following this, the chapter outlines objective of the research, highlighting significance and scope of the study and acknowledging any limitations.

**Chapter 2: Literature Review** – This chapter surveys key topics relevant to the research. It explores recent trends in power system stability, defines and classifies different stability types, and discusses the benefits of FACTS devices. Additionally, the chapter delves into power system modeling techniques and wind turbine modeling approaches, highlighting their classification and application in power systems.

**Chapter 3: Materials and Methods** – This chapter dives into mathematical modeling of Adama II wind farm, including aggregation methods. It then details the development of Adama II wind farm model for integration with IEEE 30-bus modified test system. Finally, the chapter explores utilization of PSO for optimizing location and size of a STATCOM device.

**Chapter 4: Results and Discussion** – This chapter analyzes the impact of wind energy integration on power system stability under pre-fault, fault, and fault with STATCOM scenarios. PSAT software is used to simulate the system's dynamic behavior with and without a PSO-optimized STATCOM placement. The chapter discusses and compares the results, focusing on improvements in loss reduction, voltage profile, and transient stability.

**Chapter 5: Conclusion and Recommendations** – This final chapter summarizes the key findings of the research, highlighting impact of Adama II wind farm model integration with a grid and STATCOM optimization on power system stability. It then offers recommendations for future research directions to further explore this area.

# CHAPTER TWO

# 2 LITERATURE REVIEW

## 2.1 Basic Theories and Overview

Power system stability is an essential aspect of electrical systems to ensure security and reliability of power supply. By redistributing power in crowded lines—particularly when there is high load—these devices can improve system stability. By improving power quality and impedance, FACTS controllers contribute to voltage consistency. Many studies have investigated how these devices can improve the shape of voltage profiles (voltage magnitude profiles), enhance the capability of the power system to handle power transfers (transfer stability), maintain safe voltage levels throughout the system (secure voltage profile), and minimize energy wasted during transmission (system losses). FACTS devices evolution has been closely tied to advancements in power electronic components. High-power level devices have become accessible for converters operating at different voltage levels. According to (Hingorani & Gyugyi, 2000) FACTS controllers can be categorized into four (4) main groups: series, shunt, series-series, and series-shunt controllers. The devices can be broadly classified into several groups:

I. Power electronics devices connected with the transmission line in series to control flow of power, including SSSC, TCPAR or TCPST, and TCSC.

II. Equipment installed at junctions in the power grid (shunt) to manage voltage levels, including the STATCOM and SVC.

III. Devices that combine series and shunt functionalities, like the IPFC for series-series operation and the UPFC for combined series-shunt control.

Table 2.1: Different FACTS controller comparison

| Name | Type | Utilized Controller | Control Application |
|---|---|---|---|
| SSSC | Series | GTO | Power flow |
| TCSC | Series | Thyristor | Power flow |
| TCPAR | shunt-Series | Thyristor | Power flow |
| STATCOM | Shunt | GTO | Voltage |
| SVC | Shunt | Thyristor | Voltage |
| UPFC | Shunt-Series | GTO | Power flow and Voltage |
| IPFC | Series-Series | GTO | Power flow and Voltage |

The application of FACTS device, including STATCOM, has been widely studied and implemented to enhance power stability. This literature review will explore various research works that has been conducted on the utilization of STATCOM to enhance power system stability.

## 2.2 Utilization of FACTS devices Benefits

The advantages of incorporating FACTS devices into electrical transmission systems can be outlined as follows: they increase the transmission lines loading capacity, prevent blackouts, enhance generation productivity, reduce reactive power circulation, improve stability limits, minimize voltage flickers, damping oscillations, ensure stability, reliability, security, availability, and economical operation. FACTS controllers, a family of electronic controllers, play a crucial role in enhancing power system performance. Power systems, being nonlinear and subject to a broad operating conditions, time-varying configurations, and parameters, benefit from the development of FACTS to improve weak AC systems performance and increase capabilities of transmission over long AC lines. All three power system states—steady state, transient, and post-transient steady state—can be operated in with FACTS controller. They have capacity to control voltage magnitude, active, and reactive power. The FACTS controller dynamic application encompasses improve transient stability, damping oscillation (dynamic stability), and enhancement of voltage stability. These controllers have the capability to control current, series and shunt impedance, voltage, and phase angle. There are three types of FACTS devices as shown in Figure 2.1.

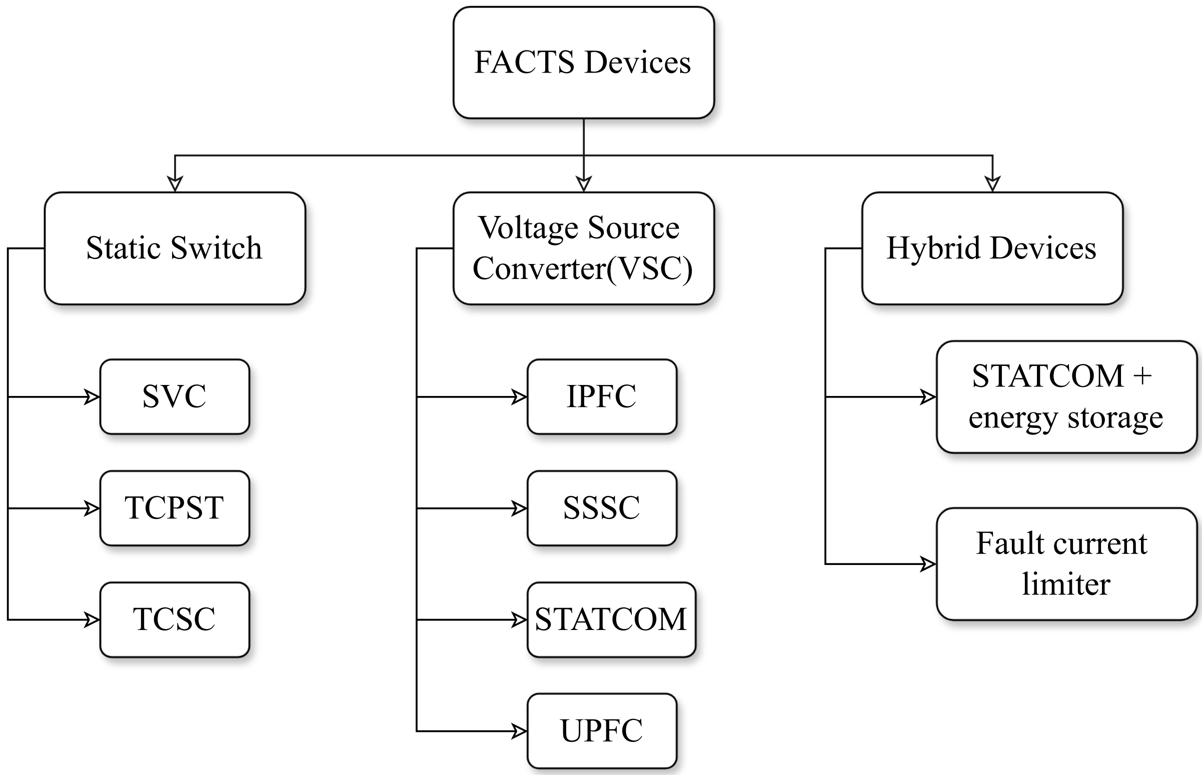


Figure 2.1: FACTS devices classification

The most promising device among FACTS controllers utilized in this study to enhance transient stability and dampen oscillations is the STATCOM. STATCOM is employed for controlling power flow and improving voltage stability. These devices operate by supplying reactive power into the power system, thereby regulating voltage and improving overall stability. STATCOM play a significant role in regulating energy flow and power quality without compromising performance expectations. Power quality has been negatively impacted by a number of devices, including transformers, motors, computers, printers, communication devices, and household machinery. Even though bus voltage magnitudes must be kept within specified limits, transporting reactive power is difficult when the network is heavily loaded (Suliman, 2020). In addition, STATCOM is used to adjust reactive power in transmission lines and loads, reduce harmonics in line currents, improve load power factor, and compensate for voltage sag/swell. It is particularly effective in mitigating bus voltage levels (Jamil et al., 2019).

### 2.2.1 Static Synchronous Compensator (STATCOM)

STATCOM, as a shunt-linked FACTS device, has the capability to absorb or produce reactive power to control voltage at the point where power system is connected. By controlling reactive power injection, STATCOM contributes to maintaining voltage stability and preventing voltage collapse following significant disruptions, including malfunctions or a loss of power. Reactive power can be generated or absorbed by it, and its output can be tuned to regulate particular power characteristics. In an AC power system, STATCOM, a power electronic-based VSC, can operate as a reactive power source or sink. A single-line STATCOM's power circuit is depicted in Figure 2.2, where utility bus and VSC are linked via magnetic coupling. Reactive current injection by a STATCOM maintains grid voltage. Conversely, the grid voltage drops when STATCOM absorbs reactive current. STATCOM, belonging to the FACTS device family, is employed for the enhancement of voltage profiles. Utilizing a VSC, STATCOM injects a variable-frequency and variable-amplitude compensatory current at the bus. Capacitance is incorporated into the DC link of this three-phase VSC.

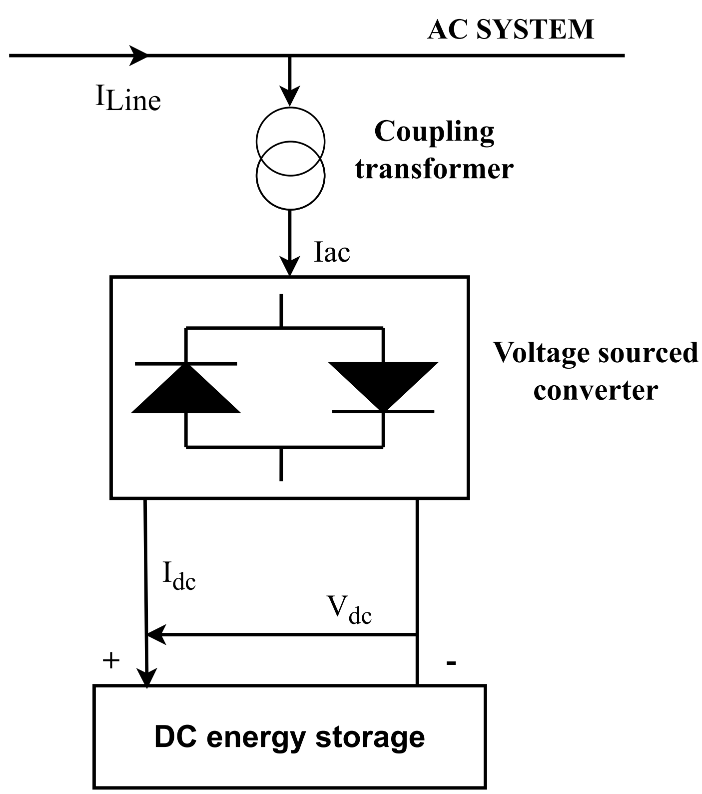


Figure 2.2: Basic STATCOM configuration

As a solid-state switching converter, STATCOM can independently generate or absorb reactive and real power that can be controlled at the output when supplied using the input terminal of an energy storage device or energy source. An energy-storage capacitor or a battery may supply the DC voltage. The three-phase voltages that make up the STATCOM output are all in phase and connected to the matching AC voltage system via a tiny reactance, which can be supplied by an interface reactor or by coupling transformer's leakage inductance. Similar to perfect synchronous machine, STATCOM functions as a fast-acting device that produces a series of three sinusoidal voltages that are balanced in terms of amplitude, phase angle, and fundamental frequency that may be adjusted. It is built on the VSC architecture and makes use of either IGBT or GTO devices. Essentially, STATCOM is a VSC that converts input DC voltage to output AC voltage for compensating reactive and active power.

**Voltage-Current*(V-I)* and Voltage-Quantity*(V-Q)* Characteristics**

The STATCOM is an alternating VSC behind a coupling reactance that has matched $v-I$ and $V-Q$ properties depicted in Figures 2.3(a) and 2.3(b) respectively. These characteristics show that even at very low (theoretically zero) voltage levels, approximately about 0.2 p.u., the STATCOM can operate over its full current output range. Essentially, the maximum absorption or generation of Var for STATCOM varies linearly with AC voltage, but it is possible to maintain the maximum output current, either inductive or capacitive, regardless of the Ac voltage.

The STATCOM's capability to provide maximum compensating current at reduced system voltage allows it to function dynamically across various applications. The highest current turn-off capacity of the power semiconductors (e.g., GTO thyristors) employed determines the maximum possible transient over current in the capacitive region. Shunt compensation provided by a STATCOM, rather than by an SVC, can increase transmittable power or decrease the STATCOM rating below that of the SVC for the same stability margin. By drawing controlled actual power at its DC terminal from an energy source, the STATCOM may supply the system with AC power. It can also regulate how much energy is absorbed from AC system in order to keep the storage device charged.

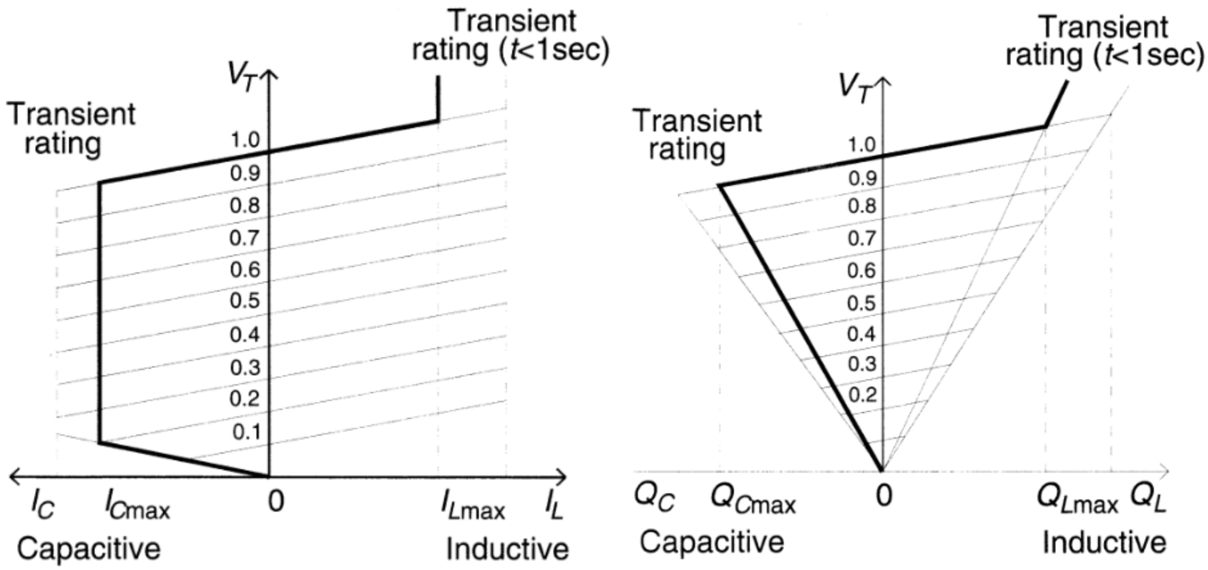


(a) *V-I* STATCOM characteristics

(b) *V-Q* STATCOM characteristics

Figure 2.3: V-I and V-Q STATCOM characteristics

## 2.3 Classification and Definition of Stability in Power System

Power system stability is the ability of a power system to recover from physical disturbance and reach a state of operational equilibrium under particular initial operating conditions. This means that most system variables remain constrained, protecting the entire system integrity. Rotor angle stability, frequency stability, and voltage stability are the three main components that make up power system stability classification, as shown in Figure 2.4 (Latt, 2019; Kundur et al., 2004). There are several subcategories within power system stability. These include:

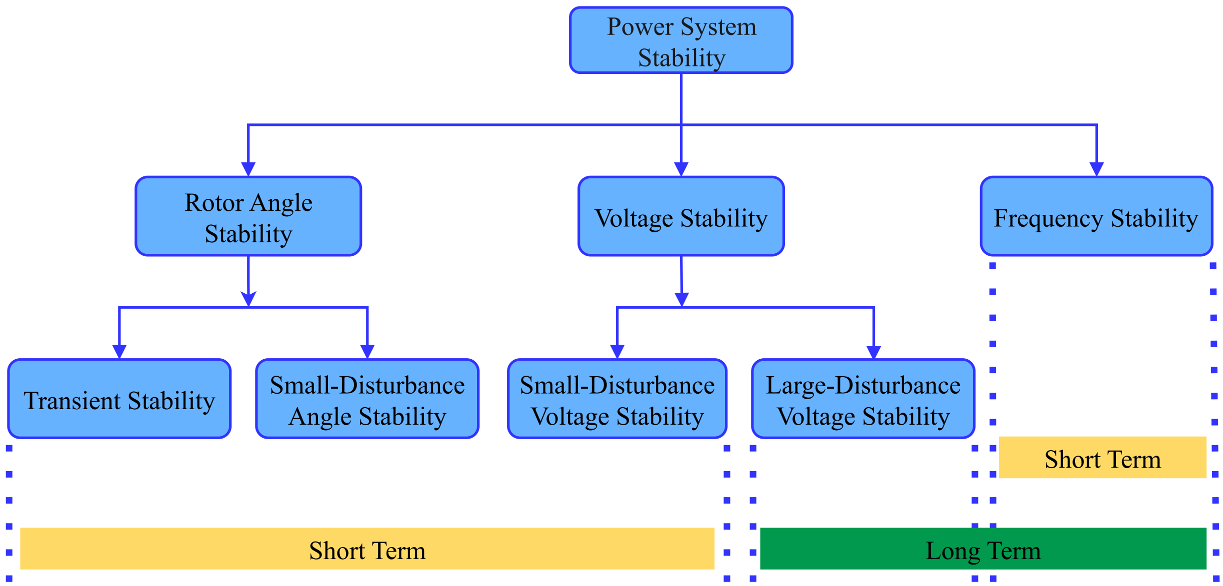


Figure 2.4: Classification of power system stability (Kundur et al., 2004)

### 2.3.1 Rotor Angle Stability

Rotor angle stability is the capability of synchronous machines in a networked power system to retain synchronism after a disruption. This stability based on the capability of system to retain or restore balance between each synchronous machine mechanical and electromagnetic torques. Potential instability manifests as escalating angular swings in certain generators, resulting in their desynchronization from other generators (Kundur et al., 2004).

### 2.3.2 Voltage Stability

When a disturbance occurs from a certain starting operating condition, power system's capacity to retain stable voltages across each bus is referred to as voltage stability. This stability relies on maintaining or restoring equilibrium between the power system's load supply and demand. Potential instability appears as a slow down or rise in voltage at specific buses. Voltage instability can cause consequences such as area load loss, tripping of transmission lines, and activation of protective systems causing a series of outages. These outages or operating situations exceeding field current limitations might cause generators to lose synchronism. Rotor angle instability may also be connected to a progressive decline in bus voltages. For instance, the loss of synchronism between two machine groups approaching a 180° rotor angle difference causes a rapid voltage drop at intermediate points near the electrical center (Kundur et al., 2004). Protective systems typically act to separate the two machine groups, allowing voltages to recover based on situations following a separation. But if the system stays together, there will be frequent "pole slips" between the machine groups, which will cause voltages close to the electrical center to fluctuate quickly between high and low levels. However, loads are involved in persistent voltage decreases associated with voltage instability, and these can happen even when there is no stability issues in the rotor angle. Constraints on voltage stability are essential for preserving power system stability. Three types of buses are typically found in a power system: generator bus (P-V bus), load bus (P-Q bus), and slack bus (reference bus). The reference voltage is defined as standard voltage at the slack bus, which is assumed to be 1.0 p.u. The difference between current bus voltage and slack bus voltage can be used to compute deviations from this reference voltage at other buses. Deviations indicate instability conditions at the corresponding bus (Kundur et al., 2004).

### 2.3.3 Frequency Stability

Frequency stability is the power system's capability to retain operating frequency following significant disturbance that causes a significant imbalance between generation and load. This stability relies on maintaining or restoring balance between the generation and load on the system, reducing unintentional load shedding. Prolonged frequency oscillations indicative of potential instability might cause loads or generating units to trip.

## 2.4 Classification of Buses in Power System

The power systems buses are primarily categorized as follows:

### 2.4.1 Load Bus

This bus has specified active and reactive power, whereas voltage magnitude and phase angle are needs to be calculated. The load bus voltage does not need to be specified because it can fluctuate within acceptable range.

### 2.4.2 Generator Bus

A voltage-controlled bus is another name for this. In this case, the voltage level and net active power are known. Reactive power and phase angle must be calculated, where active power and voltage magnitude are specified. These buses are sometimes referred to as voltage-controlled buses or generator buses. At these buses, the reactive power value is subject to set limits.

### 2.4.3 Slack Bus

The given quantities in this case are phase angle and voltage magnitude. The purpose of slack bus, which is usually a generator bus, is to supply extra active and reactive power to compensate for network losses. This kind of bus is distinct in the power system. This bus is sometimes referred to as the swing bus or the reference bus.

## 2.5 Wind Turbine Modeling

Wind energy is one of the most established and promising non-hydro renewable energy sources available. All that a wind turbine is a machine that uses air kinetic energy to create electricity by feeding it into a generator. An aerodynamic rotor is used by the wind turbine generator to harness wind energy and transform it into electrical energy. In this generation system, the wind serves as the main source of electricity. There are two categories of wind energy use: onshore and offshore. The capability of offshore wind turbines has grown from 2 to 5 MW, while the capability of onshore wind turbines has grown from 1.5 to 3 MW due to advancements in technology. Wind turbines typically employed have a capacity of 5 to 6 MW. Offshore winds are both more consistent and stronger, resulting in higher energy production compared to onshore winds. The use of wind energy at sea requires a more complicated installation system, which is why Not much study has been done in this field to date. The wind turbine axis may be horizontal or vertical. The axis along which the wind turbine vertical axis blades rotate is perpendicular to the ground, while the axis along which wind turbine horizontal axis blades rotate is parallel to the ground.

The cut-in speed, rated speed, and cut-out speed are three speeds that define a wind power curve (Singh & Santoso, 2011; Operator, 2013). The turbine operates at the cut-in speed initially, reaches its maximum power at the rated speed, and then shuts down at the cut-out speed to prevent potential damage. Since wind farms can only provide a small amount more energy than other grid sources, wind turbine generators are arranged in groups of one. All of the energy produced is combined and supplied into the grid as a single energy source. Increased installed wind power capacity is a result of rapid technological advancements in generators, mechanical drive trains, blade equipment, aerodynamics, gearboxes, wind turbine design, and converter control. These advancements have enhanced wind turbine performance and allowed wind turbines to produce more power.

### 2.5.1 Induction Machine Wind Turbines

The induction machine serves as the predominant power conversion device in commercial wind turbines. These devices not only provide a reliable connection between turbine mechanical system and grid, but also offer a more resilient and fail-safe solution. Manufacturers of wind turbines have created cutting-edge technology in addition to induction generator systems to enhance efficiency and control (Georgilakis, 2008). Sometimes Occasionally, these technologies have the ability to conceal the dynamic properties that are generally connected to rotating gear, which compromises the effectiveness of wind turbines in terms of electrical and dynamic performance. Figure 2.5 illustrates the four significant categories of generator technologies commonly used in wind turbines. Widely used wind turbines in recent decades have primarily utilized wind turbines belonging to one of the following configurations (Mastoi et al., 2023):

I. **Type I WTG:** A step-up transformer is used to link a constant−speed wind turbine with a squirrel-cage generator directly to the grid. The hub, which is coupled to an induction generator with a squirrel−cage rotor through a gearbox, is fed by the blades with stationary control (fixed pitch). Apart from having a direct connection to the mains, generator also have shunt capacitors installed, which will automatically switch on to offset reactive power. It is possible to disable the soft start mechanism once the generator has been turned on in order to keep it from making contact with the mains. The asynchronous generator's torque-speed characteristics result in the turbine operating within a defined speed range.

II. **Type II WTG:** A wind turbine with an induction generator and wound rotor that has limited speed control. This induction generator with wrapped rotor enables the regulation of the rotor current magnitude and pitch of the turbine blades to alter the speed through the use of adjustable external rotor circuit resistors. The turbine's speed range can be increased by employing external resistors.

III. **Type III WTG:** A DFIG with a variable speed wind turbine with partial electronic conversion of power. Wound rotor induction generator rotor circuit is linked to the grid terminals via a four-quadrant converter. The converter greatly increases the turbine's speed range by actively controlling the rotor circuit current vectorially, even in dynamic conditions, while taking into account the phase angle and magnitude. The primary mechanism for controlling the turbine speed is to adjust the turbine blades' pitch.

IV. **Type IV WTG:** a wind turbine with variable speed and complete electronic power conversion that works with induction or synchronous generators. The conversion of the full rated power is made possible by power converters that lie between electrical grid and wind turbine. Much of the behavior and features that are crucial for the energy system analysis could be located in the area that is directly linked to the electrical grid since power converter greatly decouples dynamics of the electrical generator from the grid.

V. **Type V WTG:** Variable-speed in which the generator's speed is adjusted to the electrical synchronous speed using a mechanical torque conversion located between high-speed generator and low-speed rotor shaft. The synchronous machine used by this kind of machine is then immediately connected to the medium-voltage grid. It consists of a synchronous generator coupled to a torque/speed converter and a standard variable speed WTG drive train. The rotor shaft's variable speed is changed into a constant output shaft speed by the torque/speed converter. A synchronization switch can then be used to connect the tightly related synchronous generator directly to the mains. This generator runs at a fixed speed that matches the mains frequency. Any required speed which usually 6-pole or 4-pole and voltage which usually medium voltage for higher capacities can be designed into the synchronous generator. The AVR, synchronization system, and generator protection system typical synchronous generator connected with grid, along with torque and speed control of the speed/torque converter, are required for this approach.

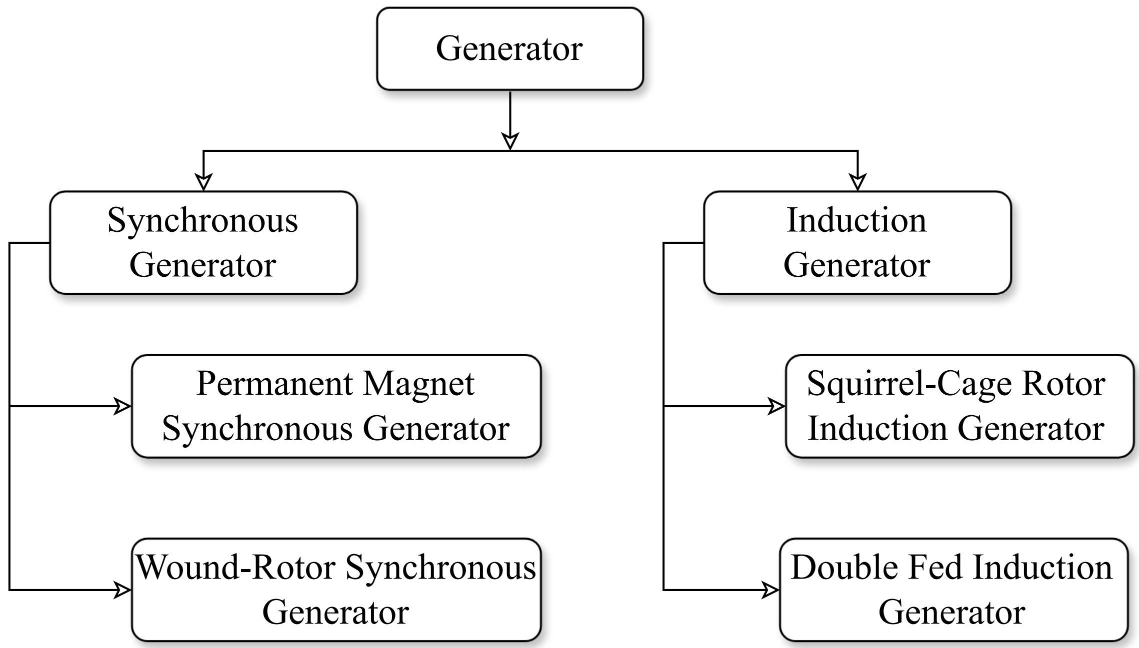


Figure 2.5: Typical wind turbine generators

### 2.5.2 Doubly Fed Induction Generator

A DFIG can use a more advanced system to control the rotor current. Across four quadrants, the converter uses voltage and current control loops to supply power to the rotor circuit. The converter output current can be regulated almost instantaneously depending on the mains frequency. Under controlled operating conditions, it is possible to achieve electromagnetic torque by controlling the current in the rotor circuit in terms of both magnitude and phase. Output reactive power to the stator terminals can also be limited by manipulating generators (Ledesma & Usaola, 2005). Vector-controlled or field-oriented induction machines, known for their high performance in industrial drive systems, offer similar advantages when applied to wind turbines. Based on the speed of the generator, grid-side converter either feeds or absorbs power into the grid. The generator runs at synchronous speed when it is operating at a grid frequency and number of poles lower than the synchronous speed (Tavoosi et al., 2022). The machine-side converter directs the output power to the rotor circuit during this synchronous speed period. When the turbine runs faster than the synchronous speed, there is an opposing power flow.

The DFIG rotor is not internally short-circuited; instead, it includes a three-phase coil winding that is coupled to a power electronic drive through slip rings with variable frequency. The stator is connected to the transformer's low-voltage side. An IGBT control circuit controls the amount of current drawn from the rotor, while the rotor itself receives active power via a connection that converts DC/AC voltage sources that draws current from the grid. When the rotor speed and a particular frequency are combined, the converter on the rotor side produces a synchronous rotating the air gap field (Din et al., 2022). The generator's rotor, which enters into a power exchange with the grid, and stator, which supplies electricity into the grid, engage in an active power exchange. Furthermore, to supply active power the stator provides reactive power to the grid.

The following benefits have led to the double-fed induction generator (DFIG) being installed more often recently:

- As opposed to an induction generator's 0%–2% range, the generator's slip range is significantly greater, ranging from 0%–16%. An induction generator's rotor frequency is also unaffected by the grid frequency.
- It can be operated at variable wind speeds, approximately $\pm 33\%$ around synchronicity, which enables the generation of power even at low wind speeds.
- Since inverter controls approximately 30% of the total power, its cost kept to a minimum.
- It has the ability to modify power factor by adjusting the amount of reactive power that the grid delivers or absorbs.
- Its efficiency is higher than that of traditional induction generators.

The schematic diagram in Figure 2.6 illustrates a wind turbine fitted with a DFIG. The stator and grid are directly connected. A back−to−back VSC and Slip rings are used to connect rotor windings to the grid. Rotation speed can be adjusted with the help of a variable frequency source that the VSC offers. Both the generator rotor's rotation and the rotational impacts of the AC current from the converter cause rotor windings' magnetic field to rotate. This results in two possible situations where the rotor rotating magnetic field occurs either in the opposite direction or in the rotor's direction of rotation. When the magnetic field of the rotor and generator's rotor are orientated in the same direction, super synchronous operation takes place. When the generator's rotor is positioned opposite to magnetic field of the rotor, sub-synchronous operation occurs. The magnetic flux density passing through the stator windings determines the induced stator voltage level. Applying a voltage proportional to the frequency to the rotor winding will keep a steady voltage on the stator. This indicates that the voltage to frequency $V/f$ ratio is maintained constant.

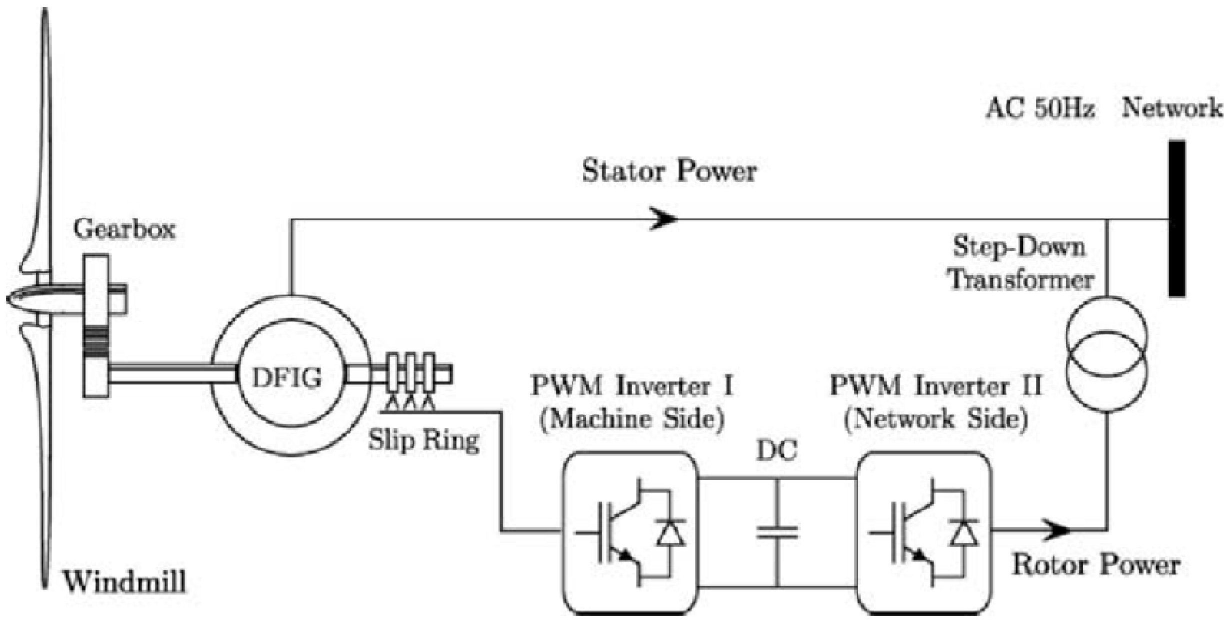


Figure 2.6: Schematic illustration of a wind turbine with DFIG (Tavoosi et al., 2022)

### 2.5.3 Aggregation of Wind Farm

A large-scale wind generating plant can comprise several wind turbines, each with a capacity in the megawatt range. A complex collector system connects these turbines to each other. Although the impact of individual turbines on the wider electricity grid is limited, the wind turbines as a whole can significantly affect the electricity grid in the event of severe disturbances, such as adjacent faults. Although it is crucial to simulate a wind turbine as nearly as possible to the real implementation, it is not feasible to model hundreds of turbines and branches that corresponding with them. Thus, an equivalent representation that is simplified is employed.

A wind turbine generator (WTG) is made up of many separate WTG coupled to a collector system with a medium voltage at the transfer point, which is then connected to the transmission grid. Modern wind turbines typically have low terminal voltage levels (575V or 690V) and rated outputs between 1.5 MW and 5 MW per turbine. A step-up transformer, typically installed on a base, connects each wind turbine to a collector system with a medium voltage, which typically operates between 12 kV and 34.5 kV. The collector network comprises one or more feeders that are interconnected in a collector network station. One or more station transformers are located at the collector system station are utilized to attain voltage of the transmission grid. A transfer line is necessary if the collector system station is far apart from the transfer point. Power factor correction at the collector station may include the installation of continuously adjustable devices such as STATCOM or SVS and mechanically switched capacitors. Reactive power compensation can be implemented at the wind turbine generator (WTG) terminals to rectify the power factor, depending on the kind of WTG. The amount and characteristics of power factor correction will be influenced by the collector system design considerations and interconnection requirements, which include factors such as voltage regulation and losses.

The total output of a wind farm can be illustrated using the diagram of a single turbine representation (STR). Generally, a medium voltage level between 12 kV and 34.5 kV is linked to collector system, with the wind turbines connected together in a string or a cluster via underground cables. Wind turbines can be grouped together in one or more clusters. The generated terminal voltage of each wind turbine is raised to the average voltage level of the collector system by means of an electrical connection to its individual transformer. The medium voltage is then raised to the transmission voltage by connecting the collector system with central substation transformer. A massive wind farm is made up of multiple separate turbines connected to one another over a considerable region of land or water, as shown in Figure 2.7. For load flow and transient stability studies, equating every wind turbine to a single machine—as shown in Figure 2.8—is a useful way to reduce its size.

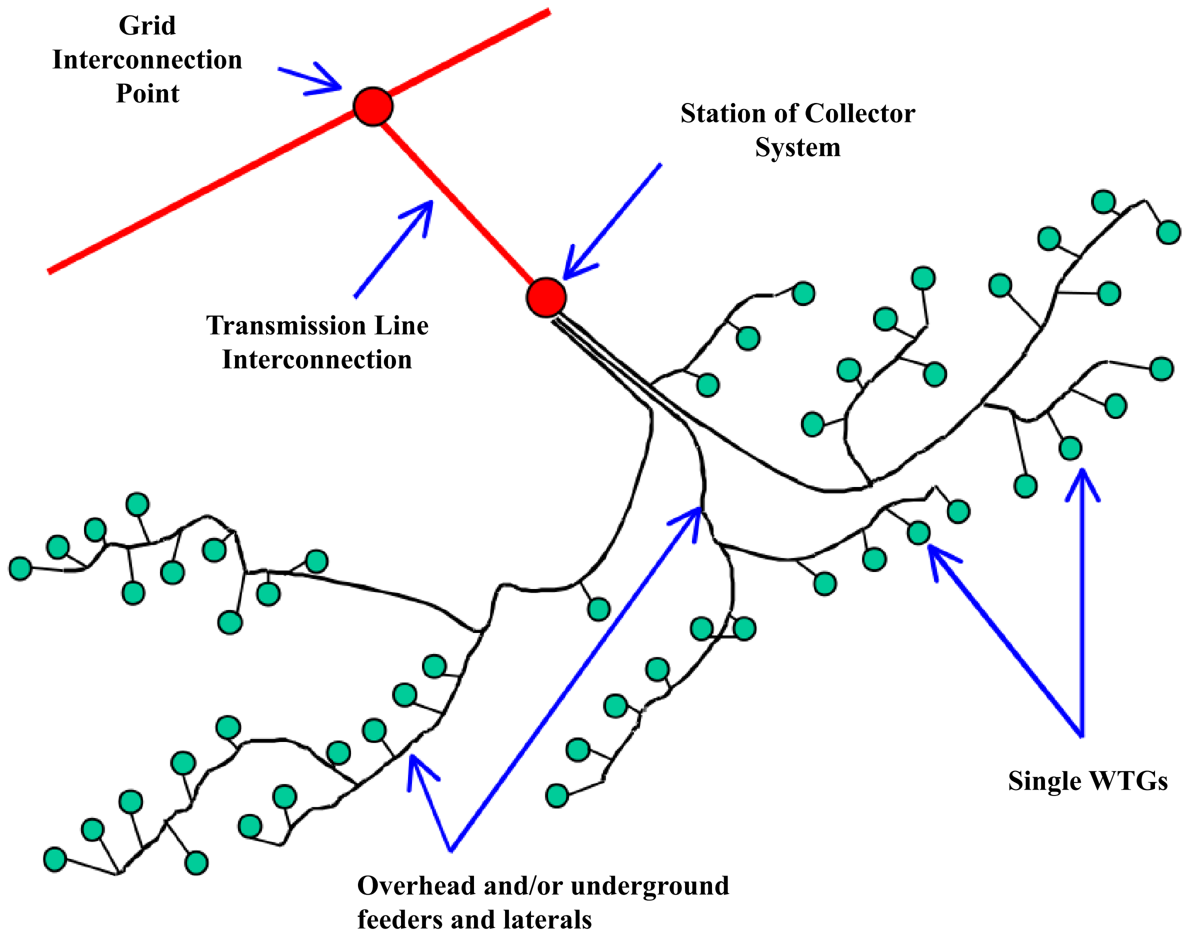


Figure 2.7: A generic wind power plant's topology

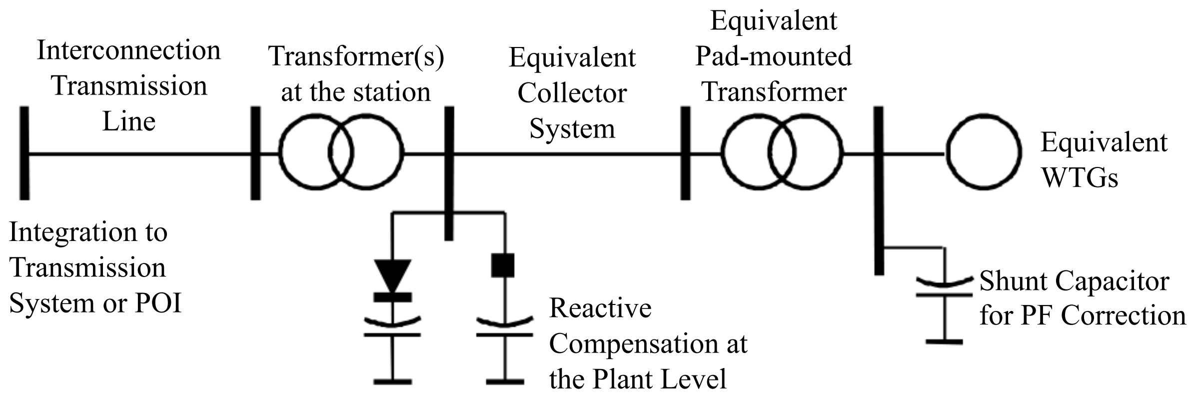


Figure 2.8: Combining several wind farms into one WTG

### 2.5.4 General Assumptions for the Modeling of Wind Farms

The subsequent derivations are grounded on the equivalent circuit for apparent power loss, encompassing real and reactive power loss. These derivations consider the following assumptions when establishing the equivalent circuit for the collector system (Jember et al., 2024).

1. All wind turbines inject current with identical magnitudes and angles.

2. The reactive power generated by line capacitive shunts assumes the bus voltage is at 1 p.u.

### 2.5.5 Steps for Aggregating Wind Farms

This thesis adopts the concept of single-unit equivalence to establish an equivalent aggregated wind turbines model. In aggregated wind turbine generator model, the results of a single equivalent wind turbine generators $(WT_{eq})$ is representation of the combined output power of multiple wind turbine generators, achieved through capacity weighting and proportional amplification.

**Step 1: Wind Turbine Equivalents**

If $N_t$ wind turbines number are reduced to a single wind turbine, the parameters derived from the equivalent machine are megawatts (MW) of active power $(P_{eq\underline{n}})$ , megavolt-amperes (MVAr) of reactive power $(Q_{eq\underline{n}})$ and megavolt-amperes (MVA) of apparent power $(S_{eq\underline{n}})$ (Jember et al., 2024).

The parameters are specified in Equation (2.1):

$$\begin{aligned} P_{\mathrm{eq\underline{n}}} &= N_t \times P_{MW\,per\,unit} \\ Q_{\mathrm{eq\underline{n}}} &= N_t \times Q_{MVAR\,per\,unit} \\ S_{\mathrm{eq\underline{n}}} &= N_t \times S_{MVA\,per\,unit} \end{aligned} \tag{2.1}$$

where, $N_t$ is the total number of wind turbines in wind farm's.

**Step 2: Pad Mount Transformer Equivalents**

A loss formula is used to evaluate the equivalency of unit transformer linked to a turbine. The system with three turbines and three unit transformers, as illustrated in Figure 2.9 (a), can be used to determine the equivalent impedance of a pad mount transformer (Jember et al., 2024).

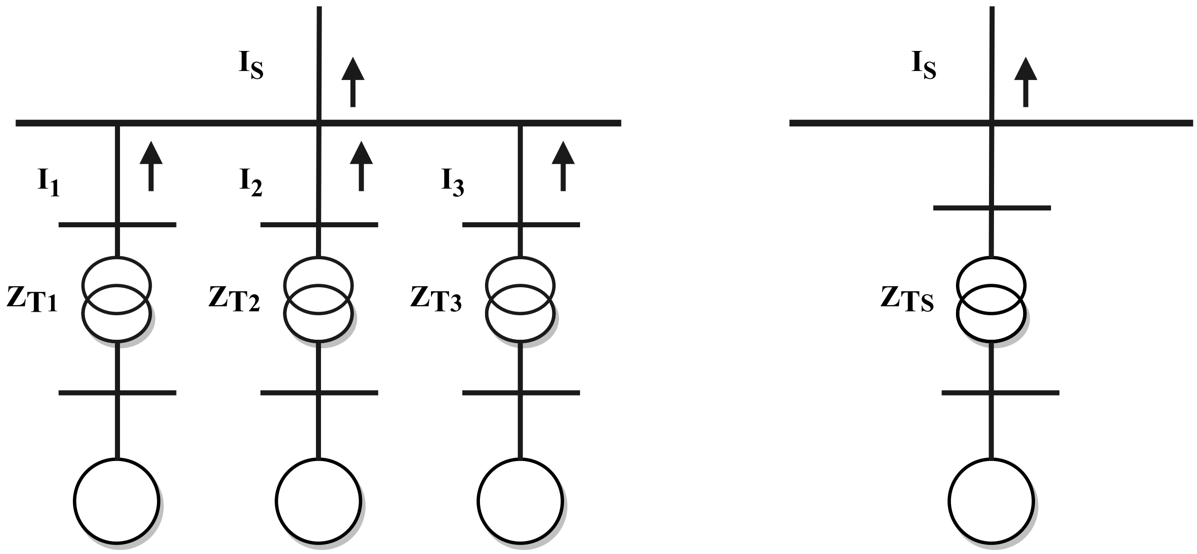

(a)

(b)

Figure 2.9: (a) A system with three turbines, and (b) A representation with single turbine

Therefore, as shown in Figure 2.9 (a) each pad mount transformer's voltage drop is;

$$\begin{aligned}
\Delta V_{T_1} &= I_1 Z_{T_1} = \left(\frac{S_1}{V}\right) Z_{T_1} = \left(\frac{P_1}{V}\right) Z_{T_1} \\
\Delta V_{T_2} &= I_2 Z_{T_2} = \left(\frac{S_2}{V}\right) Z_{T_2} = \left(\frac{P_2}{V}\right) Z_{T_2} \\
\Delta V_{T_3} &= I_3 Z_{T_3} = \left(\frac{S_3}{V}\right) Z_{T_3} = \left(\frac{P_3}{V}\right) Z_{T_3}
\end{aligned} \tag{2.2}$$

Using Equation (2.2) the individual pad mount transformer's power losses become;

$$\begin{aligned}
S_{ZT_1} &= \Delta V_{T_1} I_1^* = \left(\frac{P_1 Z_{T_1}}{V_1}\right)\left(\frac{P_1}{V}\right)^* = \left(\frac{P_1}{V}\right)^2 Z_{T_1} \\
S_{ZT_2} &= \Delta V_{T_2} I_2^* = \left(\frac{P_2 Z_{T_2}}{V_2}\right)\left(\frac{P_2}{V}\right)^* = \left(\frac{P_2}{V}\right)^2 Z_{T_2} \\
S_{ZT_3} &= \Delta V_{T_3} I_3^* = \left(\frac{P_3 Z_{T_3}}{V_3}\right)\left(\frac{P_3}{V}\right)^* = \left(\frac{P_3}{V}\right)^2 Z_{T_3}
\end{aligned} \tag{2.3}$$

Thus, the total power loss becomes;

$$S_{ZT_S} = S_{ZT_1} + S_{ZT_2} + S_{ZT_3} \tag{2.4}$$

Rearranging terms and substituting values into Equation (2.4) from Equations (2.1) to (2.2).

$$\left(\frac{P_{total}}{V}\right)^2 Z_{T_S} = \left(\frac{P_1}{V}\right)^2 Z_{T_1} + \left(\frac{P_2}{V}\right)^2 Z_{T_2} + \left(\frac{P_3}{V}\right)^2 Z_{T_3} \tag{2.5}$$

$$Z_{T_S} = \frac{\sum_{m=1}^{n} P_m^2 Z_{T_m}}{\left(\sum_{m=1}^{n} P_m\right)^2} \tag{2.6}$$

Where, $Z_{T_S}$ is unit transformers equivalent impedance in a group.

**Step 3: Representation of the shunt parameters**

The shunt parameters are the total of all the shunts in the power grid when examining the transmission line equivalent circuit diagram, as seen in Figure 2.10. This is because, under typical circumstances, bus voltage is almost unity and capacitors produce reactive power that is proportionate to the voltage squared across them (Jember et al., 2024; Mesfin, 2017).

The total shunt capacity of a wind turbine can be computed using the following formula, which is based on the aforementioned assumptions:

$$B_{total} = \sum_{i=1}^{n} B_i \tag{2.7}$$

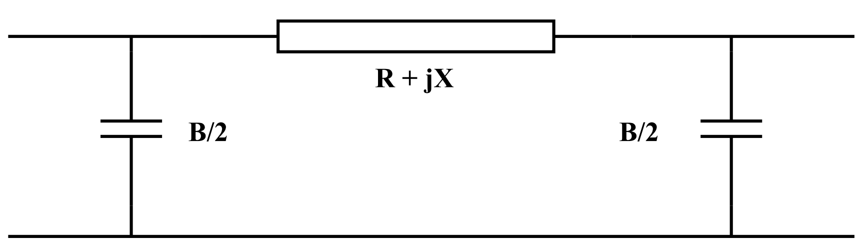


Figure 2.10: Representing the wind farm's line capacitance

**Step 4: Collector System Equivalents** Aims to replicate the large wind farm performance concerning voltage drop and power losses. The injected current from each turbine is taken to be the same, as per assumption number 1, with reference to the strand with daisy chains and its equivalent circuit shown in Figure 2.11 (taking into account that B/2 generator is considered to include the unit transformers).

Thus,

$$I_1 = I_2 = I_3 = I_4 = I$$

Then, within the representation of equivalency, the total current is provided by

$$I_S = N_t \times I$$

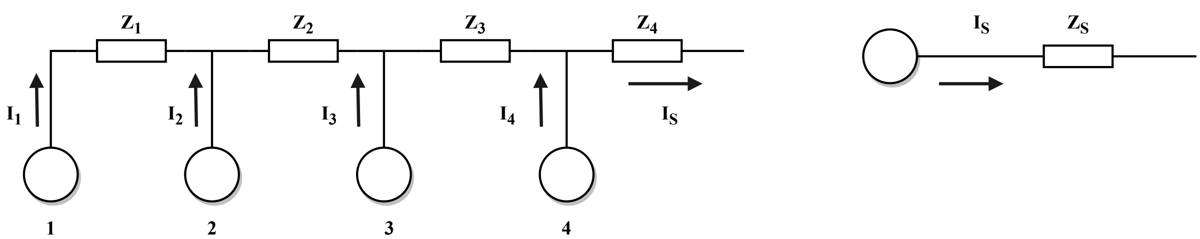


Figure 2.11: A Daisy-chained string of wind turbines connected to an equivalent circuit.

Each impedance voltage drop can be readily determined from Figure 2.11

$$\begin{aligned}
\Delta V_{Z_1} &= I_1 Z_1 = \left(\frac{S_1}{V}\right) Z_1 = \left(\frac{P_1}{V}\right) Z_1 \\
\Delta V_{Z_2} &= (I_1 + I_2) Z_2 = \left(\frac{S_1}{V} + \frac{S_2}{V}\right) Z_2 = \left(\frac{P_1}{V} + \frac{P_2}{V}\right) Z_2 \\
\Delta V_{Z_3} &= (I_1 + I_2 + I_3) Z_3 = \left(\frac{S_1}{V} + \frac{S_2}{V} + \frac{S_3}{V}\right) Z_3 = \left(\frac{P_1}{V} + \frac{P_2}{V} + \frac{P_3}{V}\right) Z_3 \\
\Delta V_{Z_4} &= (I_1 + I_2 + I_3 + I_4) Z_4 = \left(\frac{S_1}{V} + \frac{S_2}{V} + \frac{S_3}{V} + \frac{S_4}{V}\right) Z_4 \\
&= \left(\frac{P_1}{V} + \frac{P_2}{V} + \frac{P_3}{V} + \frac{P_4}{V}\right) Z_4
\end{aligned} \tag{2.8}$$

The line segment's apparent power loss can then be computed as follows:

$$
\begin{aligned}
S_{Z_1 loss} &= \Delta V_{Z_1} I^* = \left(\frac{P_1}{V}\right)\left(\frac{P_1}{V}\right) Z_1 = \left(\frac{P_{Z_1}}{V}\right)^2 Z_1 \\
S_{Z_2 loss} &= \Delta V_{Z_2} I^* = \left(\frac{P_1}{V}+\frac{P_2}{V}\right)\left(\frac{P_1}{V}+\frac{P_2}{V}\right) Z_2 = \left(\frac{P_{Z_2}}{V}\right)^2 Z_2 \\
S_{Z_3 loss} &= \Delta V_{Z_3} I^* = \left(\frac{P_1}{V}+\frac{P_2}{V}+\frac{P_3}{V}\right)\left(\frac{P_1}{V}+\frac{P_2}{V}+\frac{P_3}{V}\right) Z_3 = \left(\frac{P_{Z_3}}{V}\right)^2 Z_3 \\
S_{Z_4 loss} &= \Delta V_{Z_4} I^* = \left(\frac{P_1}{V}+\frac{P_2}{V}+\frac{P_3}{V}+\frac{P_4}{V}\right)\left(\frac{P_1}{V}+\frac{P_2}{V}+\frac{P_3}{V}+\frac{P_4}{V}\right) Z_4 = \left(\frac{P_{Z_4}}{V}\right)^2 Z_4
\end{aligned}
\tag{2.9}
$$

Hence, the overall loss is:

$$
S_{total\ loss} = \left(\frac{P_{Z_1}}{V}\right)^2 Z_1 + \left(\frac{P_{Z_2}}{V}\right)^2 Z_2 + \left(\frac{P_{Z_3}}{V}\right)^2 Z_3 + \left(\frac{P_{Z_4}}{V}\right)^2 Z_4 \tag{2.10}
$$

$$
\left(\frac{P_{Z_4}}{V}\right)^2 Z_S = \left(\frac{P_{Z_1}}{V}\right)^2 Z_1 + \left(\frac{P_{Z_2}}{V}\right)^2 Z_2 + \left(\frac{P_{Z_3}}{V}\right)^2 Z_3 + \left(\frac{P_{Z_4}}{V}\right)^2 Z_4 \tag{2.11}
$$

Therefore, the general formula for the collector circuit impedance can be obtained from Equation (2.11) by rearranging the terms.

$$
Z_S = \frac{\sum_{m=1}^{n} (P_{Z_m})^2 Z_m}{\left(\sum_{m=1}^{n} P_{Z_m}\right)^2} \tag{2.12}
$$

Where, $Z_S$ denotes the impedance of equivalent collector, while $Z_m$ represents each series impedance.

## 2.6 Techniques for Time Domain Simulation

Dynamic simulations are essential for evaluating how electric power systems react to large-scale disruptions, offering essential insights for planning, designing, operating, and ensuring the security of power networks. These simulations, commonly performed in the Time Domain Simulation (TDS), involve resolving a substantial number of stiff, hybrid, nonlinear Differential-Algebraic Equations (DAEs). These equations capture the system's interactions, control strategies, and physical dynamics. A whole transmission network consists of hundreds of thousands of these equations across different time intervals that are subject to discrete transitions forced by limiters, switching devices, and other factors. Consequently, dynamic simulations pose computational challenges, are resource-intensive, and can strain computer capabilities. In this research, the TDS tool in MATLAB® PSAT is employed, applying two integration methods—Trapezoidal rule and forward Euler. The Jacobian matrices of the system are used in these methods to evaluate the algebraic and state variable directions at each dynamic phase.

PSAT fully supports disturbances, including faults and breaker operations. Function models deal with perturbations in transient stability analysis. A time vector is constructed during the TDS period in order to perform transient stability analysis both prior to and following fault events. The network modifies its shunt admittances and recomputes the admittance matrix in response to faults or fault clearances. Responses are computed by TDS and shown on PSAT's main graphical user interface. They are compared using the PSAT TDS tool to study their responses to power oscillation before and after the FACTS device STATCOM model is included into the system in this study.

## 2.7 Literature Review on Previous Works

The concept of FACTS was initially introduced by (Hingorani & Gyugyi, 2000), denoting with electronic basis devices ability of controlling both reactive and active power flow in the power grid. FACTS controllers, being power electronic devices, improve power system performance by virtue of their injection modes and control characteristics (Sutter1 & Muriithi3, 2015). FACTS devices integration into power system stability has been a continuously intriguing research area, as explored by (Nkan et al., 2021; Biswas et al., 2021).

In the work by (Rajderkar & Chandrakar, 2023), a design and implementation were undertaken to coordinate a hybrid energy storage and fuzzy based UPFC. This coordination aimed to augment dynamic performance of the system under abnormal conditions and enhance performance. When the voltage at the DC link is not enough to meet voltage needed by the converter, hybrid energy storage can be used during transients. In their investigation (Rani, 2020), Using SVC, STATCOM, UPFC, and TCSC, to improve power system transient stability in a two-area was investigated. At matching buses to control voltage and power flow, a PI controller method for UPFC was utilized, and its effectiveness was examined using MATLAB/Simulink for the IEEE-9 bus bench mark network (Patil et al., 2023).

Another study by (Ramlochun et al., 2021) designed a wind turbine (WT) using a model of SCIG and DFIG. These generators were used in the IEEE 9-Bus test system to assess transient stability using a PSS and a DC1A excitation mechanism applied to synchronous machines. Additionally, (Sharma et al., 2022) presented an approach to enhance voltage stability by minimizing voltage deviation within the IEEE-14 bus test network, utilizing simplified voltage stability indices for STATCOM and SVC.

Another study conducted by (Hong & Nguyen, 2018) investigated the effectiveness of STATCOM in enhancing power system stability with a rapid penetration of renewable energy sources. The study employed a simulation of a power grid with significant green energy penetration and analyzed the system's performance under various scenarios. The results demonstrated that the use of STATCOM improved system stability, reduced power losses, and enhanced power quality.

A Gravitational Search Algorithm (GSA)-based optimization technique was utilized by (Kumar, 2019) to determine the optimum location for FACTS controller within IEEE 30-bus test systems. The study assessed power transfer capacity of FACTS devices on individual generators, considering both power system's reactive and active loading. In a two-area system, (Hemeida et al., 2020) investigated whether TCSC within auxiliary control could improve voltage profile of the grid and performance of overall network. The suggested technique for improving voltage profile and performance of network were shown by the simulation results.

In the work by (Oukennou et al., 2018), voltage profile is enhanced through the use of a PI controller. Another study by (Mathur & Varma, 2002) identifies optimal locations for placing STATCOM to improve the voltage profile. The utilization of SVC for enhancing the voltage profile is discussed in (Hingorani & Gyugyi, 2000). Another highly adaptable and effective FACTS devices, UPFC, has potential to improve power system stability and provide superior power flow. In order to facilitate utilizing of the maximum power transmission capacity and control natural power-sharing between two separate parallel transmission lines, TCSC (Siddula et al., 2020; Mahapatra & Jha, 2014), as well as UPFC, are put in place inside the power system.

## 2.8 Research Gaps

Despite advancements in transient stability enhancement of a power system using FACTS device based on Optimization techniques, several critical gaps remain. Optimization methods for the precise placement and sizing of devices like STATCOM have not been employed, missing opportunities for enhanced efficiency and performance. The integration of UPQC and fuzzy controllers to shorten settling time and mitigate power fluctuations has been overlooked, and the robustness of optimization techniques across various grid configurations remains underexplored. Additionally, the complexities of modern power systems and the integration of renewable energy with advanced control techniques have not been adequately addressed. To fill these gaps, Particle Swarm Optimization (PSO) for the optimal placement and sizing of STATCOM devices proposed to enhance transient stability and reduce power losses.

## 2.9 Summary

Most of the related works in this research study use different Meta-Heuristic optimization techniques to address problems in transmission lines, by controlling voltage, current, power flow, power quality, transient and dynamic, reactive power, loss reduction. However, these reviews often overlook the optimum sizing and placement of FACTS devices that are in series and shunt, which contribute to congestion, line losses, voltage fluctuations, and operating costs in transmission lines. These limitations encourage this study to use shunt FACTS devices, utilizing STATCOM with PSO to choose the optimum location and size for STATCOM within the dynamic modified 30-Bus IEEE Standard Test Transmission Network. It was found that STATCOM has some advantages in terms of reactive power injection, response time, and implementation cost, as mentioned earlier. Therefore, STATCOM is the main FACTS device used in this research work and has been extensively discussed and thoroughly reviewed. In addition, most available articles did not find application of particle swarm optimization for optimizing STATCOM devices to reduce power dissipation and minimize bus voltage profile deviation, hence this work. Achieving the above objectives by implementing an optimally placed STATCOM device using independent optimization algorithms involving PSO formed the starting point for the conclusions drawn from the review of literature in this chapter.

# CHAPTER THREE

# 3 MATERIALS AND METHODS

## 3.1 Methodology

Methodology of this study begins with problem identification and an extensive review of relevant literature, including books, articles, and web pages. The primary issue addressed is the occurrence of blackouts, sudden load changes, oscillations, loss of synchronism, and system faults in the power grid of Ethiopia, resulting in frequent power system breakdowns and momentary instability. The need to automate power system transient stability control through the integration of FACTS device STATCOM serves as the driving force behind this research. The aim is to enhance transient stability by determining optimal locations, sizes, and compensation properties of these FACTS device. The combined interconnection of a dynamic IEEE 30-bus modified system and wind farm Adama II is the main subject of the study, chosen for their multi-machine network characteristics that can be generalized to other networks. The investigation begins with a literature survey on transient stability enhancement in power systems, gathering insights to address the identified problems. MATLAB/PSAT is utilized for analysis and control power system. Power flow analysis, optimal power flow, continuation power flow, small signal stability analysis, and time domain simulation are among the features that PSAT provides. Graphical user interfaces (GUI) and a Simulink−based library make the operations easier to use and offer a convenient tool for network design. The TDS tool in the MATLAB®/ PSAT is utilized to perform dynamic transient stability improvement simulations. Simulations are conducted with and without FACTS devices. Flow chart of the methods are shown in Figure 3.1 for accomplishment of this thesis. PSAT is selected due to its robustness and TDS tool's ability to efficiently examine different transient stability parameters.

## 3.2 Case Study Test System Selections

The wind farm's high-voltage terminal side of Adama II, equipped with 230 kV overhead transmission lines, is connected to the Koka substation, an integral part of the Ethiopian National

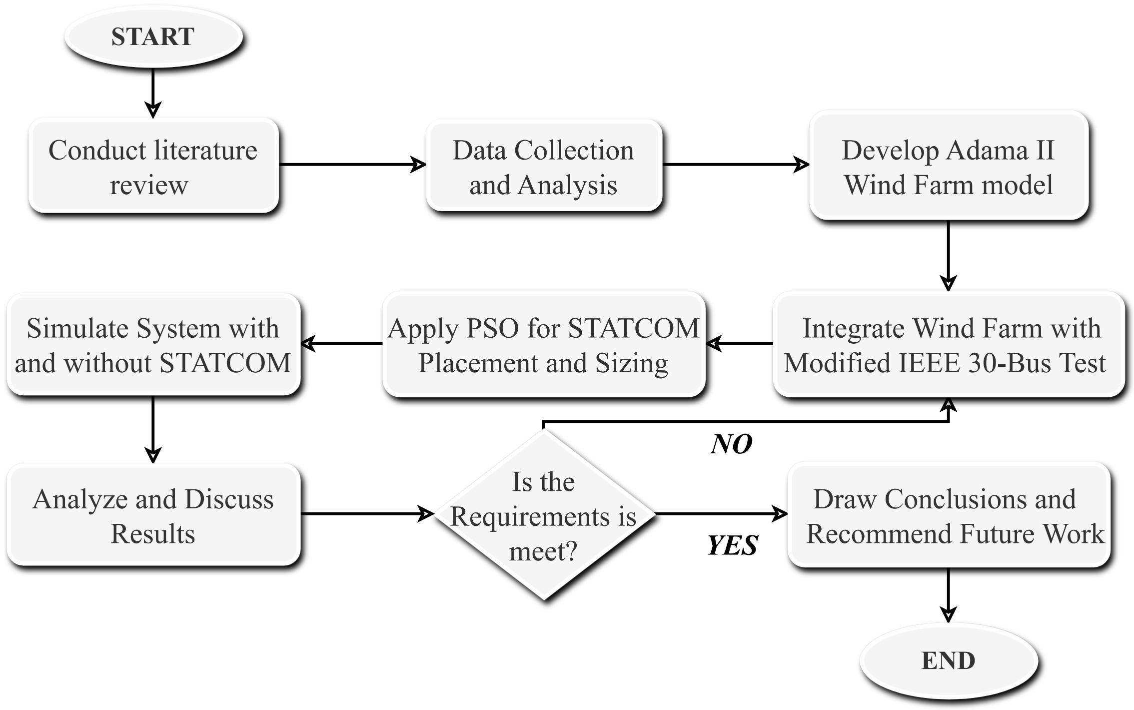


Figure 3.1: Flow chart of the methods

Grid. The Koka substation further links to the eastern and central parts of the Ethiopian National Grid's transmission line system. However, due to the challenges associated with collecting detailed parameters and specifications for various generation stations and substations (such as Koka, Melka Wakena, and Awash II and III power plants), a comprehensive modeling representation of the entire Ethiopian transmission network in the MATLAB® PSAT software toolbox version is unavailable. This limitation is attributed to cost, time constraints, and the unavailability of certain data.

The combined interconnection of dynamic IEEE 30-bus modified system within wind farm Adama II is used for this study in order to address these gaps. The IEEE 30-bus modified bench mark system serves as a multiple-machine network that can be considered as a representative basis and can be generalized to the broader Ethiopian transmission network and other networks. In this configuration, the wind farm is integrated into large load of the IEEE 30-bus modified system, comprising 30 buses, 6 synchronous machines, synchronous generator at bus 1 and 2, as well as reactive power support synchronous capacitors at buses 5, 8, 11, and 13, 21 loads, 2 shunt capacitors, 7 tap-changing transformers and 41 transmission lines. Bus number 03 in this system has a substantial load compared to other bus numbers.

The wind farm itself is made up of 102 turbines arranged into eight clusters, one with eleven turbines and the other seven with thirteen turbines, all grouped together. Depending on each unit's location and distance from the 33 kV collector bus, several overhead and underground cables with different capacities and lengths are used for the connectivity. Out of the six generators in the system, two generators supply active power, while the remaining four, operating as synchronous compensators, are solely utilized for reactive power generation. Generator 1 acts as the slack generator, and each generator's AVR controls the voltages. As per the IEEE model-I standard, the machine has a Type-II AVR. The AVRs are essential in reducing electro-mechanical oscillations and improve transient stability.

## 3.3 Data Collection

The data necessary for this thesis encompasses all parameters of power system IEEE-30 modified bench mark system, generator, transmission line, transformer, and wind farm Adama II. Appendices A.2 to A.9 give comprehensive data for IEEE-30 bus modified bench mark system connected with wind farm Adama II used for this study. The topological scheme of this system is illustrated in Figure 3.4. All necessary data for the thesis study have been collected. The static data of wind farm Adama II connected with IEEE-30 bus modified bench mark system is outlined in Appendices A.2 and A.3, while the dynamic data is presented in Appendices A.5 to A.9. The common data for the wind farm Adama II integrated into IEEE-30 bus modified test system includes:

a. Base Power: 100 MVA.

b. Base Frequency: 50 Hz.

c. Base Voltages: 132 kV for buses 1-8 and 28, 33 kV for buses 10, 12, 14-27 and 29-30, 11 kV for bus 11 and 13, and 1 KV for bus 9.

Device nominal ratings match system base unless otherwise noted. Parameters concerning device nominal ratings are expressed in terms of per unit $P.U$.

## 3.4 Data Analysis

Depending on the collected data, study characteristics of IEEE 30 bus modified bench mark system interlinked into wind farm Adama II power system is carried out. The system's characteristics are analyzed and interpreted according to international standards under different circumstances. Drawing from existing literature, potential causes of transient stability issues are identified, and suggestions for improving these problems are implemented. The power grid studied in this thesis serves as a basis study in combination, involving the interconnection of a large wind farm with IEEE 30-bus modified bench mark system and examine utilization of FACTS device STATCOM to mitigate system stability issues. The test system has a total reactive load of 100.95 MVAr and a total real load of 283.4 MW. The base MVA of IEEE-30 bus test network is 100 MVA in all configurations. In the test system, total real and reactive power generation is 300.1 MW and 133.93 MVAr, respectively. The losses in the test system are calculated to be 17.56 MW and 32.98 MVAr. Bus 1 acts as the reference angle and slack bus for power flow analysis. Voltage security limitations of $V_{max} = 1.20$ P.u. and $V_{min} = 0.8$ P.u. are implemented in optimal power flow analysis. The collected data from original and secondary sources are manipulated and converted to MATLAB/PSAT compatible formats for further analysis.

## 3.5 Adama II Wind Farm Model

Adama II wind farm is located in the central of our country, approximately 90 km far from capital city, Addis Ababa, to the east and 3 km far from Adama city to the north west, with an elevation ranging from 1741 to 2173 meters. The wind park is centrally positioned at $8°34'18''N, 39°12'10''E$, experiencing wind speed on average in the range of 8 to 9 m/s. The wind farm employs DFIG type. The total installed capacity of the wind farm power is 153 MW with each turbines producing 1.5 MW power each, with each of the 102 wind turbines generating 690V as the rated voltage. Each wind turbine is connected to unit transformer in order to increase the voltage (690V) at the generator's terminal to a medium voltage level of 33 kV. These 102 turbines are organized into eight (8) clusters denoted as clusters A to H, with one cluster comprising eleven (11) turbines and the remaining seven (7) clusters having thirteen (13) turbines each. They are arranged in groups, and each cluster is linked to the main substation by a 33 kV overhead line. The interconnection involves 33kV overhead transmission lines and underground cables with varying lengths and capacities based on unit locations and distances to collector bus of 33 kV. The 102 wind turbines are aggregated into a single representation using aggregation process, creating a wind power plant, which is then verified using load flow analysis. The two transformers in the main substation have a voltage level of 33/230 kV and a capacity of 90 MVA each. The structure of wind farm Adama II is represented in Figure 3.2. The Koka substation is connected to the high−voltage terminal side of the wind farm by a single 230 kV overhead transmission line. The wind power plant has interconnected with a compatible IEEE 30−bus modified system, allowing its 102 wind turbines to be represented as a single turbine.

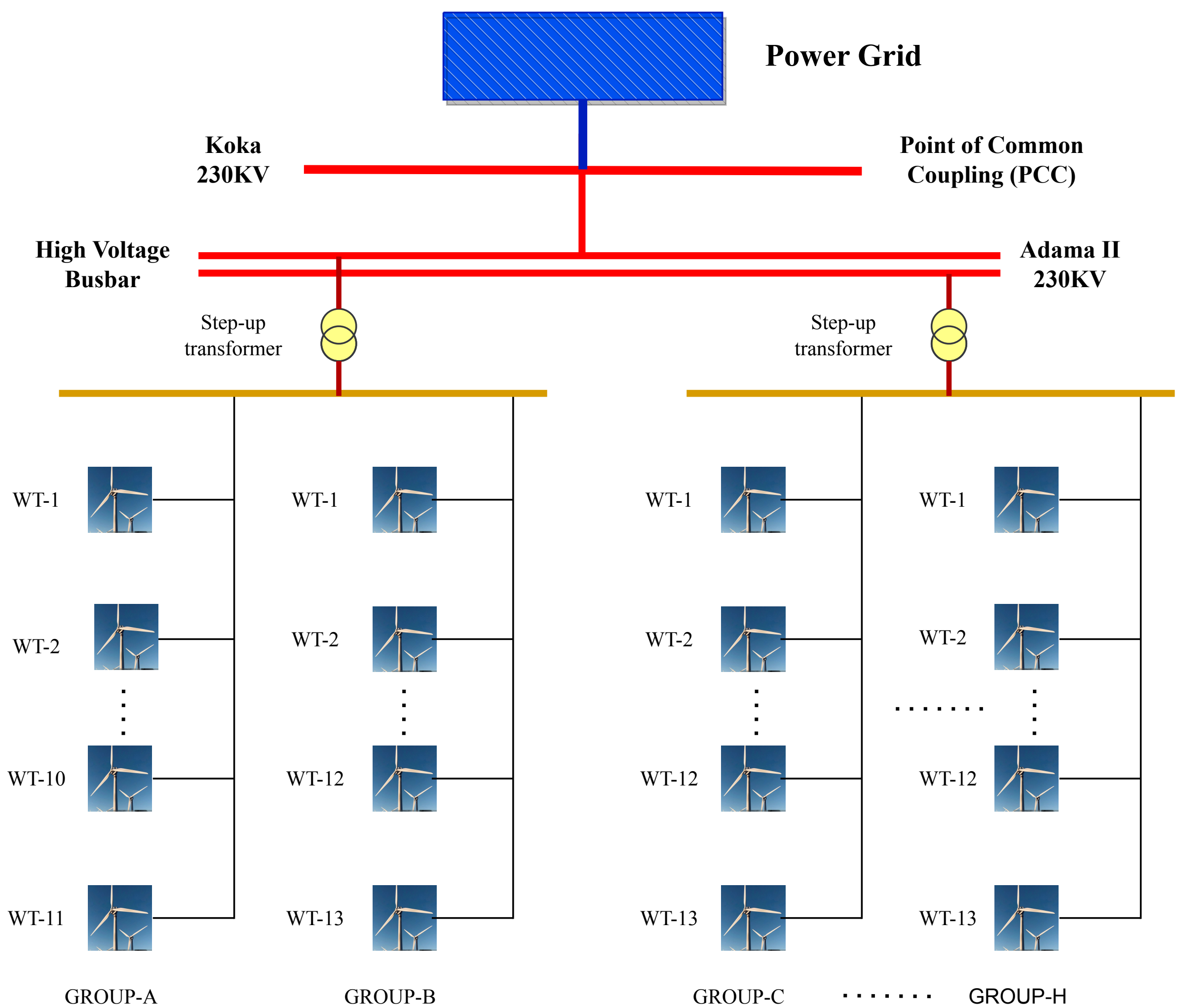


Figure 3.2: The structure of the Adama II wind farm

Table 3.1: Data input for power flow modeling of wind farm Adama II (Source: Adama II WF)

| Parameter or symbol | Values with Unit |
|---|---|
| **A. Generator data for a wind turbine** | |
| Apparent power ($S_t$) | 1.60 MVA |
| Maxi (Min) reactive power ($Q_{max}(Q_{min})$) | 0.90 (-0.80) MVAr |
| Source impedance ($Z_{source}$) | 0.00 + j 0.80 p.u. |
| Maxi (Min) active power ($P_{max}(P_{min})$) | 1.50(0.00) MW |
| Base apparent power (M base) | 1.60 MVA |
| **B. Transformer data for a Wind turbine** | |
| Apparent power ($S_t$) | 1.60 MVA |
| Transformer voltage ratio ($Unp/Uns$) | 0.690/33.0 KV/KV |
| Transformer impedance ($Z_{tr}$) | 0.00120 + j 0.00570 p.u. |
| Base apparent power (M base) | 1.60 MVA |
| **C. Transformer data for a substation** | |
| Apparent power ($S_t$) | 90.0 MVA |
| Transformer voltage ratio ($Unp/Uns$) | 33.0/230.0 KV/KV |
| Transformer impedance ($Z_{tr}$) | 0.003610+j0.12995 p.u. |
| Transformer admittance ($Y_{tr}$) | 0.00050 - j 0.001490 p.u. |
| Base apparent power (M base) | 100MVA |

The following are the useful steps for aggregating wind farm Adama II:

**Step 1: Wind Turbine Equivalent**

The large wind farm Adama II consists 102 DFIGs, with each unit supplying active power of 1.5 MW. Consequently, as per Equation (2.1):

$$P_{\text{eq\underline{n}}} = 102 \times 1.5MW = 153MW$$

**Step 2: Pad Mount Transformer Equivalent**

The mathematical expressions for resistance and reactance component in single transformers can be expressed as:

$$Z_{TS} = R_{TS} + X_{TS}$$

Where,

$$R_{TS} = \frac{\Delta V_r \times V_1^2}{100 S_{tr}} \tag{3.1}$$

$$X_{TS} = \frac{\Delta V_q \times V_1^2}{100 S_{tr}} \tag{3.2}$$

Where, $\Delta V_r$: Rated voltage drop at resistance (%)=1.3%.

$\Delta V_q$: Rated voltage drop at reactance (%)=$\sqrt{Z_{sc}^2 - \Delta V_r^2}$.

$V_1$: Primary voltage of the transformer (0.69 KV).

$S_{tr}$: Apparent power of the transformer (1.6 MVA).

$Z_{sc}^2$: Transformer short circuit impedance (%)=6.5%

Thus,

$$\Delta V_q = \sqrt{Z_{sc}^2 - \Delta V_r^2} = \sqrt{6.5^2 - 1.3^2} = 6.37\%$$

Therefore, substituting the values into Equation (3.1) and (3.2):

$$R_{T_S} = 0.003870\Omega$$

$$X_{T_S} = 0.01870\Omega$$

$$Z_{T_S1} = 0.003870 + j0.01870\Omega$$

**Group one (1) of Cluster A's Unit Transformer Modeling**

The micro setup of the wind farm illustrates how the four unit transformers in Group A of Cluster A are connected in parallel. Therefore, by applying Equation (2.6), we obtain:

$$Z_{T_S}^1 = \frac{P_1^2 Z_{T_S1} + P_2^2 Z_{T_S2} + P_3^2 Z_{T_S3} + P_4^2 Z_{T_S4}}{(P_1 + P_2 + P_3 + P_4)^2}$$

Where, $P_1$, $P_2$, $P_3$, and $P_4$ represent the rated output power for each individual wind turbine, and $Z_{T_S1} = Z_{T_S2} = Z_{T_S3} = Z_{T_S4}$ is the leakage reactance of a transformer. Therefore, the equation will be simplified to

$$Z_{T_S}^1 = \frac{Z_{T_S1}}{4}$$

This mean that,

$$Z_{T_S}^1 = \frac{Z_{T_S1}}{N_t} \tag{3.3}$$

Where $N_t$ represents the total turbines number in a group. Given that group (1) comprises (4) wind turbines, we can substitute the value of the transformer leakage reactance into the Equation (3.3).

$$Z_{T_S}^1 = \frac{(0.003870 + j0.01870)}{4}\Omega = 0.0009680 + j0.004680\Omega$$

In per units,

$$Z_{T_S}^1 = \frac{1.6}{(0.69)^2}(0.000968 + j0.00468) = 0.00325 + j0.0157 p.u$$

**Group two (2) of Cluster A's Unit Transformer Modeling**

Cluster A's Group 2 is consists of seven parallel-operating unit transformers. Similarly, Equation (3.3) can be used to determine the equivalent impedance.

$$Z_{T_S}^2 = \frac{(0.003870 + j0.01870)}{7} = 0.00055290 + j0.002670\Omega$$

In per units,

$$Z_{T_S}^2 = \frac{1.6}{(0.69)^2}(0.0005529 + j0.00267) = 0.001858 + j0.008978 p.u$$

Accordingly, using Equation (2.6), the resulting equivalent impedance of the pad-mounted transformer in Cluster A, represented as $Z_{T_SA}$, calculated as follows:

$$Z_{T_S}A = \frac{\sum_{m=1}^{n} P_{gm}^2 Z_{T_S}^m}{\left(\sum_{m=1}^{n} P_m^2\right)}$$

Where, $n$ represents the number of groups in Cluster A.

$$Z_{T_S}A = \frac{P_{g1}^2 Z_{T_S}^1 + P_{g2}^2 Z_{T_S}^2}{(P_1 + P_2)^2}$$

Where, $P_{g1}^2$ and $P_{g2}^2$ indicate the total amount of power that was transferred to Groups 1 and 2, accordingly.

$$P_{g1}^2 = P_1^2 + P_2^2 + P_3^2 + P_4^2$$

$$P_{g2}^2 = P_5^2 + P_6^2 + P_7^2 + P_8^2 + P_9^2 + P_{10}^2 + P_{11}^2$$

But, $P_1 = P_2 = \cdots = P_{11} = 1.5MW$

Therefore,

$$P_{g1}^2 = (4 \times 1.5)^2 = (6)^2 MW$$

$$P_{g2}^2 = (7 \times 1.5)^2 = (10.5)^2 MW$$

$$Z_{T_S}A = \frac{(6)^2(0.003250 + j0.01570) + (10.50)^2(0.0018580 + j0.0089780)}{(6.0 + 10.50)^2}$$

$$Z_{T_S}A = 0.0011820 + j0.0057120 p.u$$

**Step 3: Shunt Impedance Equivalent**

The equivalence shunt admittance is determined by applying Equation (2.7).

1. Shunt admittance of Group 1 in Cluster A

$$B_{g1} = 4 \times 8.84 \mu s = 35.36 \mu s$$

2. Shunt admittance of Group 2 in Cluster A

$$B_{g2} = 7 \times 8.84 \mu s = 61.88 \mu s$$

$$B_{total} = \sum_{i=1}^{n} B_i$$

**Step 4: Collector Circuit Equivalent**

**Modeling of Group (1) Collector Circuit**

Group (1) consists (4) wind turbines; therefore, equivalency can be computed by utilizing Equation (2.12).

$$Z_S = \frac{\sum_{m=1}^{n} (P_{Z_m})^2 Z_m}{\left(\sum_{m=1}^{n} P_{Z_m}\right)^2}$$

$$ZC_{g1} = \frac{P_1^2 Z_1 + P_2^2 Z_2 + P_3^2 Z_3 + P_4^2 Z_4}{(P_1 + P_2 + P_3 + P_4)^2}$$

The impedance of the branch between wind turbines $WT_{G14} - WT_{G15}$, $WT_{G15} - WT_{G16}$, $WT_{G16} - WT_{G17}$, and $WT_{G17} - WT_{GCCG1}$ is represented by $Z_1$, $Z_2$, $Z_3$, and $Z_4$, respectively, as shown in the micro$-$siting of the wind farm. The branch flows are shown by $P_1$, $P_2$, $P_3$, and $P_4$. Equivalency can then be computed by changing the branch impedance and power flow quantities.

$$Re(ZC_{g1}) = \frac{1.5^2R_1 + 3^2R_2 + 4.5^2R_3 + 6^2R_4}{(1.5+3+4.5+6)^2}$$
$$Re(ZC_{g1}) = \frac{1.5^2 \times 0.01 + 3^2 \times 0.0082 + 4.5^2 \times 0.009 + 6^2 \times 0.006}{(1.5+3+4+6)^2}$$
$$Re(ZC_{g1}) = 0.04191 p.u$$

$$Im(ZC_{g1}) = \frac{1.5^2X_1 + 3^2X_2 + 4.5^2X_3 + 6^2X_4}{(1.5+3+4.5+6)^2}$$
$$Im(ZC_{g1}) = \frac{1.5^2 \times 0.0067 + 3^2 \times 0.0051 + 4.5^2 \times 0.055 + 6^2 \times 0.003}{(1.5+3+4+6)^2}$$
$$Im(ZC_{g1}) = 0.005701 p.u$$

Thus,

$$ZC_{g1} = 0.041910 + j0.005701 p.u$$

**Modeling of Group (2) Collector Circuit**

Group (2) consists (7) wind turbines, hence we can compute the equivalency using Equation (2.12).

$$ZC_{g2} = \frac{P_1^2Z_5 + P_2^2Z_6 + P_3^2Z_7 + P_4^2Z_8 + P_5^2Z_9 + P_6^2Z_{10} + P_7^2Z_{11}}{(P_1+P_2+P_3+P_4+P_5+P_6+P_7)^2}$$

As shown in the micro−siting of the wind farm, the impedance of the branch between wind turbines $WT_{G18}$-$WT_{GCCG}$, $WT_{G18}$-$WT_{G19}$, $WT_{G19}$-$WT_{G20}$, $WT_{G21}$-$WT_{G22}$, $WT_{G22}$-$WT_{G23}$, and $WT_{G23}$-$WT_{G24}$, respectively, are represented by $Z_5$, $Z_6$, $Z_7$, $Z_8$, $Z_9$, and $Z_{11}$. The branch flows are represented by $P_1$, $P_2$, $P_3$, $P_4$, $P_5$, $P_6$ and $P_7$. Equivalency can then be computed by replacing the given branch impedance and power flow quantities.

$$Re(ZC_{g2}) = \frac{1.5^2R_5 + 3^2R_6 + 4.5^2R_7 + 6^2R_8 + 7.5^2R_9 + 9^2R_{10} + 10.5^2R_{11}}{(1.5+3+4.5+6+7.5+9+10.5)^2}$$
$$Re(ZC_{g2}) = \frac{1.5^2 \times 0.015 + (3^2+6^2) \times 0.008 + (4.5^2+9^2+10.5^2) \times 0.007 + 7.5^2 \times 0.0018}{(1.5+3+4+6+7.5+9+10.5)^2}$$
$$Re(ZC_{g2}) = 0.00163 p.u$$

$$Im(ZC_{g2}) = \frac{1.5^2X_5 + 3^2X_6 + 4.5^2X_7 + 6^2X_8 + 7.5^2X_9 + 9^2X_{10} + 10.5^2X_{11}}{(1.5+3+4.5+6+7.5+9+10.5)^2}$$

$$Im(ZC_{g2}) = \frac{1.5^2 \times 0.007 + 3^2 \times 0.028 + (4.5^2 + 6^2 + 7.5^2 + 9^2 + 10.5^2) \times 0.005}{(1.5+3+4+6+7.5+9+10.5)^2}$$

$$Im(ZC_{g2}) = 0.001087p.u$$

Thus,

$$ZC_{g2} = 0.001630 + j0.001080p.u$$

The impedance of Groups One and Two must be reduced in order to depict the cluster using a single turbine setup. Consequently, the Cluster A collector circuit can be made simpler as follows:

$$Z_{CA} = \frac{P_{g1}^2 ZC_{g1} + P_{g2}^2 ZC_{g2}}{(P_{g1} + P_{g2})^2}$$

$$Z_{CA} = \frac{6^2(0.04191 + j0.005701) + 10.5^2(0.00163 + j0.00108)}{(6+10.5)^2}$$

$$Z_{CA} = 0.0062 + j0.00119p.u$$

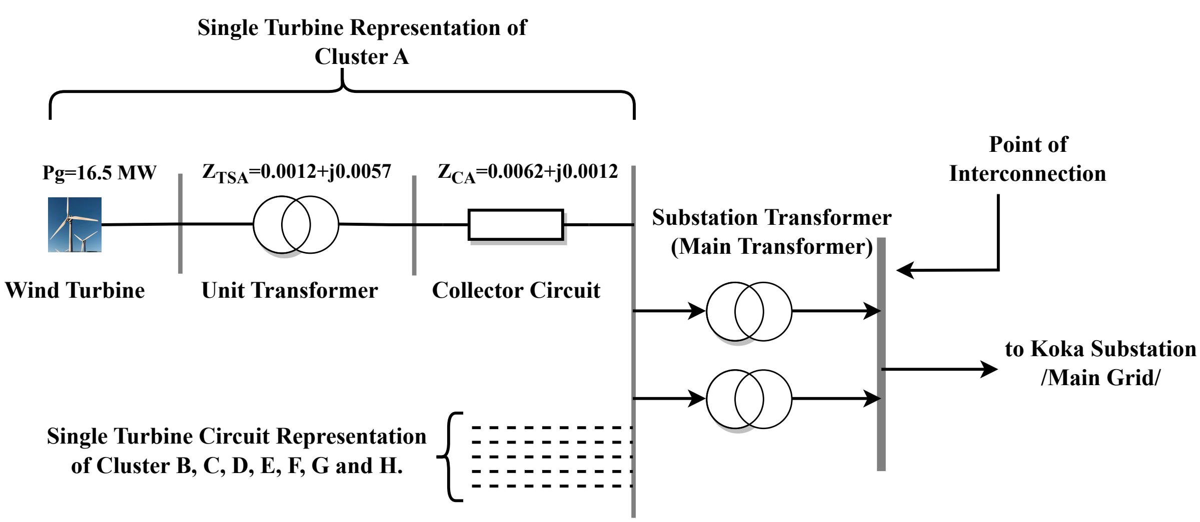


Figure 3.3: Cluster A represented with a single turbine in the Adama II WPP

The equivalent unit transformer and collector circuit impedances for the remaining clusters, which are modeled using a single turbine system, have been displayed in Tables 3.2 and 3.3.

Table 3.2: An overview of the unit transformer's equivalent impedance for each cluster

| Cluster | $N\underline{O}$. of Transformer | Total Power (MW) | Equivalent Transformer Impedance of each cluster | |
|---|---|---|---|---|
| | | | $R_{eq}$ (pu) | $X_{eq}$ (pu) |
| A | Eleven (11) | 16.50 | 0.00120 | 0.00570 |
| B | Thirteen (13) | 19.50 | 0.0010 | 0.00480 |
| C | Thirteen (13) | 19.50 | 0.0010 | 0.00480 |
| D | Thirteen (13) | 19.50 | 0.0010 | 0.00480 |
| E | Thirteen (13) | 19.50 | 0.0010 | 0.00480 |
| F | Thirteen (13) | 19.50 | 0.0010 | 0.00480 |
| G | Thirteen (13) | 19.50 | 0.0010 | 0.00480 |
| H | Thirteen (13) | 19.50 | 0.0010 | 0.00480 |

In general, the STR parameters for the Adama II wind farm were established based on a base voltage of $V_B = 33$ kV and apparent power at base of $S_B = 100$ MVA. consequently, the equivalent impedance of the unit transformer was computed using Equation (2.12), by inserting values sourced from Table 3.2.

$$Z_{T_S} = 0.0001270 + j0.00061560 p.u$$

Table 3.3: An overview of each cluster's equivalent impedances across all collector circuits

| Cluster | Length (km) | Total Power (MW) | Impedance of Collector | |
|---|---|---|---|---|
| | | | $R_{eq}$ (pu) | $X_{eq}$ (pu) |
| A | 1.40 | 16.50 | 0.00620 | 0.00120 |
| B | 3.570 | 19.50 | 0.10690 | 0.01450 |
| C | 0.150 | 19.50 | 0.00450 | 0.00060 |
| D | 5.0 | 19.50 | 0.14980 | 0.02040 |
| E | 5.610 | 19.50 | 0.16810 | 0.02280 |
| F | 5.0 | 19.50 | 0.14980 | 0.02040 |
| G | 5.450 | 19.50 | 0.16330 | 0.02220 |
| H | 5.0 | 19.50 | 0.14980 | 0.02040 |

Then, the equivalent impedance of the collector circuit has been computed by substituting the values from Table 3.3 into Equation (2.12).

$$Z_{CC} = 0.000748 + j0.000125 p.u$$

### 3.5.1 An integrated model of wind farm Adama II with IEEE 30 bus modified test systems

This thesis work includes a case study of Adama II wind farm, which has representation of single turbine made up of 102 wind turbines and is incorporated into IEEE 30-bus modified system. The analysis is focuses on enhance transient stability, improve voltage profile, and reduce loss. Dynamic TDS has been utilized to validate the effects of STATCOM controller in the case study. Buses 5, 8, 11, and 13's synchronous condensers, along with the generators at Buses 1 and 2, are all represented using sub-transient models with AVRs.

To induce transient instability, a fault is introduced between Bus 1 and 30. Specifically, a transient three-phase fault is introduced at Bus 08, accompanied by sudden load changes. The quantity of power flow over the network without a wind farm linked the best place to connect a wind farm, the bus with the highest voltage drop; a comparison analysis of high voltage drop revealed that bus number 30 had the highest voltage drop from Table 4.2. The interconnection of a wind farm disturbed the test system with a total reactive load of 395.36 MVAr and a total real load of 151.44 MW. The total active and reactive power generation is 432.6 MW and 258.45 MVAr, and real and reactive losses are 137.206 MW and 107.01 MVAr, respectively. In this integrated test system, the aggregated Adama II wind turbine is linked to bus number 30 of IEEE 30−bus modified system. The fault bus is selected at random since faults in the system can happen wherever. The transient instability analysis considers both the faulted buses and generation units. The single-line diagram of wind farm Adama II interconnected with IEEE 30−bus modified system is presented in Figure 3.4. This diagram shows that all generators maintaining a steady mechanical input power and steady excitation, while constant impedance are considered for loads. The IEEE-30 bus system modeled in MATLAB/PSAT with a base voltage of 132 kV and a base MVA of 100. Six state variables included in the system: rotor angle and speed, transient voltage along the d-axis and q-axis, sub-transient voltage along the d-axis and q-axis.

The test system that is being proposed incorporates two different kinds of generators: grid side synchronous generators and a representation of single turbine DFIG from wind farm Adama II. Under typical operating circumstances, synchronous generators do not operate with its full capacity to allow for system power reserve. Synchronous generators react quickly to disruptions in the system due to the presence of AVRs, while wind turbines, with their complex control systems, are more challenging to make responsive in a similar manner. Therefore, additional equipment such as FACTS devices is necessary to ensure stability during and after disturbances. While individual wind turbines have a minimal effect on the larger power system network, the collective effect of wind turbines can be significant during significant disruptions, like adjacent faults. The 102 wind turbines reduced into representation of a single equivalent in order to perform simulations.

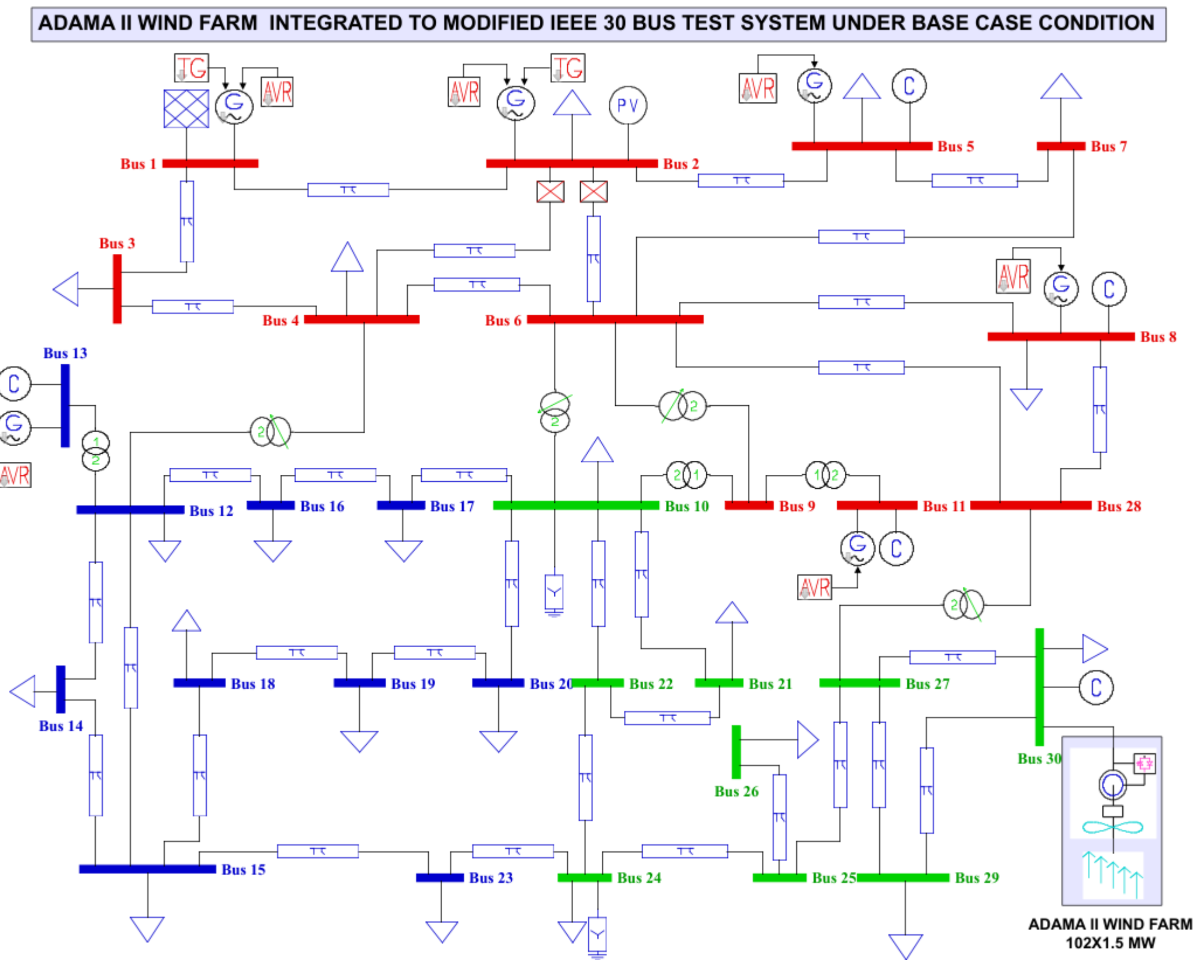


Figure 3.4: Dynamic IEEE 30-bus modified test systems with integration of wind farm Adama II in MATLAB/PSAT

## 3.6 Load Flow Analysis

Load flow studies play a crucial role in planning of power system, economic operation, expansion, and enhancement of existing systems, as well as in scheduling and power exchange among electric utilities. These studies are also essential for conducting various analyses, including stability analysis of voltage, transient, contingency and state estimation. Consequently, load flow analysis serves as fundamental computational tool for determining power system operating conditions. The key information obtained from load flow analysis includes each bus phase angle and voltage magnitude, each line reactive and active power loss, and injection of both reactive and active power at each bus. For each bus, two of the four variables—active power, reactive power, voltage magnitude, and phase angle—are given, and the remaining two are calculated. The bus kinds determine the specified quantity. The most popular techniques for load flow analysis are the Gauss-Seidel, Newton-Raphson, and Fast Decoupled Load Flow methods. The Newton-Raphson approach is especially recommended for larger systems because of its accuracy, dependability, and versatility.

## 3.7 Particle Swarm Optimization

In 1995, Drs. James Kennedy and Russell Eberhart introduced PSO, an algorithmic approach inspired by nature (Okelola et al., 2021). PSO is a population−based meta−heuristic algorithm that are modeled by natural phenomena, such as fish schools and bird flocking (Sirjani et al., 2012). PSO algorithm is utilized to solve problems with constraints and has proven to be one of the most effective meta−heuristic algorithm, especially in power systems. The utilization of PSO for allocating and sizing STATCOM will implement within dynamic IEEE 30− bus test system interlinked with wind farm Adama II. This choice was made due to the precision and quick convergence of PSO compared to other techniques. PSO is considered more effective than Genetic Algorithms (GA) and exhibits a balanced approach to improving both local and global exploration capabilities (Sadati et al., 2006; Fogel, 2006). In many cases, PSO is considered as a clear, user-friendly, and computationally effective method. PSO was first created to handle constrained nonlinear optimization issues involving both discrete variable and continuous variable. It was first intended to solve continuous nonlinear optimization problems (Eajal & El-Hawary, 2010; Liang et al., 2013). The fundamental concept of PSO algorithm is to randomly create a population, or swarm. This swarm comprises individuals called particles, with each particle representing a remedy for issue at hand. Each particle traverses a random velocity in a dimensional search space. Throughout the generations, particles adjust their positions based on own and their neighborhood experiences. The algorithm aims to balance exploitation and exploration by integrating local and global search methods, velocity update and position of each particle accordingly. As explained by (Okelola et al., 2021), PSO algorithms operate as follows:

a. The attributes of each individual particle $i$ are as follows: a current position in the search space $X_i$, an individual optimum position in the search space $Y_i$, and a current velocity $\vec{V}_i$.

b. According to the objective function $F$, assuming a minimization goal, the individual optimum position $Y_i$ denotes the place in the search space where particle $i$ shows the smallest error.

c. Among all the $Y_i$, the location with the lowest error is referred to as the global optimum position $Y$.

The PSO is defined by (Majumdar et al., 2009) with Equations (3.4) and (3.5), updating the individual (personal) and global optimum modifications expressed as follows:

$$Y_i^{t+1} = \begin{cases} Y_i^t & \text{if} \quad F(Y_i^t \leq F(X_i^{t+1})) \\ X_i^{t+1} & \text{if} \quad F(Y_i^t > F(X_i^{t+1})) \end{cases} \tag{3.4}$$

$$Y(t) = \min\{F(Y)|F(Y(t))\} \tag{3.5}$$

$$Y \in \{Y_0^t, Y_1^t, \ldots, Y_S^t\} \qquad i \in \{1, 2, \ldots, S\}$$

Equations (3.6) and (3.7) are used to modify the current velocity and the next position:

$$\vec{V}_{i,j}^{\,t+1} = \omega \times \vec{V}_{i,j}^{\,t} + C_1 \times rand_{1,j}^t [Y_{i,j}^t - X_{i,j}^t] + C_2 \times rand_{2,j}^t [Y_{i,j}^t - X_{i,j}^t] \tag{3.6}$$

$$X_i^{t+1} = X_i^t + \vec{V}_i^{\,t+1} \tag{3.7}$$

Smaller inertia weights can help with local searches, but larger inertia weights can aid with global searches. Equation (3.8) gives the inertial weight ($\omega$) that governs the PSO convergence behavior according to:

$$\omega = \omega^{\max} - \left( \frac{\omega^{\max} - \omega^{\min}}{\text{iterat}^{\max}} \right) \times \text{iterat} \tag{3.8}$$

where: iterat is the current iteration number, $\text{iterat}^{\max}$ is the maximum iteration number, $\omega^{\min}$ and $\omega^{\max}$ are the minimum and maximum values of weighting factors, respectively.

### 3.7.1 PSO Parameters

The fundamental and crucial parameters of PSO algorithm are briefly outlined and explained accordingly:

**a) Particle Velocity**

The particle velocity in the PSO algorithm plays a significant role in finding the movement of particles within the search space. The velocity is updated in each iteration based on the current velocity of the particles, its local optimum or optimum position, and global optimum or the entire swarm optimum position. Regarding the bounds, $V_{\max}$ and $V_{\min}$ are typically set based on a percentage of the variable's dynamic range on each axis. The choice of this percentage is a tuning parameter and may vary depending on the specific problem and characteristics of the optimization. A common range is 12–25% of the variable's dynamic range. This restriction helps balance exploitation and exploration phases of the algorithm, preventing particles from moving too fast or too slow in the search space.

**b) Random Numbers**

Random values in the range [0, 1] used in the PSO algorithm. These random values, denoted as $rand_1^t$ and $rand_2^t$, are crucial for introducing stochastic behavior in the algorithm. These random values introduce a level of randomness into the movement of particles, allowing for investigation of the search space. The stochastic nature helps to the algorithm from becoming trapped in one's own local best, improving its ability to find global optima in the solution space.

#### c) Weighting Coefficients

The coefficients of weighting, represented by these parameters, govern the stochastic acceleration terms in the PSO algorithm. These coefficients play a crucial role in determining the unexpected movement towards or past target regions. High values result in a more pronounced impact, while low values allow particles to cover longer distances before experiencing a pullback effect. As the iteration numbers increases, these parameters can be set within the range of 1 to 2. Typically, for their conventional values, $C_1$ and $C_2$ are set as constants equal to 2, regulating the rate of relative influence in their respective applications.

#### d) Inertia Weight

A well-chosen inertia weight ($\omega$) is essential for achieving a balanced mix of global and local searches in the PSO algorithm. Typically, the initial inertia weight is set to a high value and is then gradually reduced during the optimization process. The adjustment of the inertia weight ($\omega$) is generally guided by Equation (3.8), where values between 0.2 and 0.9 are considered acceptable.

#### e) Termination Criterion

After the initial phase, the assessment steps undergo multiple iterations and subjected to objective function tolerances before reaching a stopping criterion. The termination condition is defined by either completing a predetermined maximum number of iterations or achieving a specified level of accuracy in the solution.

### 3.7.2 PSO Implementation Procedures

The population of the PSO algorithm is consists of $n$ particles, each of which represents a possible outcome. As a result, every optimized parameter in the problem space corresponds to a certain dimension. Figure 3.5 shows the procedure by which the applicable PSO was implemented to address the optimization problem, and procedures of the PSO technique steps are explained accordingly.

**Step 1:** (Initialization) involves inputting system parameters and Establish proper PSO parameter values, construct control variables within allowable bounds, and enter data for buses and transmission lines.

**Step 2:** Involves initiating a feasible solution randomly, ensuring it adheres to the defined practical constraints. Set the iteration counter to 0.

**Step 3:** The particle population and its velocity should be randomly generated.

**Step 4:** Utilize the Newton Raphson method for each particle to compute transmission losses, load flow, and voltage performance index.

**Step 5:** Use the evaluation function to determine each particle's estimated value. Utilizing Equation (3.17), determine each particle's objective function.

**Step 6:** Determine each particle's individual optima ($P_{best}$) and global optima ($G_{best}$) by taking into account their objective function. Compare the projected value of each particle with its Pbest.

**Step 7:** (Update weight) Use Equation (3.8) to change the inertia weight $W$.

**Step 8:** (Update velocity), As per Equation (3.6), calculate the velocity (V) of each particle and update it in the event that its limit is exceeded.

**Step 9:** (Update position), Equation (3.7) can be used to modify the position of each particle.

**Step 10:** For every particle, $P_{best} = P$ indicates that the individual optima of the current fitness (P) is superior to the individual optima of the previous fitness.

**Step 11:** The current value is modified to $P_{best}$ when the estimation of each particle value surpasses the previous $P_{best}$. The value is changed to $G_{best}$ when the optimum $P_{best}$ is superior to $G_{best}$.

**Step 12:** (Updating iteration), While (termination is not met) do, iteration counter = iteration + 1.

**Step 13:** The particle that produces the most recent $G_{best}$ is the optimal value. Concerning voltage magnitudes and power losses within given limitations, the $G_{best}$ particle minimizes values through coordination of optimum values for control variables.

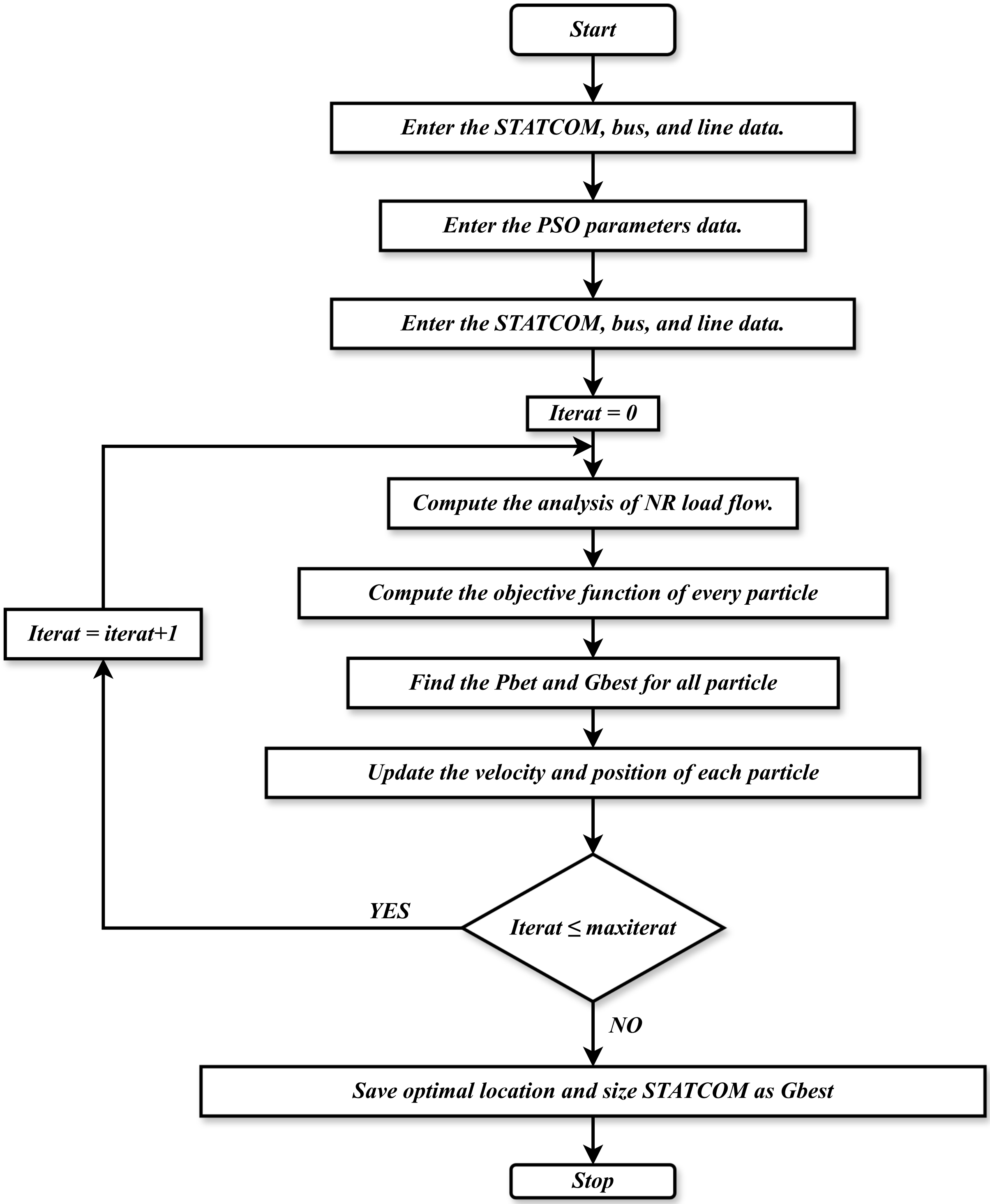


Figure 3.5: Flow chart of particle swarm optimization algorithm

## 3.8 Optimal Allocation and Size of STATCOM

The thesis successfully fulfilled the overall criteria for reducing power loss, enhancing the voltage profile, and ensuring transient stability through the application of particle swarm optimization algorithms. The objective is to determine the most efficient STATCOM size and candidate buses are identified for the optimal placement of STATCOM by employing PSO with the latest system configuration. While voltage stability indices offer a useful approach, their effectiveness can be limited by variations in network configurations and unexpected events like load changes or tripped lines. These fluctuations can lead to sub optimal solutions when identifying the weakest buses for STATCOM placement. To address these limitations, meta−heuristic optimization techniques come into play, employing algorithms in order to determine the best location, number, and size of STATCOM depending on specified constraints and objectives. Various optimization methods, including conventional approaches like linear, sequential quadratic, and nonlinear programming, along with meta−heuristic methods, have been implemented in order to determine the best placement and size of reactive power compensation devices. In this study, PSO technique is employed due to its greater flexibility, rapid convergence, low computational burden, easy implementation, and robustness compared to conventional methods, making it more suitable for exploring complex and uncertain areas.

## 3.9 Problem Formulation

The primary goal of this research is to optimize the fitness function, aiming to minimize transmission loss within the network and voltage deviations at various buses. This thesis involves the pursuit of two minimization objective functions to determine the optimal size and placement of STATCOM for enhancing transient stability and reducing power loss. Consequently, voltage deviation index and active power loss serve as the designated objective functions.

### 3.9.1 Power Loss Minimization

The redistribution of reactive power in a network is mainly influenced by transmission losses. Therefore, the minimization of transmission losses leads to adjustments in the active power generated by the slack bus. The mathematical expression for calculating losses in a network is provided as:

Active power losses,

$$
\begin{aligned}
F_1 &= Min \sum P_{loss} = Min \sum_{t=1}^{n} R_t I_t \\
&= \sum_{i=1}^{Nb} \sum_{\substack{j=1 \\ i \neq j}}^{Nb} [V_i^2 + V_j^2 - 2V_i V_j \cos(\alpha_i \alpha_j)] Y_{ij} \cos\beta_{ij} \\
&= \sum_{t=1}^{m} G_t \left(V_i^2 + V_j^2 - 2V_i V_j \cos\theta_{ij}\right)
\end{aligned}
\tag{3.9}
$$

where, $F_1$ represents real power loss, $n$ number of lines, $I_t$ line current, $R_t$ line resistance, $G_t$ transmission line conductance $t^{th}$, $Nb$ transmission lines total number or buses, $V_i$ and $\alpha_i$ magnitude of voltage and angle at bus i, $V_j$ and $\alpha_j$ voltage magnitude and angle at bus j, and $Y_{ij}$ and $\beta_{ij}$ line admittance magnitude and angle and $\theta_{ij}$ the power angle.

### 3.9.2 Voltage Deviation Minimization

Maintaining load bus voltages in a power system within designated deviation limits of ±5% from the nominal value is preferred. Maintaining voltage deviations within the range of ±5% is essential to prevent voltage collapses during faulty conditions. Unacceptable service quality may result from excessively low voltages, leading to voltage instability issues. Typically, the voltages at related buses may decrease under 0.95 per unit when load requirements increase, requiring additional voltage support at those particular buses. The strategic placement of FACTS devices on suitable buses and lines can effectively minimize voltage deviations and enhance voltage stability. Thus, Connecting FACTS controllers to optimal locations becomes crucial to enhance the system's voltage profile and prevent voltage collapse. This voltage deviation can be computed as:

$$
F_2 = Min \sum_{t=1}^{Nb} |V_{tref} - V_t| = Min \sum_{t=1}^{Nb} (1 - V_t)^2 \tag{3.10}
$$

Where, $F_2$ voltage deviation, $V_t$ voltage magnitude of $t^{th}$ bus, $Nb$ transmission lines total number or buses and $V_{tref}$ nominal voltage of bus t. This study considers an acceptable bus voltage range within the 0.90 to 1.10 per unit (p.u.) range.

### 3.9.3 Power System Constraints

Transformer taps, shunt reactors, bus voltages, generator units real power, and transformer taps are the control variables for the optimal power flow. The optimization problem described above is subject to various constraints, includes reactive power generation limits, voltage, load flow, and STATCOM controller constraint. These can be classified into inequality and equality constraints. The equalities involve fundamental load flow equations, ensuring a balance of reactive or active power. In contrast, the inequalities encompass reactive power, bus voltage, and decision variables, each adhering to their respective limits. The generator's bus voltage magnitude, tap setting transformer, and STATCOM controller VAR output are the control variables that need to be optimized. These parameters values are shown in Table 3.4.

Table 3.4: Control Variables Boundaries

| S/N | Control Variable | Boundaries |
|---|---|---|
| 1 | Voltage of Generator ($V_{Gt}$) | $(0.950 - 1.050)$ p.u. |
| 2 | Settings for Transformer Tap ($T_{pt}$) | $(0.9 - 1.1)$ p.u |
| 3 | Static Compensator's MVAR ($Q_{STC}$) | $(0.0 - 100.0)$ MVAR |

**Equality Constraints** The load flow equation, which requires active and reactive power net injection at each bus to be zero, imposes the limits in the load flow, which define power system grid physical state.

$$
\begin{aligned}
P_{Gt} - P_{Dt} = P_t(V,\delta) = \sum_{k=1}^{Nb} V_t V_k \left(G_{tk}\cos\delta_{tk} + B_{tk}\sin\delta_{tk}\right) \\
Q_{Gt} - Q_{Dt} = Q_t(V,\delta) = \sum_{k=1}^{Nb} V_t V_k \left(G_{tk}\cos\delta_{tk} + B_{tk}\sin\delta_{tk}\right)
\end{aligned}
\tag{3.11}
$$

**Inequality Constraints** The physical equipments are constrained by inequality limitations to a certain extent, highlighting the utility power system's security. All of the inequality constraints needed for the implementation of OPF will be set forth in this section. The system's operational bounds are determined by the inequality constraints, which also include limitations on the apparent power of transmission lines and transformers, reactive power injections, voltages at generator and load bus voltages, transformer tap settings (tap ratio (T)), and FACTS parameters. These constraints can be expressed through the following equations:

$$
\begin{aligned}
&\quad\text{Active power at bus t.}\\
&P_{Gt}^{min} \leq P_{Gt} \leq P_{Gt}^{max}, \quad t \in \{1,2,\ldots,NG\}\\
&\quad\text{Reactive power at each PV bus.}\\
&Q_{Gt}^{min} \leq Q_{Gt} \leq Q_{Gt}^{max}, \quad t \in \{1,2,\ldots,NPV\}\\
&\quad\text{Magnitude of voltage at each PQ bus.}\\
&V_t^{min} \leq V_t \leq V_t^{max}, \quad t \in \{1,2,\ldots,Nbus\}\\
&\quad\text{Tap setting of transformers.}\\
&T_k^{min} \leq T_k \leq T_k^{max}
\end{aligned}
\tag{3.12}
$$

The condition specified is $0.9 \leq T_k \leq 1.0$ and $0.8 < V_t < 1.2$.

Where (Equations (3.11) and (3.12))

$V_t$ the voltage magnitude at bus t,

$V_k$ stands for the magnitude of voltage at bus k,

$N_b$ is the total number of buses,

$Q_{Gt}, P_{Gt}$ the reactive and real power generated at bus number t,

$Q_{Dt}, P_{Dt}$ reactive and real power demand at bus number t, and

$\delta_{tk}$ the angle of the line connecting t and k in terms of bus admittance.

**Transformer Tap Setting Constraints** Constraint on transformer tap settings dictate the allowable range for adjusting the taps of transformer. When it comes to auto transformers, the minimum and maximum tap setting should be zero and one respectively, denoted by $0 \leq t \leq 1$. Likewise, in the case of tapping on the secondary side of a two−winding transformer, the limitation is expressed as $0 \leq t \leq n$, where n is transformation ratio. The voltage stability index (VSI) values should fall within the range of 0 to 1.

$$0 \leq VSI_t < 1 \tag{3.13}$$

The following describes the limitations for power flow limits on each transmission line:

$$S_t \leq S_t^{max} \tag{3.14}$$

The weighting factor serves the purpose of converting multi-objective functions into single-objective functions. Therefore, considering equations 3.6, 3.7 and 3.8,

$$MinF = \omega_1 F_1 + \omega_2 F_2 \tag{3.15}$$

Where, $\sum_{t=1}^{2} \omega_t = \omega_1 + \omega_2 = 1$

The inequality requirements are handled using a static square penalty function. Consequently, the fitness function, or enhanced objective function, which is expressed as follows:

$$\begin{gathered} \text{objective function (fitness function)} = MinF + \text{penalty function}, \\ \text{Penalty function} = p_1 f(Q_{Gt}) + p_2 f(V_t) + p_3 f(VSI_t) + p_4 f(S_t) \end{gathered} \tag{3.16}$$

Where, $p_1$, $p_2$, $p_3$, $p_4$ are Penalty factors

$$\text{objective function (fitness function)} = \omega_1 F_1 + \omega_2 F_2 + \text{Penalty function} \tag{3.17}$$

The system reaches convergence when the difference between its functional value in successive iterations becomes very small (or it reaches a set limit on the number of iterations).

Table 3.5: Particle swarm optimization algorithm parameters and constraint of the decision variables of the objective function

| | | | |
|---|---|---|---|
| PSO algorithm parameters | Particle Number ($N\underline{o}.p$) for PSO | | 50 |
| | Maximum Iteration | | 100 |
| | Inertia Weight ($\omega$) | $\omega_{min}$ | 0.2 |
| | | $\omega_{max}$ | 0.9 |
| | Personal best ($P_{best}$) value ($c_1$) | | 1.5 |
| | Global best ($G_{best}$) value ($c_2$) | | 2 |
| Decision variable of Objective function | | Bus Number (Location) | Size of STATCOM (MVAr) |
| Boundary | Lower bound (Lb) | 2 | 0.0 |
| | Upper bound (Ub) | 30 | 100.0 |

# CHAPTER FOUR

# 4 RESULTS AND DISCUSSIONS

## 4.1 Integration of STATCOM Controller into IEEE 30-Bus System

The simulation analysis was performed using MATLAB 2023a on an Intel(R) Core(TM) i7-8700U CPU @ 3.20 GHz, 3.19 GHz, 8.00 GB RAM DESKTOP-E9GUIJH computer. By applying input parameters of particle swarm optimization algorithms and constraints of decision variables as shown in Table 3.5. The weighting factors are $\omega_1$ = 0.6 and $\omega_2$ = 0.4 for the multi-objective function.

The main goals of this study are bus voltage profile deviation and minimization of power loss; as a results line losses, voltage magnitude, and line flows that directly relate to these goals were noticed and documented. The data used to model the system is presented in Appendices A.1 and A.2. Two test cases were taken into consideration for the performance assessment of the PSO algorithm regarding best allocation and sizing for the STATCOM controller.

**Test case I (Base case):** The Base scenario represents load flow of test system without the device, indicating current state of the network.

**Test case II (STATCOM−placed PSO):** This test case resembles test case one, with the distinction that PSO employed in order to determine the best location and size of the STATCOM. Utilizing PSO algorithm for optimal configuration of the STATCOM enhances the device's performance.

**Simulation Results**

Newton−Raphson power flow analysis used in each scenario to calculate the bus voltages and examine load flow. For comparison study, plots of the voltage magnitudes, line flows, and total losses were made in each scenario. The following sections explain results obtained for the two distinct case studies as described. The demonstrations adhered to the goals of lowering reactive and active power losses as well as bus voltage deviation.

### 4.1.1 Bus Voltage Profiles

The voltage level profiles for the load flow solutions of the test system for two test scenarios are shown in Figure 4.1. The voltage values at bus 5 and 7 for the test case I are 0.9215 and 0.9386 p.u. respectively, from the graphical representation. These values below the lower voltage limit due to insufficient compensation of reactive power, indicating that these locations are suitable for STATCOM placement by analytical method. One STATCOM controllers were installed by using PSO at bus five (5) with 39.93 MVar reactive power injection to maintain the voltages within its limit. Upon incorporating STATCOM controller voltage values at buses 5 and 7, were improved to 0.9719 and 0.9615 p.u., as opposed to their base values of 0.9215 and 0.9386 p.u. when STATCOM controllers weren't used by the system, corresponding to 5.2% and 2.4% improvement respectively.

The network voltage profile was enhanced by the integration of STATCOM controllers, with voltage magnitudes at most buses falling within permissible limit of ±5%.

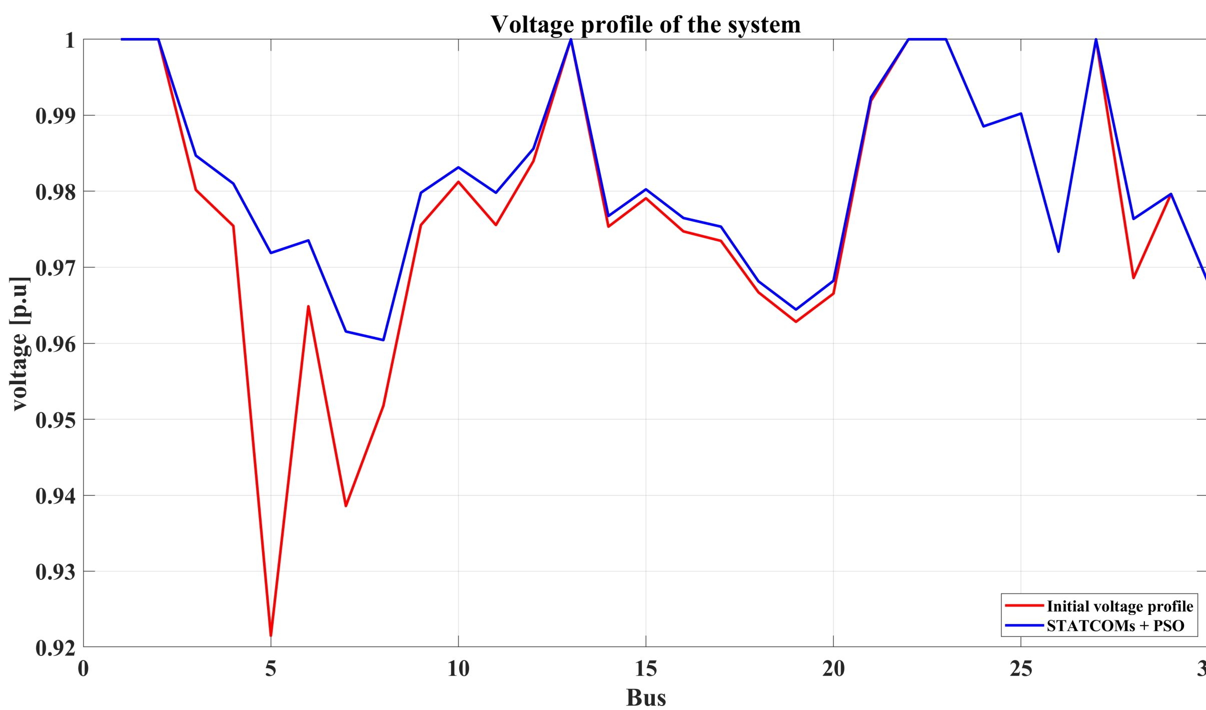


Figure 4.1: Bus voltage profile for each of the two test scenarios

The integration of PSO-positioned STATCOM ensures that there are no further violations of specified limits of bus voltage at any of the buses. Applying this method further enhances the overall network voltage profile. Figure 4.1 shows a comparison of two test cases' voltage profiles. When STATCOM was properly integrated with the artificial intelligence technique known as PSO, bus voltage enhancement greatly improved. The inference suggests that while STATCOM has the capability to enhance bus voltage, achieving optimal performance requires careful optimization. All terminal voltages in test case two fall within the permissible limits of 0.95 to 1.05 p.u., leading to an improved performance and a more stable operation of network.

### 4.1.2 Active Power Loss Minimization

The total active power loss without STATCOM controller was 9.003 MW, which decreased to 8.4173 MW when the STATCOM was placed by using PSO. The integration of the PSO algorithm with the STATCOM resulted in a decrease of 0.5857 MW. PSO integration of the STATCOM device resulted in a 6.5% reduction in active power loss. Branch five (5) experiences high power losses due to its peak loading conditions, with a real load ($PL_5$) of 94.2 MW and a reactive load ($QL_5$) of 19 MVAr, as documented in Appendix A.2.

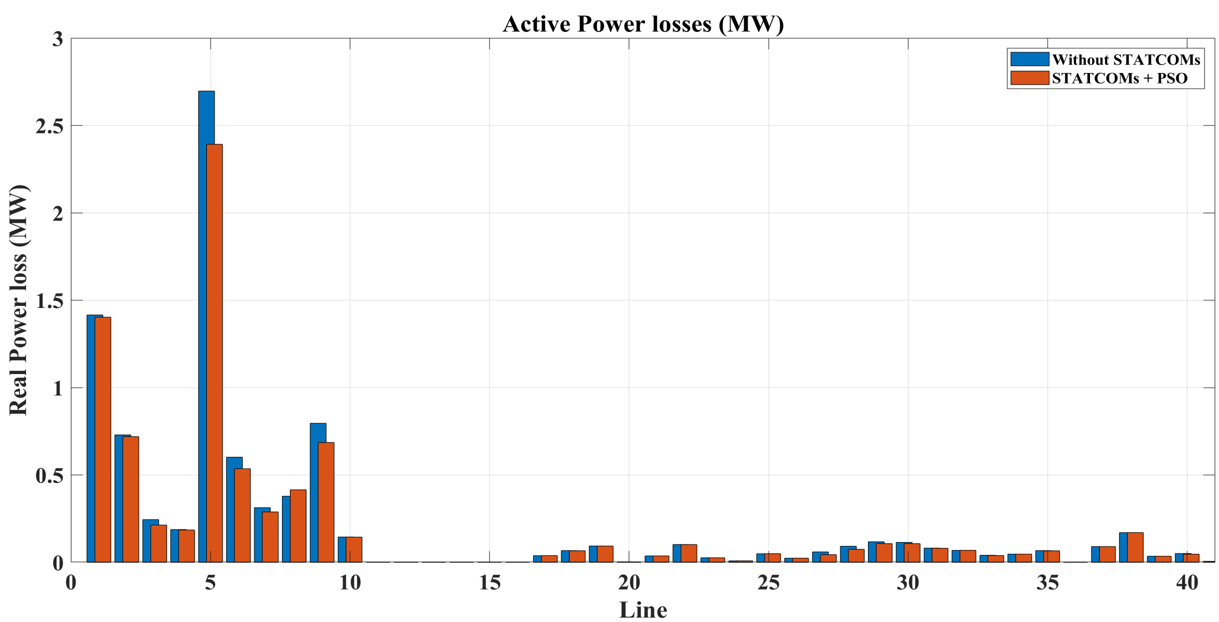


Figure 4.2: Minimization of active power loss in both scenarios

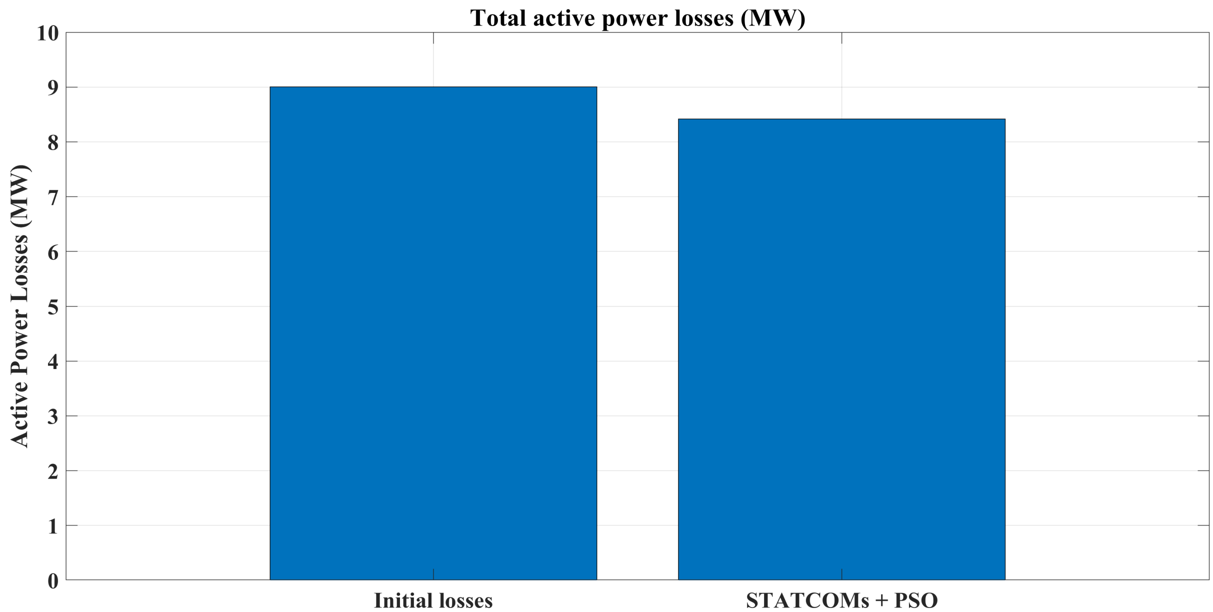


Figure 4.3: Total active power loss minimization in both scenarios

The minimization of losses was accomplished by redistributing line flows on the network, facilitated by the STATCOM device, which supplied reactive power. Figure 4.2 illustrates the comparison of the STATCOM device's effectiveness in reducing active power loss using optimally placed methods for better comprehension. It is clear that when the STATCOM was installed using the PSO technique, the network's loss was minimized. The total power loss reduction is depicted in Figure 4.3, providing a clearer understanding performance of the optimum integration of STATCOM inside a test network.

### 4.1.3 Minimization of Reactive Power Loss

The total reactive power loss which was 32.6309 MVAr without STATCOM was reduced to 30.2954 MVAr when STATCOM was incorporated using PSO. When PSO was utilized to site the device, an achievement of 2.3355 MVAr—or a 7.157% total reduction—was seen. It is important to highlight that positioning the FACTS device appropriately is necessary to achieve the intended outcomes. For better presentation, the comparison of the PSO methods utilized in STATCOM placement shown in Figure 4.4. Figure 4.5 shows the total reactive loss decrease after and before STATCOM placement using PSO. This allows for a more visual representation and understanding of the overall advantages of utilizing the optimization technique in the

FACTS location. The system's reactive loss has been greatly reduced as a result. It is impossible to overstate the PSO's performance because it reduced costs while simultaneously improving voltage profile and minimizing active and reactive power loss. For better understand, Figure 4.4 compares the methods utilized in STATCOM placement by PSO graphically. Figure 4.5 shows the total decrease in reactive losses before STATCOM and after optimally placed STATCOM.

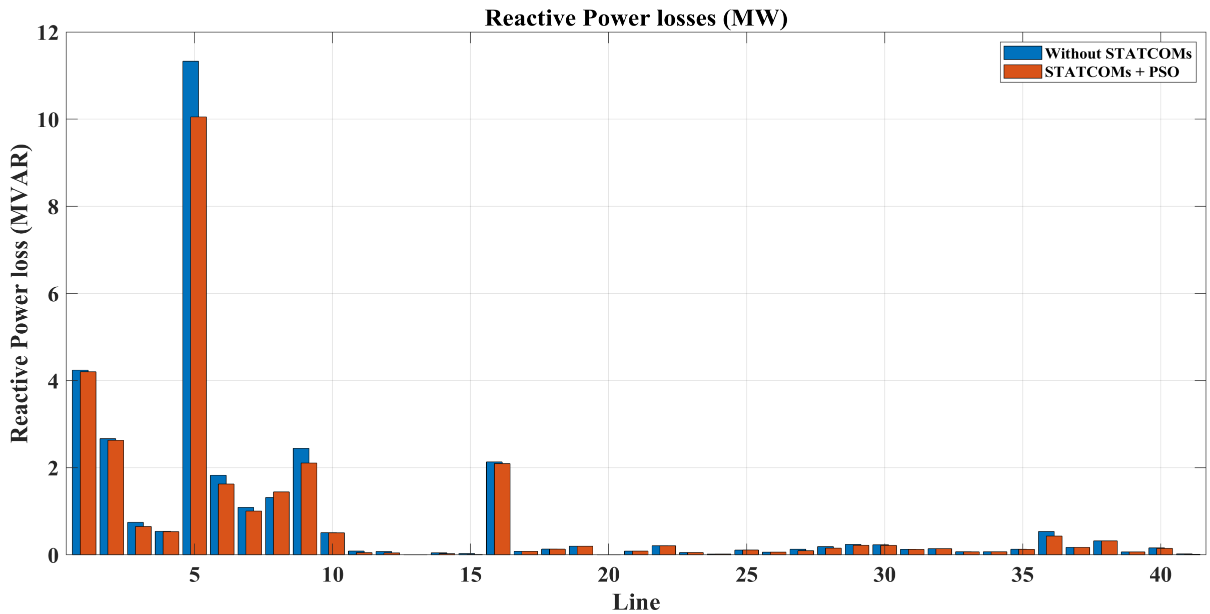


Figure 4.4: Reduction of reactive power loss in the two scenarios

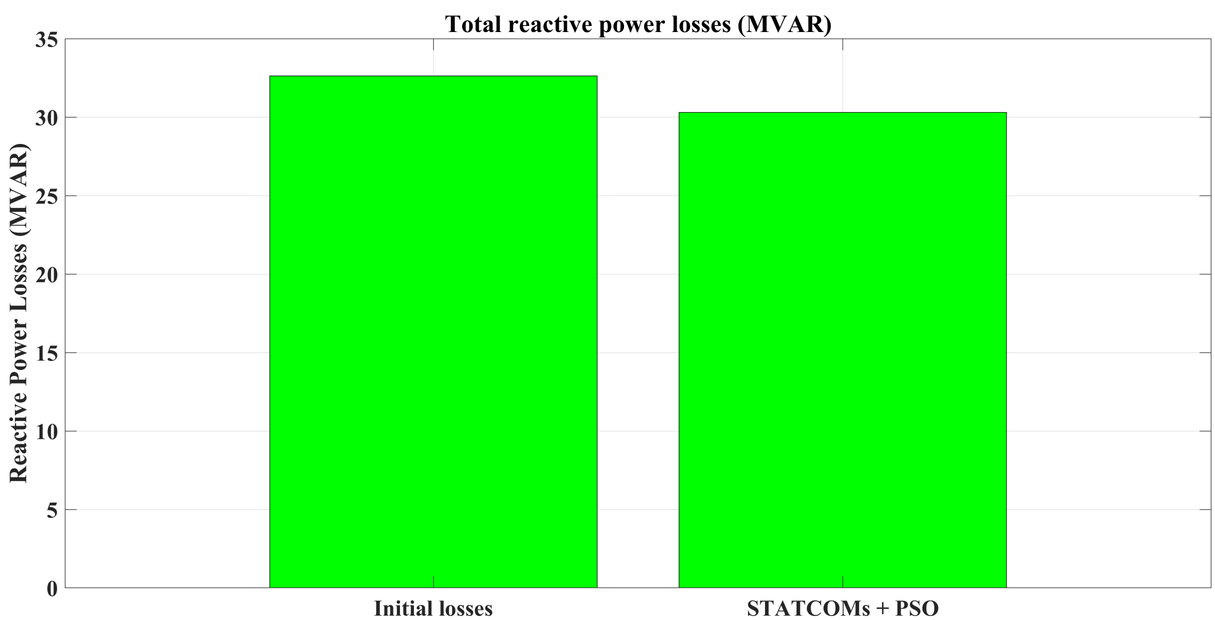


Figure 4.5: Reduction of total reactive power loss in both scenarios

The PSO technique was used to insert the single STATCOM devices into the test network in an optimal manner, resulting in a total reactive power injection of 39.93 MVAr. Reducing costs is one of the algorithm's primary achievements. Table 4.1 provides an summary of the total power loss reduction that can be achieved by incorporating a STATCOM device.

Table 4.1: Results of the test network's total active and reactive power losses

| **Overall Power Loss** | **Base case (Steady State)** | **PSO placed STATCOM** |
|---|---|---|
| P (MW) | 9.003 | 8.4173 |
| Q (MVAR) | 32.6309 | 30.2954 |
| STATCOM bus (MVAr) | – | 5 (39.93) |

## 4.2 Enhancement of Transient Stability Using Case Study Analysis

The first step in transient stability analysis usually entails using steady-state power flow analysis to evaluate the system's static stability and make sure it can function in a stable state. Analysis of transient stability focus on how the system behaves in the face of large disruptions, such faults. In particular, the study looks at the case of a fault at the grid-connected wind farm's output bus. The analysis examines how the wind farms linked to the grid affects power system safe operation by assessing the system's level of recovery following the disturbance. As for transient stability of power system, there are three primary oscillations to consider:

**1. Inter-machine mode:** In this mode, the rotors of several synchronous machines in the system oscillate with one another. It is mostly affected by the machines' inertia and the electrical strength of the transmission lines that link them, and its frequency is normally between one and three hertz.

**2. Local Mode:** Oscillations between a particular machine and its adjacent loads or generators are a feature of this mode. It is primarily influenced by the local control systems of the machine and the impedance of the surrounding network, and it operates at a greater frequency than the inter-machine mode (2–5 Hz).

**3. Torsional Mode:** This mode is characterized by oscillations between a machine's turbine and shaft system. Out of the three modes, it has the maximum frequency (10-30 Hz) and is affected by the spinning masses' inertia and the shaft's torsional stiffness.

The main task of the simulation study is to simulate the test systems and apply traditional power flow (PF) methodologies for analysis. A MATLAB toolbox called PSAT is intended for the power system analysis, modeling and control. PSAT can perform a number of tasks, such as simulation in the time domain, stability study of small signals, analyzing optimal power flow, continuation power flow, and conventional power flow.

- **Power Flow Analysis:** This looks into the system's power flow and steady-state voltage under various operation scenarios.
- **Continuation Power Flow Analysis:** This method tracks the power flow solution as system parameters change to evaluate voltage stability.
- **Analyzing Optimal Power Flow:** minimizes expenses or losses while adhering to system limitations by operating the power system as efficiently as possible.
- **Stability Study of Small Signals:** This assesses how well the system recovers from minor disruptions to synchronism.
- **Simulation in the Time Domain:** This mimics how the system would react in real time to a variety of disruptions, like as failures, load variations, and generator trips.

Using MATLAB/PSAT software to mimic IEEE 30 bus modified test system, the study investigated how wind farm Adama II integrated with it. The use of voltage stability indices alone to identify potential or vulnerable buses may not provide the best results due to variances in topology of networks, settings, and load changes contingencies, generator, or line failures. By assisting in the selection of the most appropriate number, location, and size of STATCOM taking into account given objectives and constraints, meta−heuristic optimization approaches provide an answer to these limits. With this configuration, the efficacy of the FACTS device STATCOM with PSO for the ideal positioning and sizing of STATCOM models created in this thesis was assessed. The IEEE 30-bus system with the Adama II wind farm will be investigated under three conditions.

**Test system scenarios for case studies**

In order to ensure the performance of the power system under a range of transient scenarios, such as a three-phase $(3-\phi)$ Fault and abrupt load fluctuations, an analysis was carried out. The system operates under normal conditions without any faults or additional control devices. A fault is simulated on bus number 8 was cleared in 1.25 seconds after it occurred at 1.00 seconds under fault condition. The same fault on bus number 8 will occur, but with a STATCOM installed on bus number 5 (as determined by PSO analysis) to regulate the voltage and improve stability for the fault with STATCOM condition.

### 4.2.1 Scenario 1: Base Case Condition

The integration of wind farm Adama II with an IEEE 30−bus modified system is analyzed conventionally using the Newton−Raphson power flow approach using MATLAB/PSAT. An analysis and evaluation of the bus with the lowest magnitude of voltage profile and lines with the largest active power losses are crucial in analytical approaches for determining the best locations for FACTS devices. These characteristics aid in locating crucial points in the power system where FACTS devices can improve system stability and performance most effectively. The single-line diagram of wind farm Adama II interconnected with IEEE 30−bus modified system under base condition is presented in Figure 4.6.

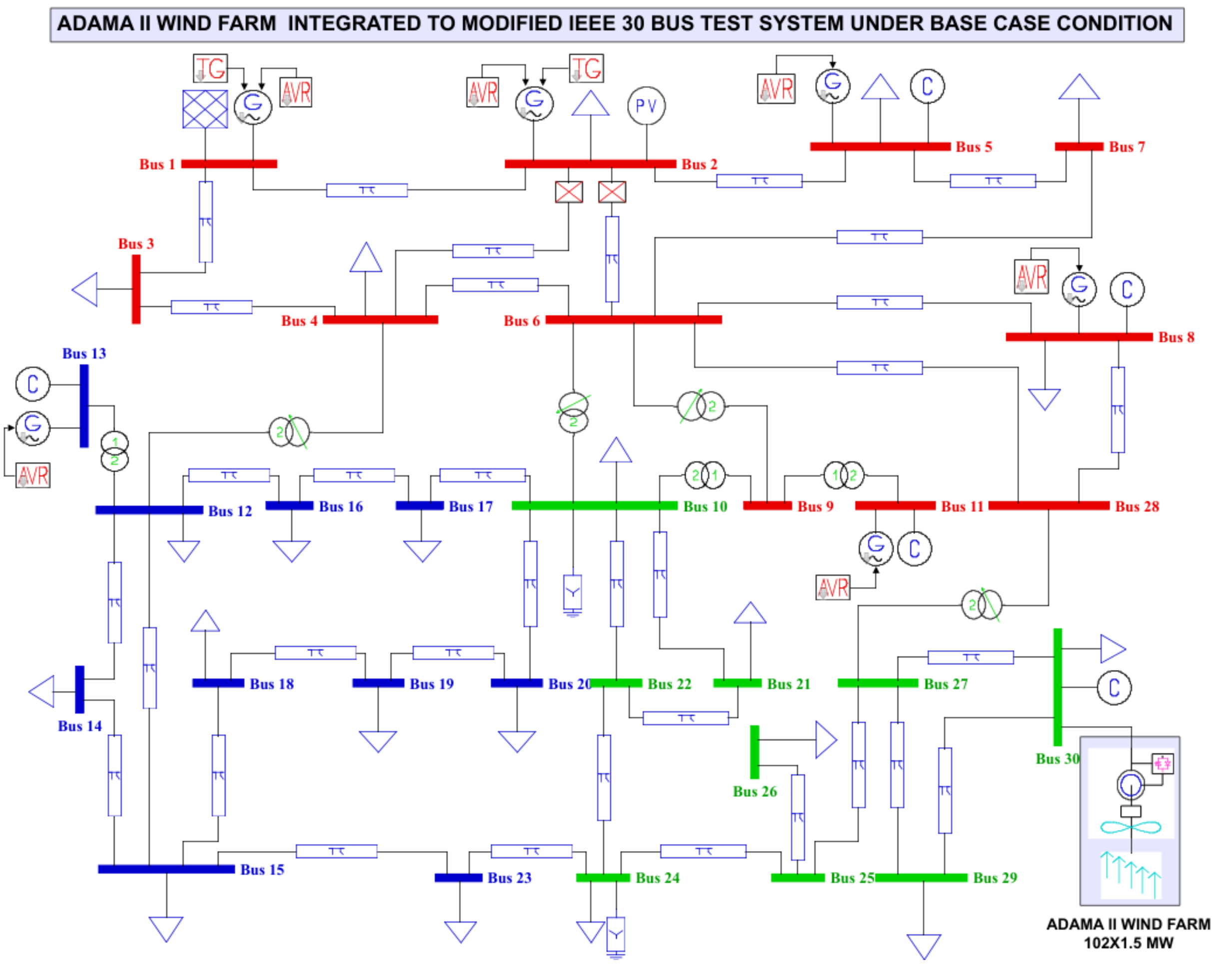


Figure 4.6: IEEE 30−bus dynamic test systems with Wind farm Adama II under base case condition

In order to assess how FACTS devices affect the system's power dissipation, transient stability, and voltage deviation, it is essential to ascertain corresponding values of these parameters in the most favorable circumstances. Under base case conditions, a Newton−Raphson load flow for uncompensated wind farm Adama II integrated with IEEE 30-bus modified test system reveals that the line from bus #1 to #2 has the largest line loss, which is recorded as 0.05474 p.u. Furthermore, bus No. 26 exhibits the weakest bus voltage under heavy load conditions. This bus voltage was measured at 1.02004 p.u, according to the power flow results displayed in Table 4.2. PSAT software was used to run the power flow calculations, and the outcomes are displayed below:

Table 4.2: Results of Power Flow for IEEE 30 bus system for base case condition in PSAT

| Bus | V | Phase | P gen | Q gen | P load | Q load |
|---|---|---|---|---|---|---|
| | [p.u.] | [rad] | [p.u.] | [p.u.] | [p.u.] | [p.u.] |
| Bus 1 | 1.06000 | 0.00000 | 3.5203 | −0.35115 | 0.00000 | 0.00000 |
| Bus 10 | 1.04936 | −0.27242 | 0.00000 | 0.00000 | 0.05800 | −0.18922 |
| Bus 11 | 1.08200 | −0.24481 | 0.00000 | 0.14390 | 0.00000 | 0.00000 |
| Bus 12 | 1.06196 | −0.25999 | 0.00000 | 0.00000 | 0.11200 | 0.07500 |
| Bus 13 | 1.07100 | −0.25999 | 0.00000 | 0.06914 | 0.00000 | 0.00000 |
| Bus 14 | 1.04711 | −0.27535 | 0.00000 | 0.00000 | 0.06200 | 0.01600 |
| Bus 15 | 1.04247 | −0.27684 | 0.00000 | 0.00000 | 0.08200 | 0.02500 |
| Bus 16 | 1.04903 | −0.26977 | 0.00000 | 0.00000 | 0.03500 | 0.01800 |
| Bus 17 | 1.04428 | −0.27534 | 0.00000 | 0.00000 | 0.09000 | 0.05800 |
| Bus 18 | 1.03281 | −0.28730 | 0.00000 | 0.00000 | 0.03200 | 0.00900 |
| Bus 19 | 1.03021 | −0.29021 | 0.00000 | 0.00000 | 0.09500 | 0.03400 |
| Bus 2 | 1.04500 | −0.09292 | 0.40000 | 0.45404 | 0.21700 | 0.12700 |
| Bus 20 | 1.03422 | −0.28675 | 0.00000 | 0.00000 | 0.02200 | 0.00700 |
| Bus 21 | 1.03705 | −0.28010 | 0.00000 | 0.00000 | 0.17500 | 0.11200 |
| Bus 22 | 1.03760 | −0.27986 | 0.00000 | 0.00000 | 0.00000 | 0.00000 |
| Bus 23 | 1.03188 | −0.28344 | 0.00000 | 0.00000 | 0.03200 | 0.01600 |
| Bus 24 | 1.02613 | −0.28628 | 0.00000 | 0.00000 | 0.08700 | 0.02172 |
| Bus 25 | 1.02185 | −0.27864 | 0.00000 | 0.00000 | 0.00000 | 0.00000 |
| Bus 26 | 1.00425 | −0.28590 | 0.00000 | 0.00000 | 0.03500 | 0.02300 |
| Bus 27 | 1.02769 | −0.26942 | 0.00000 | 0.00000 | 0.00000 | 0.00000 |
| Bus 28 | 1.01085 | −0.20254 | 0.00000 | 0.00000 | 0.00000 | 0.00000 |
| Bus 29 | 1.00795 | −0.29070 | 0.00000 | 0.00000 | 0.02400 | 0.00900 |
| Bus 3 | 1.04500 | −0.13703 | 0.00000 | 0.45862 | 0.02400 | 0.01200 |
| Bus 30 | 0.99653 | −0.30596 | 0.00000 | 0.00000 | 0.10600 | 0.01900 |
| Bus 4 | 1.02499 | −0.16330 | 0.00000 | 0.00000 | 0.07600 | 0.01600 |
| Bus 5 | 1.01000 | −0.24499 | 0.00000 | 0.33141 | 0.94200 | 0.19000 |
| Bus 6 | 1.01544 | −0.19202 | 0.00000 | 0.00000 | 0.00000 | 0.00000 |
| Bus 7 | 1.00547 | −0.22293 | 0.00000 | 0.00000 | 0.22800 | 0.10900 |
| Bus 8 | 1.01000 | −0.20354 | 0.00000 | 0.22600 | 0.30000 | 0.30000 |
| Bus 9 | 1.05434 | −0.24481 | 0.00000 | 0.00000 | 0.00000 | 0.00000 |

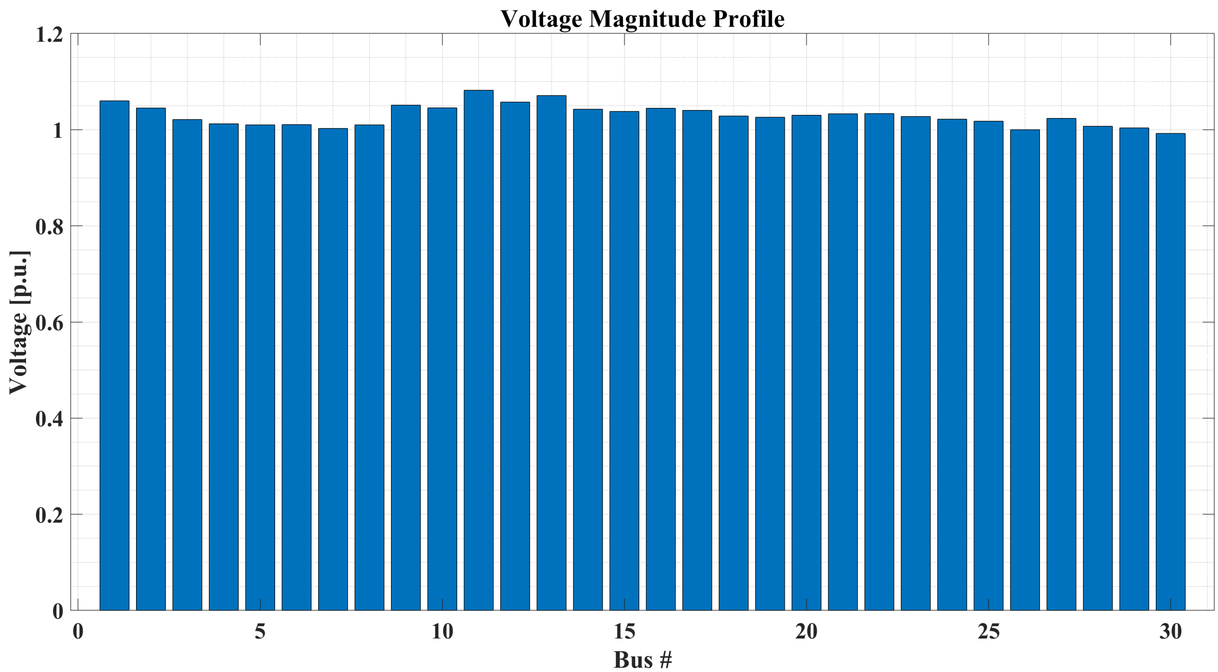


Figure 4.7: Magnitude of voltage profile for base case condition of IEEE 30 bus in PSAT

The incorporation of wind farm Adama II into IEEE−30 bus modified test system guarantees that, even with different phase angles, the voltage values stay within the required limits. Bus 01, the slack bus, keeps the voltage at 1.06 pu at a zero degrees angle. Bus number twenty six (26) is the most sensitive, as evidenced by Table 4.2 and Figure 4.7 analysis, since bus number twenty six's voltage drops to its lowest point at any reactive load. Thus, this bus is determined analytically to be the best place to place STATCOM devices in order to increase transient stability. In this simulation, we employed PSO to find the best location for a STATCOM. With a size of 39.9316 MVAR reactive power, bus number 5 was determined to be the optimum size and location for the STATCOM based on PSO analysis. The effectiveness of this placement was then evaluated through analysis of the simulation results. The results of the line flow for the IEEE 30 bus system installed into the Adama II wind farm are displayed in Table 4.3 for the base case scenario in PSAT.

Table 4.3: Results of Line Flow for IEEE 30 bus system for base case condition in PSAT

| From bus | To bus | Line | P flow [p.u.] | Q flow [p.u.] | P loss [p.u.] | Q loss [p.u.] |
|---|---|---|---|---|---|---|
| Bus 2 | Bus 1 | 1.00000 | −1.66509 | 0.33766 | 0.05111 | 0.09457 |
| Bus 6 | Bus 8 | 2.00000 | 0.29518 | 0.04415 | 0.00104 | −0.00558 |
| Bus 12 | Bus 14 | 3.00000 | 0.07849 | 0.02440 | 0.00074 | 0.00153 |
| Bus 12 | Bus 15 | 4.00000 | 0.17831 | 0.06941 | 0.00215 | 0.00423 |
| Bus 16 | Bus 12 | 5.00000 | −0.07111 | −0.03418 | 0.00053 | 0.00112 |
| Bus 1 | Bus 3 | 6.00000 | 0.89265 | −0.10806 | 0.03235 | 0.07302 |
| Bus 14 | Bus 15 | 7.00000 | 0.01575 | 0.00687 | 0.00006 | 0.00005 |
| Bus 17 | Bus 16 | 8.00000 | −0.03604 | −0.01590 | 0.00007 | 0.00027 |
| Bus 18 | Bus 15 | 9.00000 | −0.05949 | −0.01621 | 0.00038 | 0.00078 |
| Bus 19 | Bus 18 | 10.00000 | −0.02744 | −0.00711 | 0.00005 | 0.00010 |
| Bus 20 | Bus 19 | 11.00000 | 0.06773 | 0.02723 | 0.00017 | 0.00034 |
| Bus 10 | Bus 20 | 12.00000 | 0.09054 | 0.03603 | 0.00081 | 0.00180 |
| Bus 17 | Bus 10 | 13.00000 | −0.05396 | −0.04210 | 0.00014 | 0.00036 |
| Bus 10 | Bus 21 | 14.00000 | 0.15779 | 0.09958 | 0.00110 | 0.00237 |
| Bus 10 | Bus 22 | 15.00000 | 0.07614 | 0.04566 | 0.00052 | 0.00107 |
| Bus 22 | Bus 21 | 16.00000 | 0.01831 | 0.01480 | 0.00001 | 0.00001 |
| Bus 2 | Bus 4 | 17.00000 | 0.43164 | −0.02611 | 0.00973 | −0.00978 |
| Bus 23 | Bus 15 | 18.00000 | −0.04967 | −0.02938 | 0.00031 | 0.00063 |
| Bus 24 | Bus 22 | 19.00000 | −0.05686 | −0.02908 | 0.00045 | 0.00069 |
| Bus 24 | Bus 23 | 20.00000 | −0.01761 | −0.01325 | 0.00006 | 0.00012 |
| Bus 24 | Bus 25 | 21.00000 | −0.01253 | 0.02061 | 0.00010 | 0.00018 |
| Bus 25 | Bus 26 | 22.00000 | 0.03544 | 0.02366 | 0.00044 | 0.00066 |
| Bus 27 | Bus 25 | 23.00000 | 0.04832 | 0.00369 | 0.00024 | 0.00046 |
| Bus 27 | Bus 29 | 24.00000 | 0.06189 | 0.01667 | 0.00085 | 0.00162 |
| Bus 27 | Bus 30 | 25.00000 | 0.07091 | 0.01660 | 0.00161 | 0.00303 |
| Bus 30 | Bus 29 | 26.00000 | −0.03670 | −0.00542 | 0.00033 | 0.00063 |
| Bus 4 | Bus 3 | 27.00000 | −0.82697 | −0.24773 | 0.00934 | 0.01781 |
| Bus 6 | Bus 28 | 28.00000 | 0.18757 | 0.01909 | 0.00059 | −0.01126 |
| Bus 2 | Bus 5 | 29.00000 | 0.81843 | 0.02824 | 0.02906 | 0.07796 |
| Bus 2 | Bus 6 | 30.00000 | 0.59802 | −0.01275 | 0.01903 | 0.01804 |
| Bus 8 | Bus 28 | 31.00000 | −0.00586 | −0.02427 | 0.00000 | −0.04369 |
| Bus 4 | Bus 6 | 32.00000 | 0.73244 | 0.03164 | 0.00609 | 0.01182 |

Continued on next page

Table 4.3 – continued from previous page

| **From bus** | **To bus** | **Line** | **P flow** | **Q flow** | **P loss** | **Q loss** |
|---|---|---|---|---|---|---|
| | | | **[p.u.]** | **[p.u.]** | **[p.u.]** | **[p.u.]** |
| Bus 5 | Bus 7 | 33.00000 | −0.15264 | 0.09168 | 0.00152 | −0.01688 |
| Bus 7 | Bus 6 | 34.00000 | −0.38216 | −0.00043 | 0.00386 | −0.00551 |
| Bus 6 | Bus 9 | 35.00000 | 0.27771 | −0.07281 | 0.00000 | 0.01590 |
| Bus 6 | Bus 10 | 36.00000 | 0.15886 | 0.00368 | 0.00000 | 0.01278 |
| Bus 9 | Bus 11 | 37.00000 | −0.00000 | −0.14022 | 0.00000 | 0.00368 |
| Bus 9 | Bus 10 | 38.00000 | 0.27771 | 0.05150 | −0.00000 | 0.00789 |
| Bus 4 | Bus 12 | 39.00000 | 0.44045 | 0.18377 | 0.00000 | 0.04821 |
| Bus 13 | Bus 12 | 40.00000 | 0.00000 | 0.06914 | 0.00000 | 0.00058 |
| Bus 28 | Bus 27 | 41.00000 | 0.18111 | 0.04977 | 0.00000 | 0.01281 |

### 4.2.2 Scenario 2: Under fault condition without STATCOM devices

A dynamic model of the IEEE 30−bus system is built using PSAT toolkit to simulate a system upset. The scenario involves a sudden load rise and a three phase $(3-\phi)$ fault applied at bus number 8. The single-line diagram of wind farm Adama II interconnected with IEEE 30-bus modified system with fault incorporated is presented in Figure 4.8. The fault is initiated at 1.00 seconds and cleared after 0.25 seconds, intentionally causing a disturbance in the system. Three-phase faults, in which all three conductive phases of a power grid unintentionally touch each other, are serious events caused by infrastructure problems, earthing problems, or external influences. These faults lead to drastic current peaks, voltage instability, and potential equipment damage. However, their effects can be mitigated by protective relays, earthing systems, and a general system design that emphasizes redundancy and resilience. In addition FACTS devices, like STATCOM and UPFCs, can act as mitigation tools by injecting current to counter the fault current and by regulating voltage, ultimately improving the system's resilience to these events. It's important to note that this simulation deliberately excludes STATCOM devices for mitigation purposes.

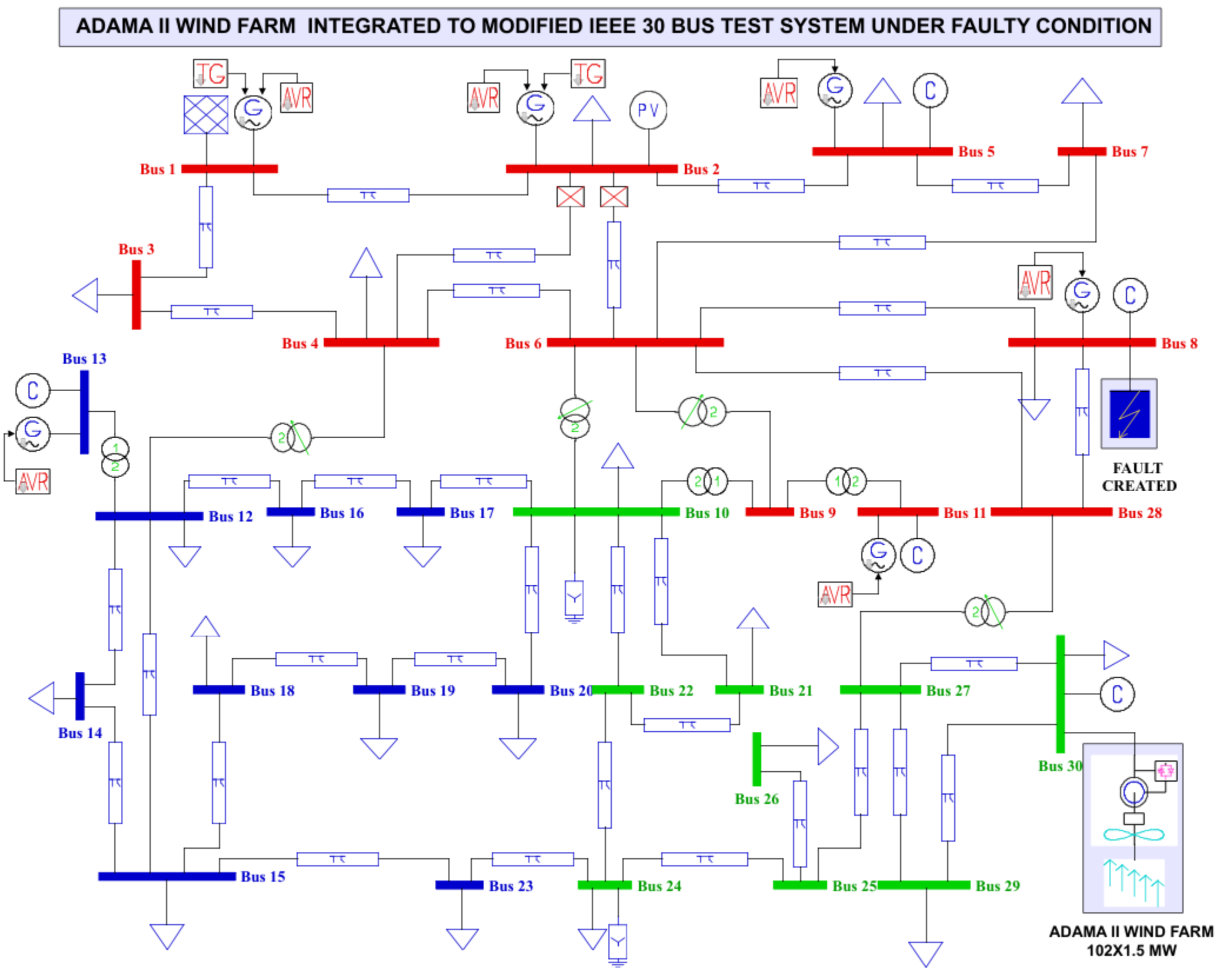


Figure 4.8: Dynamic IEEE 30-bus modified test systems with integration of wind farm Adama II in MATLAB/PSAT under faulty condition

### 4.2.3 Scenario 3: Under Faulty Conditions With PSO-Determined STATCOM Placement

Transient Stability Enhancement (TSE) simulations were performed using TDS tool within the MATLAB® PSAT toolbox. Initially, simulations were run under normal conditions and during a fault without any FACTS devices present. Subsequently, simulations were repeated with PSO-placed STATCOM included, and the results were compared. The single-line diagram of wind farm Adama II interconnected with IEEE 30-bus modified system with fault and PSO-positioned STATCOM incorporated is presented in Figure 4.9. While numerous TSE variables were explored, this work focuses on analyzing generator power, rotor speed, and rotor angle during the simulations. These simulations assessed the effectiveness of the PSO-optimized STATCOM placement in mitigating the disturbances caused by a three phase $(3-\phi)$ fault (applied at 1.00

seconds and cleared at 1.25 seconds) and a sudden load change.

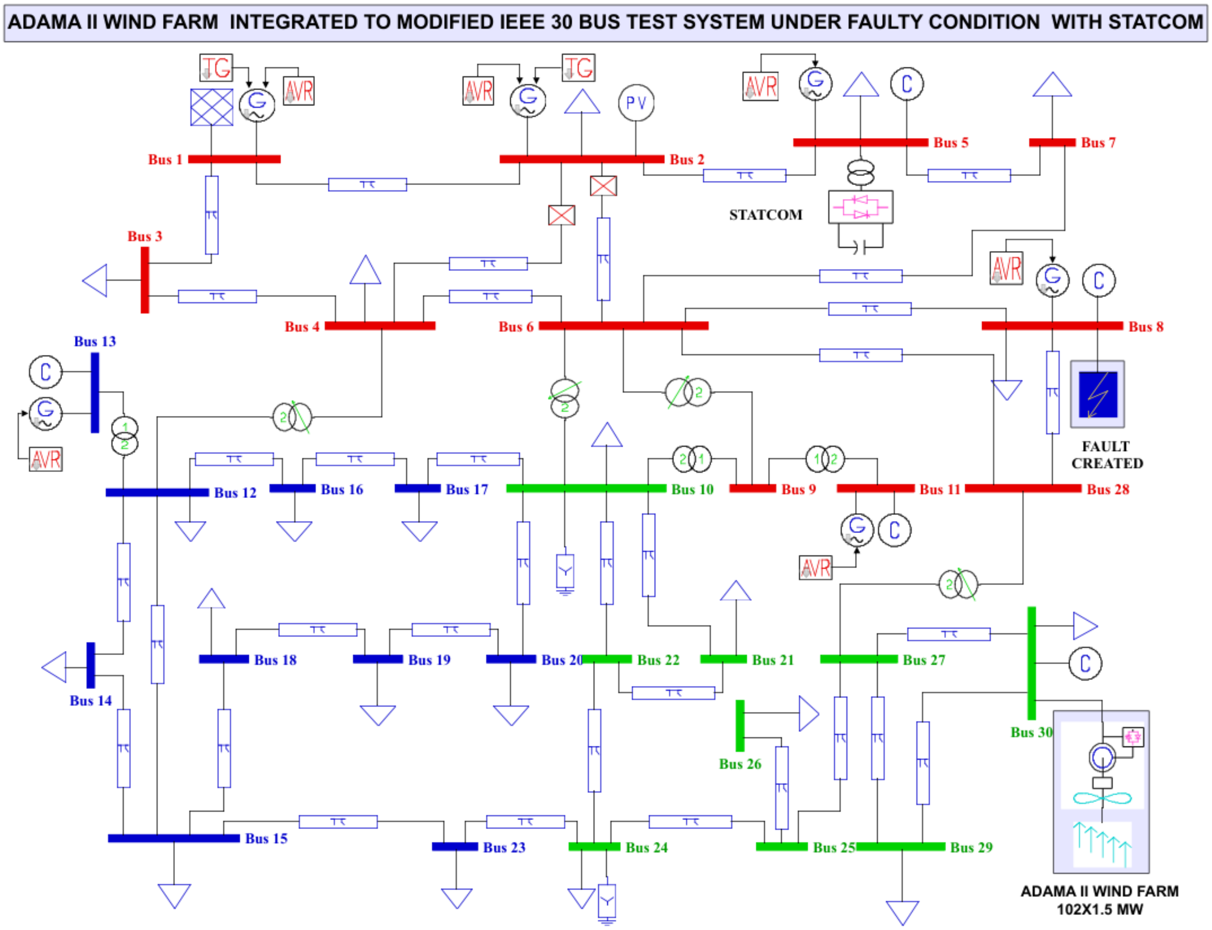


Figure 4.9: IEEE 30−bus modified dynamic test systems interlinked with wind farm Adama II under faulty with PSO−placed STATCOM

### Rotor Angle and Speed Responses of the Generator 1

The Figures (4.10 to 4.21) illustrate how a generator's performance changes under different conditions. The green curve represents prefault condition, the red curve shows response during a faulty conditions without additional devices, and the blue curve depicts response during a faulty with STATCOM condition.

Simulating a fault at bus eight (8), with a sudden load increase in the dynamic model with PSO-placed STATCOM at bus number five (5) with a size of 39.93 MVAr as shown by the blue curve in Figure 4.10, reveals a significant reduction in rotor angle oscillations around the 40-second mark. This damping effect from the STATCOM FACTS devices is also observed in rotor speed as shown by the blue curve in Figure 4.11, significantly reducing its oscillations at around 40 seconds.

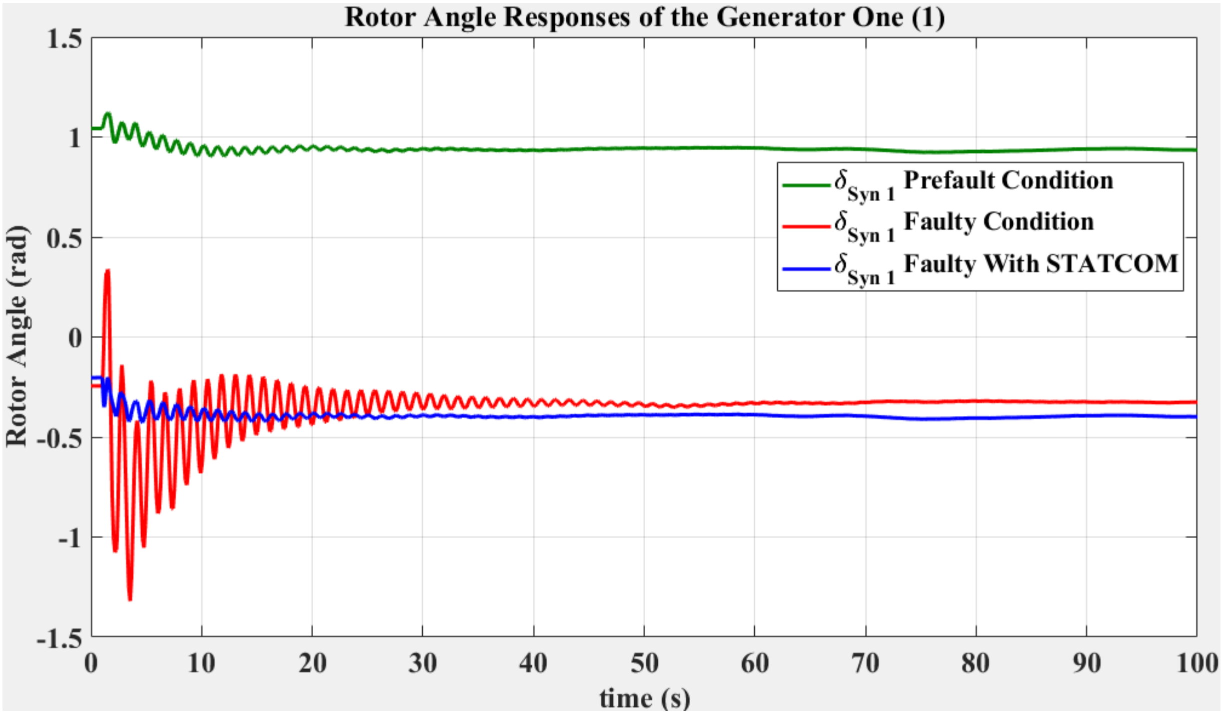


Figure 4.10: Rotor angle responses of the generator 1

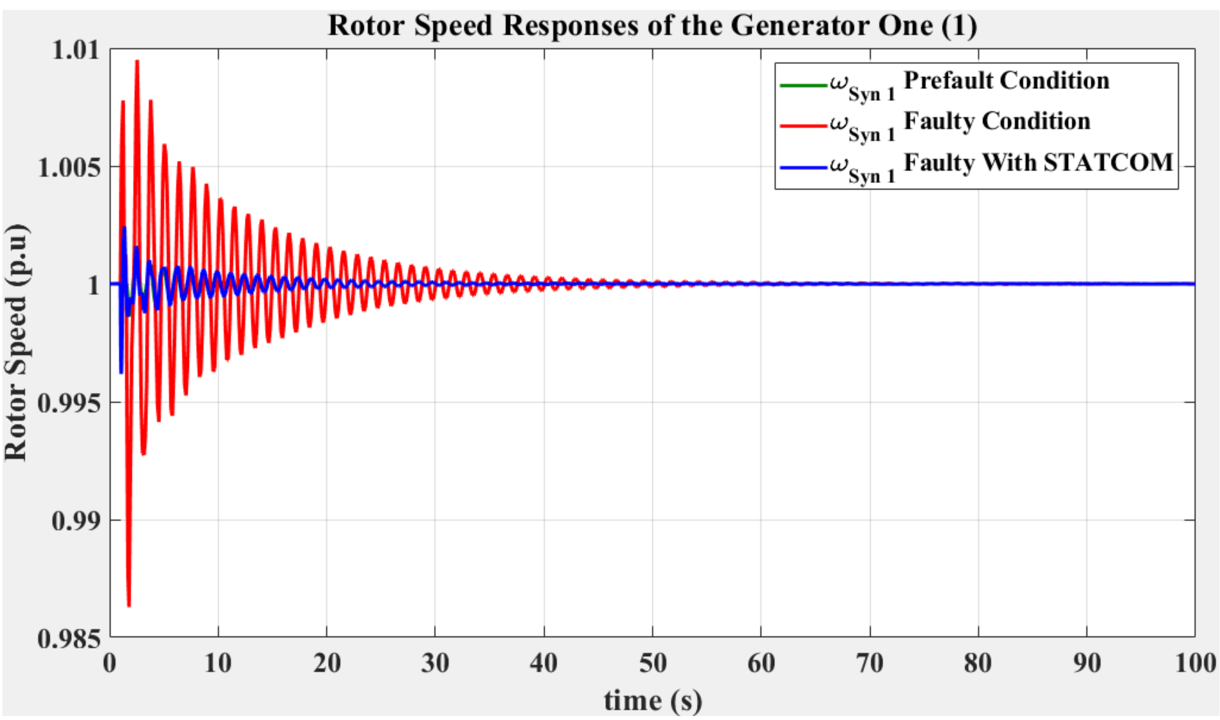


Figure 4.11: Rotor speed responses of the generator 1

**Rotor Angle and Speed Responses of the Generator 2**

Simulating a fault at bus eight (8) with a sudden load change in the dynamic model with PSO−placed STATCOM as shown by the blue curve in Figure 4.12, reveals a significant reduction in rotor angle oscillations around the 50-second mark. This damping effect from the STATCOM FACTS devices is also observed in rotor speed as shown by the blue curve in Figure 4.13, significantly reducing its oscillations at around 50 seconds.

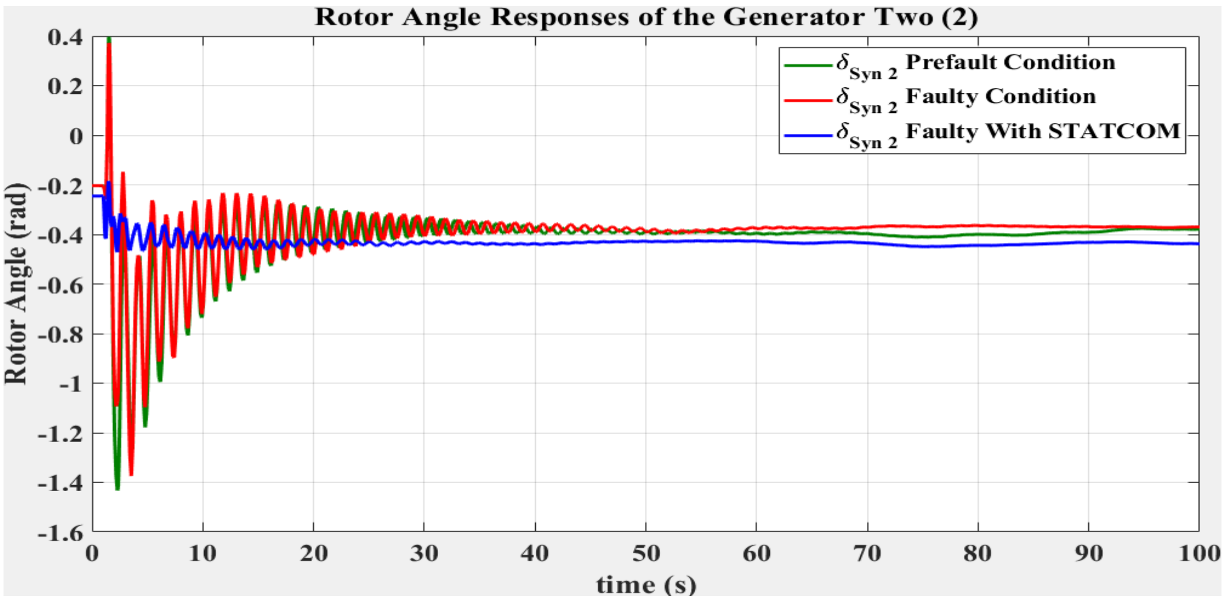


Figure 4.12: Rotor angle responses of the generator 2

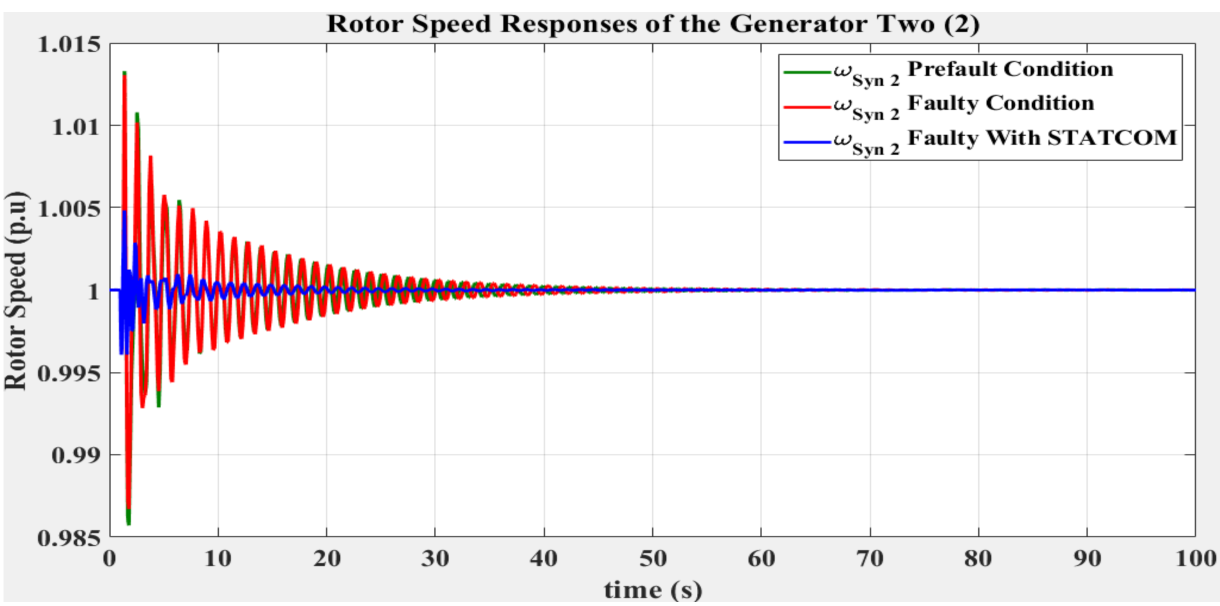


Figure 4.13: Rotor speed responses of the generator 2

**Rotor Angle and Speed Responses of the Generator 3**

Simulating a fault at bus eight (8) along with a sudden load change in the dynamic model with PSO−placed STATCOM as shown by the blue curve in Figure 4.14, reveals a significant reduction in rotor angle oscillations around the 35−second mark. This damping effect from the STATCOM FACTS devices is also observed in rotor speed as shown by the blue curve in Figure 4.15, significantly reducing its oscillations at around 35 seconds.

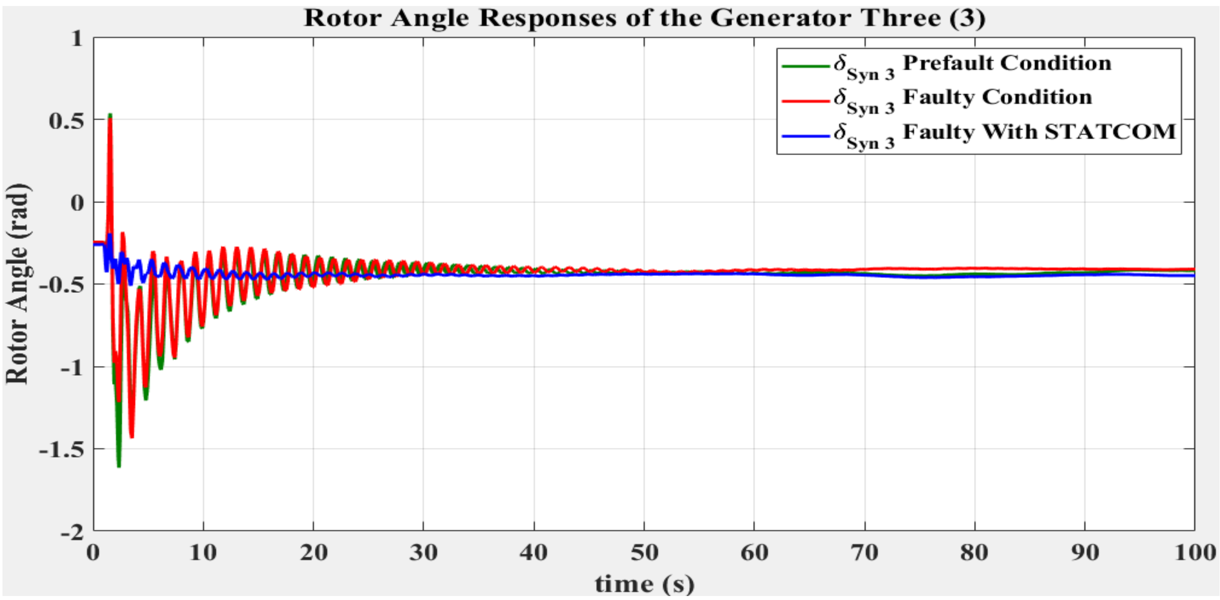


Figure 4.14: Rotor angle responses of the generator 3

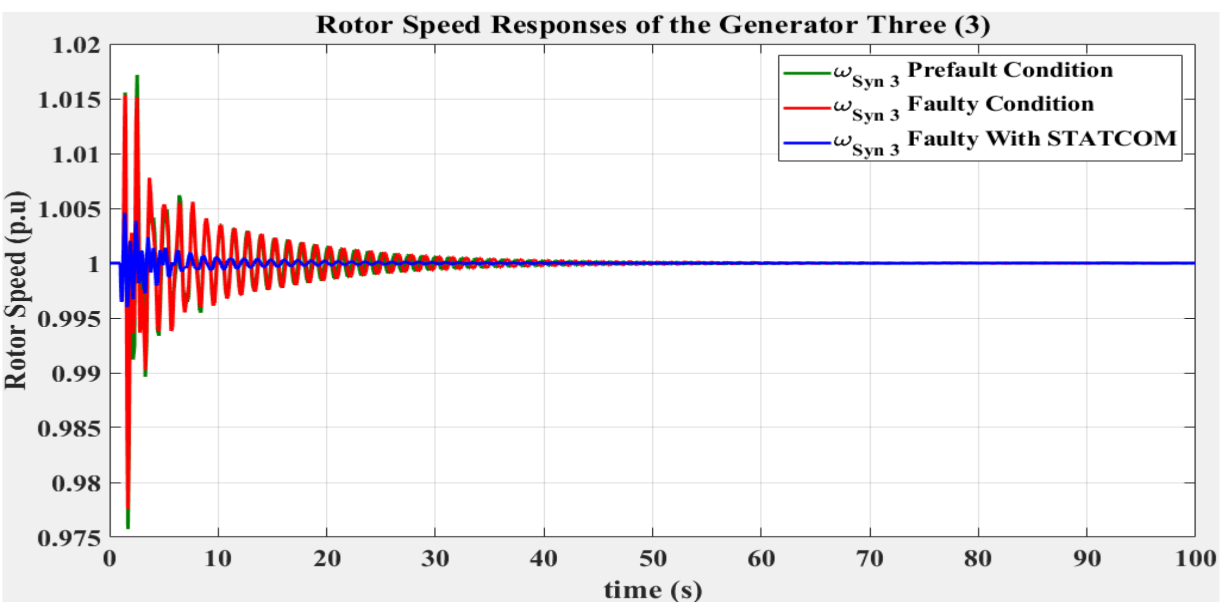


Figure 4.15: Rotor speed responses of the generator 3

**Real and Reactive Power Responses of the Generator 1**

Simulating the dynamic model with a fault applied at bus eight (8), a sudden load increase, and STATCOM placement determined by PSO shown by the blue curve in Figure 4.16, revealed that the STATCOM devices significantly damped the oscillations in the real power response. This damping effect was most prominent at approximately 60 seconds. When optimally placed and sized STATCOM are included in the model with a fault at bus eight (8) and a sudden load increase, the reactive power response stabilizes significantly faster as shown by the blue curve in Figure 4.17, reaching a steady state around 40 seconds. The STATCOM may not return reactive power and rotor angle to normal operating conditions immediately after a fault due to system dynamics and control strategies that prioritize stability and safety over rapid restoration to pre-fault levels. Grid conditions and protective mechanisms also influence the STATCOM's response, ensuring it adjusts gradually to maintain grid stability and equipment protection.

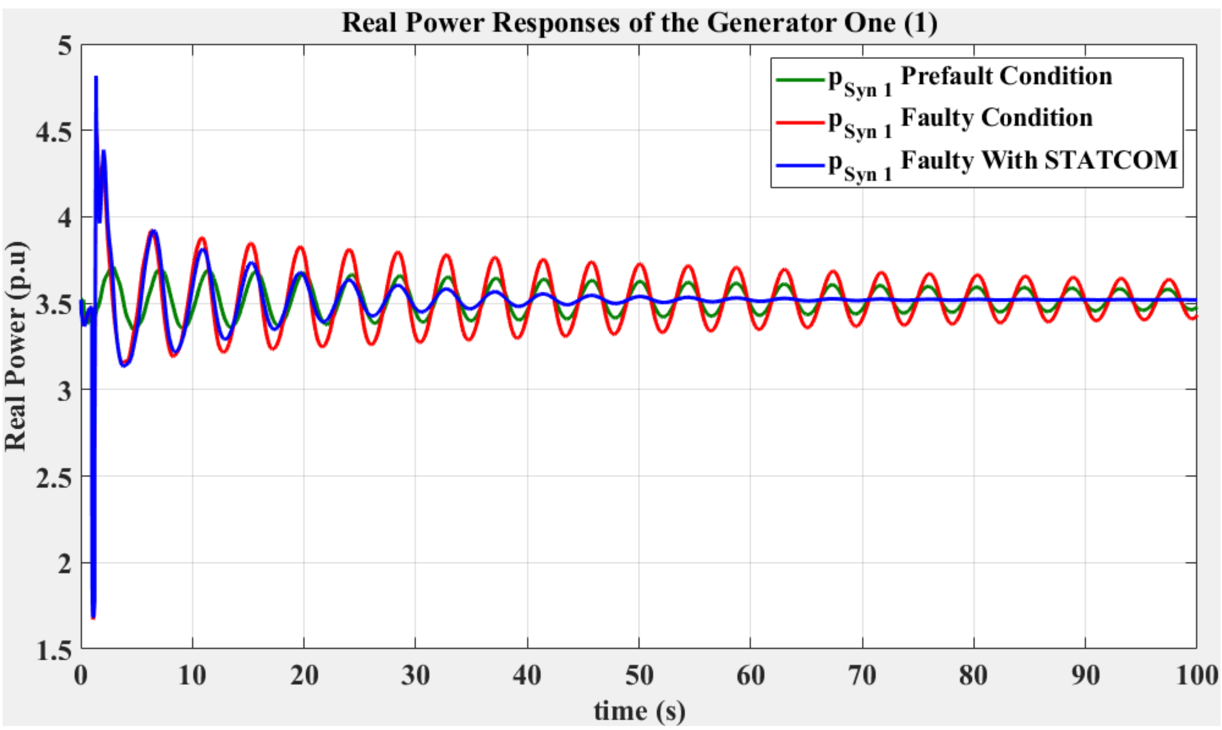


Figure 4.16: Real power responses of the generator 1

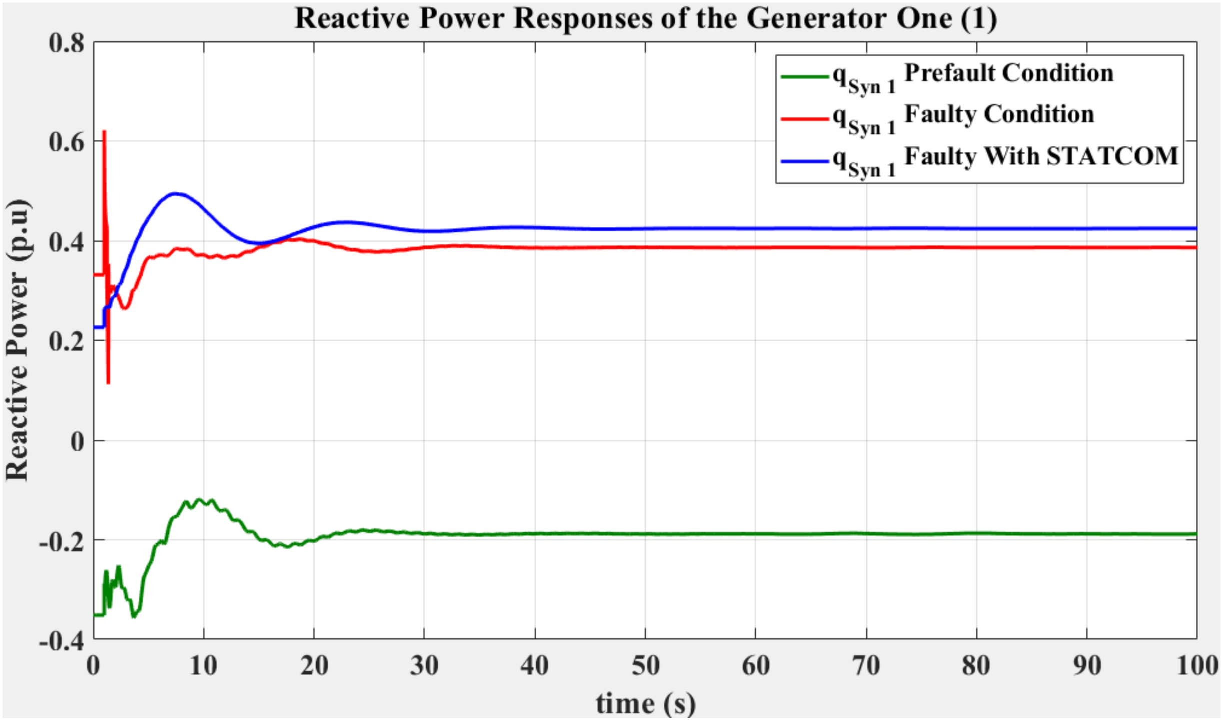


Figure 4.17: Reactive power responses of the generator 1

**Real and Reactive Power Responses of the Generator 2**

Simulating dynamic model with a fault applied at bus eight (8), a sudden load increase, and STATCOM placement determined by PSO as shown by the blue curve in Figure 4.18, revealed that the STATCOM FACTS devices significantly damped the oscillations in the real power response. This damping effect was most prominent at approximately 60 seconds. When optimally placed and sized STATCOM are included in the model with a fault at bus eight (8) and a sudden load increase, the reactive power response stabilizes significantly faster as shown by the blue curve in Figure 4.19, reaching a steady state around 30 seconds. The real power settles at a steady−state value of 0.4 p.u, which is the same as initial value.

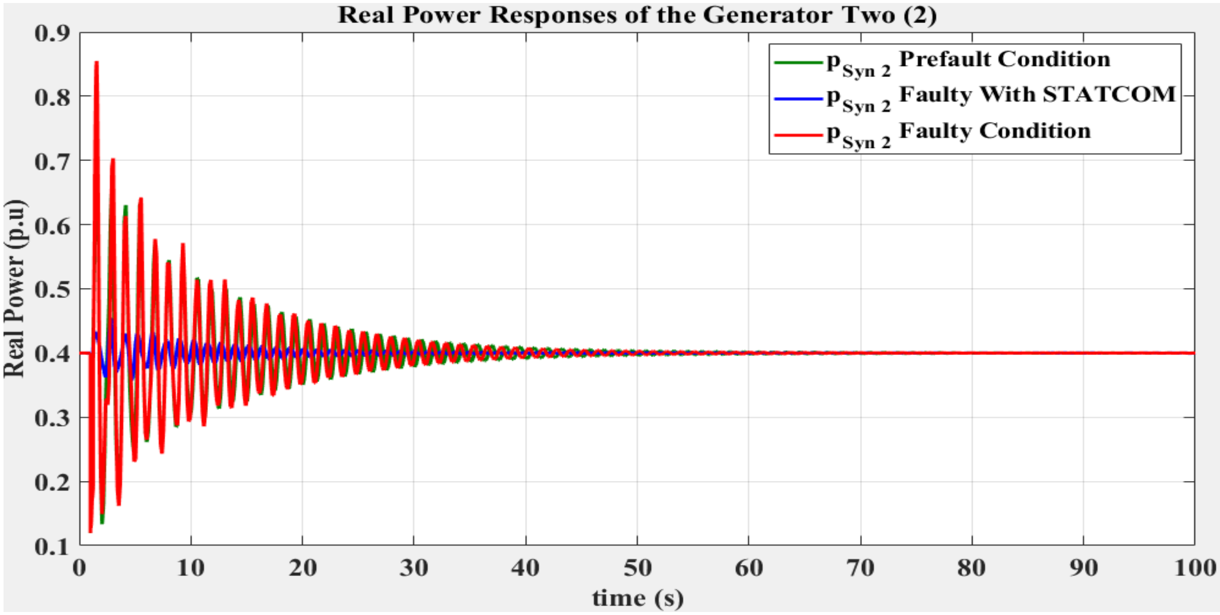


Figure 4.18: Real power responses of the generator 2

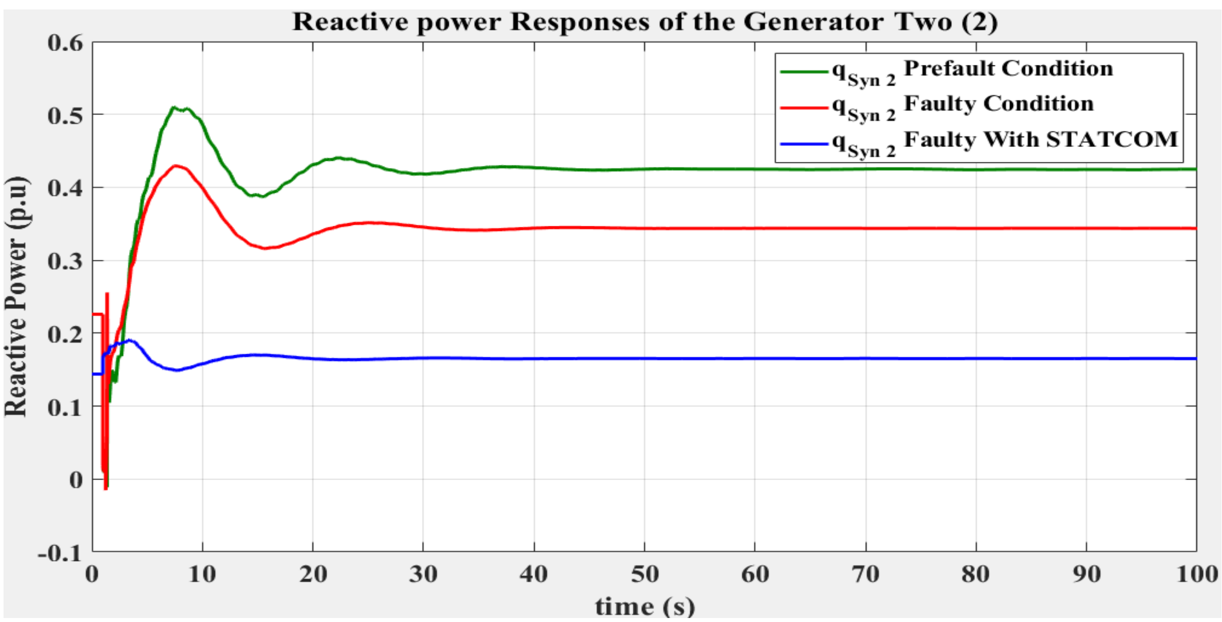


Figure 4.19: Reactive power responses of the generator 2

**Real and Reactive Power Response of the Generator 3**

Simulating dynamic model with a fault applied at bus eight (8), a sudden load increase, and STATCOM placement determined by PSO as shown by the blue curve in Figure 4.20, revealed that the STATCOM FACTS devices significantly damped the oscillations in the real power response. This damping effect was most prominent at approximately 30 seconds. When optimally placed and sized STATCOM are included in the model with a fault at bus eight (8) and a sudden load increase, the reactive power response stabilizes significantly faster as shown by the blue curve in Figure 4.21, reaching a steady state around 30 seconds.

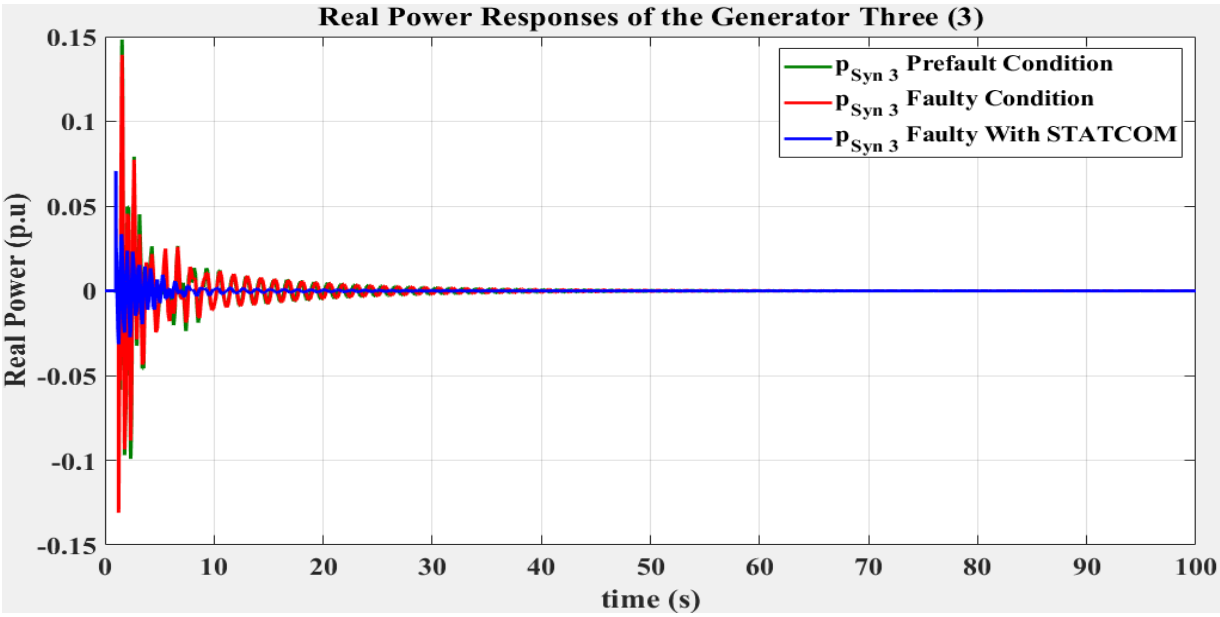


Figure 4.20: Real power responses of the generator 3

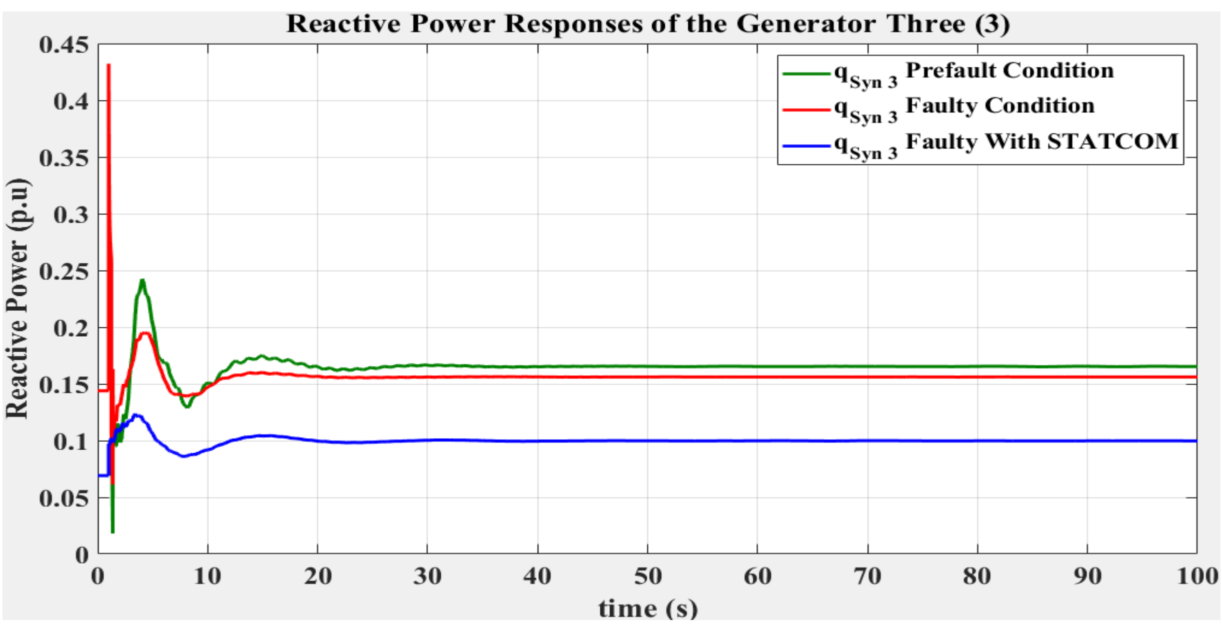


Figure 4.21: Reactive power responses of the generator 3

# CHAPTER FIVE

# 5 CONCLUSIONS AND RECOMMENDATIONS

## 5.1 CONCLUSIONS

The dynamic wind farm Adama II that represented as single turbine made up of 102 wind turbines coupled into IEEE 30-bus modified test network selected in this thesis. This thesis showed and examined STATCOM device location and size optimization. PSO utilized in order to determine the optimum location and size of STATCOM. The results showed that reduced power loss and improved voltage profile achieved with a PSO optimized STATCOM device were compared with the normal operating condition presented previously.

The overall voltage profile of the grid has been shown to have improved much more once PSO was implemented. In addition, the loss of active power was reduced by 0.5857 MW when STATCOM was allocated by PSO. This indicates after the STATCOM device was optimized with PSO, the active power was decreased by 6.50%. Similarly, the reactive power was reduced by 2.3355 MVAr, which corresponds to a total reduction of 7.157% when the STATCOM was optimally allocated. PSO enabled improved voltage profile and better loss minimization, resulting in minimum cost.

Time domain simulations were performed for wind farm Adama II connected into IEEE 30-bus modified network using MATLAB/PSAT under base case conditions, under faulted conditions, and under faulted conditions with PSO-placed STATCOM devices. The dynamic wind farm Adama II interlinked into IEEE 30-bus modified test network with PSO-placed STATCOM leads to a significant damping of grid oscillations and improvement in transient stability. STATCOM were most effective for damping the oscillations and improving transient stability of multiple-machine system with the most reduced settling time between 30 and 60 seconds.

## 5.2 RECOMMENDATIONS

The thesis work presented in this intends to expand research investigations into the dynamic analysis of power systems employing FACTS devices and makes a contribution to the field of study on power system stability in the near future. This work serves as a basis for suggestions about the creation of new work initiatives. In order to achieve transient stability with other FACTS devices, future study should incorporate models of renewable energy generators, such as solar arrays. The comparative performance of independent and integrated models of other FACTS devices needs to be investigated. The ability of an optimized STATCOM device to minimize bus voltage deviation and reduce grid losses showed how competent and naturally capable this controller is at influencing the grid parameters to meet the desired system objectives in a steady-state environment. Future research comparing the effectiveness of other FACTS controllers and STATCOM controllers under various fault scenarios have to be taken into account. Various techniques of optimization for optimum sizing and locating of STATCOM controllers, such as the tabu search algorithm, cuckoo search algorithm, ant colony, genetic algorithm and others, should be investigated in the power transmission system, analyzed, and contrasted with this finding works.

## 5.3 FUTURE WORKS

Future work in the area of improving transient stability using STATCOM based on PSO, particularly in the context of the IEEE 30-bus test system integrated into the Adama II wind farm, includes the need to evaluate the robustness of the control strategy to uncertainties associated with renewable energy sources and grid disturbances. Optimal allocation strategies for STATCOMs within the grid, taking into account the grid topology and renewable energy characteristics, need to be further investigated, as well as the development of dynamic models for wind farms to accurately capture their transient behavior. In addition, exploring adaptive control strategies, coordinating with other FACTS devices and addressing cyber-security concerns are essential for practical deployment and ensuring grid resilience. Field validation studies are necessary to evaluate the scalability and effectiveness of the proposed methodology in real-world applications.

# REFERENCES


Biswas, P. P., Arora, P., Mallipeddi, R., Suganthan, P. N., & Panigrahi, B. K. (2021). Optimal placement and sizing of facts devices for optimal power flow in a wind power integrated electrical network. *Neural Computing and Applications*, *33*, 6753-6774.

Din, Z., Zhang, J., Xu, Z., Zhang, Y., & Song, Y. (2022). Impact of dead-time on resonance in doubly fed induction generator system under weak grid. *CSEE Journal of Power and Energy Systems*. doi: https://doi.org/10.17775/CSEEJPES.2021.00760

Eajal, A. A., & El-Hawary, M. E. (2010). Optimal capacitor placement and sizing in unbalanced distribution systems with harmonics consideration using particle swarm optimization. *IEEE transactions on power delivery*, *25*, 1734-1741.

Fogel, D. B. (2006). *Evolutionary computation: toward a new philosophy of machine intelligence*. John Wiley & Sons.

Georgilakis, P. S. (2008). Technical challenges associated with the integration of wind power into power systems. *Renewable and Sustainable Energy Reviews*, *12*, 852-863.

Hemeida, A. M., Hamada, M. M., Mobarak, Y. A., El-Bahnasawy, A., Ashmawy, M. G., & Senjyu, T. (2020). Tcsc with auxiliary controls based voltage and reactive power controls on grid power system. *Ain Shams Engineering Journal*, *11*, 587-609.

Hingorani, N. G., & Gyugyi, L. (2000). *Understanding facts: concepts and technology of flexible ac transmission systems*. Wiley-IEEE Press.

Hong, Y.-Y., & Nguyen, M.-T. (2018). Optimal design of it2-fcs-based statcom controller applied to power system with wind farms using taguchi method. *IET Generation, Transmission & Distribution*, *12*, 3145-3151.

Jamil, E., Hameed, S., et al. (2019, 10). Mitigation of power system transients in a multi-machine system using unified power flow controller. In (p. 119-124).

Jember, Y. B., Workineh, T. G., Yetayew, T. T., & Dinkayow, M. (2024). Application of facts devices for transient stability enhancement in the adama ii grid-connected wind farm.. doi: 10.1007/978-3-031-41173-1_1

Khan, M. M., Husain, T., & Ansari, M. M. (2017). Stability enhancement in multimachine power system by facts controller. *Proceedings - International Conference on Global Trends in Signal Processing, Information Computing and Communication, ICGTSPICC 2016*, 414-418. doi: 10.1109/ICGTSPICC.2016.7955337

Kumar, S. (2019). Stability Improvement of Multi-Machine Power System Network using STATCOM and UPFC. *International Journal for Research in Applied Science and Engineering Technology*, *7*, 179-188. doi: 10.22214/ijraset.2019.10030

Kundur, P., Paserba, J., Ajjarapu, V., Andersson, G., Bose, A., Canizares, C., ... others (2004). Definition and classification of power system stability ieee/cigre joint task force on stability terms and definitions. *IEEE transactions on Power Systems*, *19*, 1387-1401.

Latt, A. Z. (2019, 12). Transient stability analysis of 3-machine 7-bus system using etap. *sTA*, *1*, 1.

Ledesma, P., & Usaola, J. (2005). Doubly fed induction generator model for transient stability analysis. *IEEE transactions on energy conversion*, *20*, 388-397.

Liang, X., Li, W., Zhang, Y., Zhong, Y., & Zhou, M. (2013). Recent advances in particle swarm optimization via population structuring and individual behavior control. In (p. 503-508).

Mahapatra, S., & Jha, A. N. (2014). Modeling and simulation of tcsc based controller in a multi machine power system. In (p. 1-6).

Majumdar, S., Chakraborty, A. K., & Chattopadhyay, P. K. (2009). Active power loss minimization with facts devices using sa/pso techniques. In (p. 1-5).

Mastoi, M. S., Zhuang, S., Haris, M., Hassan, M., & Ali, A. (2023). Large-scale wind power grid integration challenges and their solution: a detailed review. *Environmental Science and Pollution Research*, *30*, 103424-103462. Retrieved from `https://doi.org/10.1007/s11356-023-29653-9` doi: 10.1007/s11356-023-29653-9

Mathur, R. M., & Varma, R. K. (2002). *Thyristor-based facts controllers for electrical transmission systems*. John Wiley & Sons.

Mesfin, M. (2017). *Impact of large scale wind power integration non ethiopian power system transient stability* (Unpublished doctoral dissertation). ASTU.

Nkan, I. E., Okpo, E. E., & Okoro, O. I. (2021). Multi-type facts controllers for power system compensation: A case study of the nigerian 48-bus, 330 kv system. *Nigerian Journal of Technological Development*, *18*, 63-69.

Okelola, M. O., Ayanlade, S. O., & Ogunwole, E. I. (2021). Particle swarm optimization for optimal allocation of statcom on transmission network. In (Vol. 1880, p. 12035). doi: http://dx.doi.org/10.1088/1742-6596/1880/1/012035

Operator, A. E. M. (2013). Wind turbine plant capabilities report. *Wind Integration Studies*.

Oukennou, A., Sandali, A., & Elmoumen, S. (2018). Coordinated placement and setting of facts in electrical network based on kalai-smorodinsky bargaining solution and voltage deviation index. *International Journal of Electrical & Computer Engineering (2088-8708)*, *8*.

Patil, V., Jadhav, A. S., Nandakumara, C., Pawar, R. V., Koluragi, V., & Gadad, S. (2023). Optimization of power system transients in a multi-machine system using unified power flow controller. In (p. 385-390).

Rajderkar, V. P., & Chandrakar, V. K. (2023). *Design coordination of a fuzzy-based unified power flow controller with hybrid energy storage for enriching power system dynamics* (Vol. 13). Retrieved from www.etasr.com

Ramlochun, B., Vaithilingam, C. A., Alsakati, A. A., & Alnasseir, J. (2021, 12). Transient stability analysis of ieee 9-bus system integrated with dfig and scig based wind turbines. In (Vol. 2120). IOP Publishing Ltd. doi: 10.1088/1742-6596/2120/1/012023

Rani, M. P. Y. G. (2020). Comparison of enhancement of power system transient stability with various facts devices. *International Journal of Scientific Development and Research (IJSDR)*, *5*, 79-85.

Sadati, N., Zamani, M., & Mahdavian, H. R. F. (2006). Hybrid particle swarm-based-simulated annealing optimization techniques. In (p. 644-648).

Sharma, S., Bhardwaj, A., & Nawaz, S. (2022). Voltage stability enhancement by optimal allocation of statcom and svc. *SKIT Research Journal*. doi: https://doi.org/10.47904/IJSKIT.12.1.2022.58-64

Siddula, S., Achyut, T. V., Vigneshwar, K., & Teja, M. V. U. (2020). Improvement of power quality using fuzzy based unified power flow controller. *Proceedings of the International Conference on Smart Technologies in Computing, Electrical and Electronics, ICSTCEE 2020*, 55-60. doi: 10.1109/ICSTCEE49637.2020.9276496

Singh, M., & Santoso, S. (2011). *Dynamic models for wind turbines and wind power plants.*

Sirjani, R., Mohamed, A., & Shareef, H. (2012). Optimal allocation of shunt var compensators in power systems using a novel global harmony search algorithm. *International Journal of Electrical Power & Energy Systems*, *43*, 562-572. doi: http://doi.org/10.1016/j.ijepes.2012.05.068

Suliman, M. Y. (2020). Voltage profile enhancement in distribution network using static synchronous compensator statcom. *International Journal of Electrical and Computer Engineering*, *10*, 3367-3374. doi: 10.11591/ijece.v10i4.pp3367-3374

Sutter1, J. N. N. J. R., & Muriithi3, C. (2015). Power system oscillations damping and transient stability enhancement with application of sssc facts devices. *European Journal of Advances in Engineering and Technology*, *2*, 73-79.

Tavoosi, J., Mohammadzadeh, A., Pahlevanzadeh, B., Kasmani, M. B., Band, S. S., Safdar, R., & Mosavi, A. H. (2022). A machine learning approach for active/reactive power control of grid-connected doubly-fed induction generators. *Ain Shams Engineering Journal*, *13*, 101564.

# APPENDICES

## A. 1 IEEE 30-Bus System Single Line Diagram

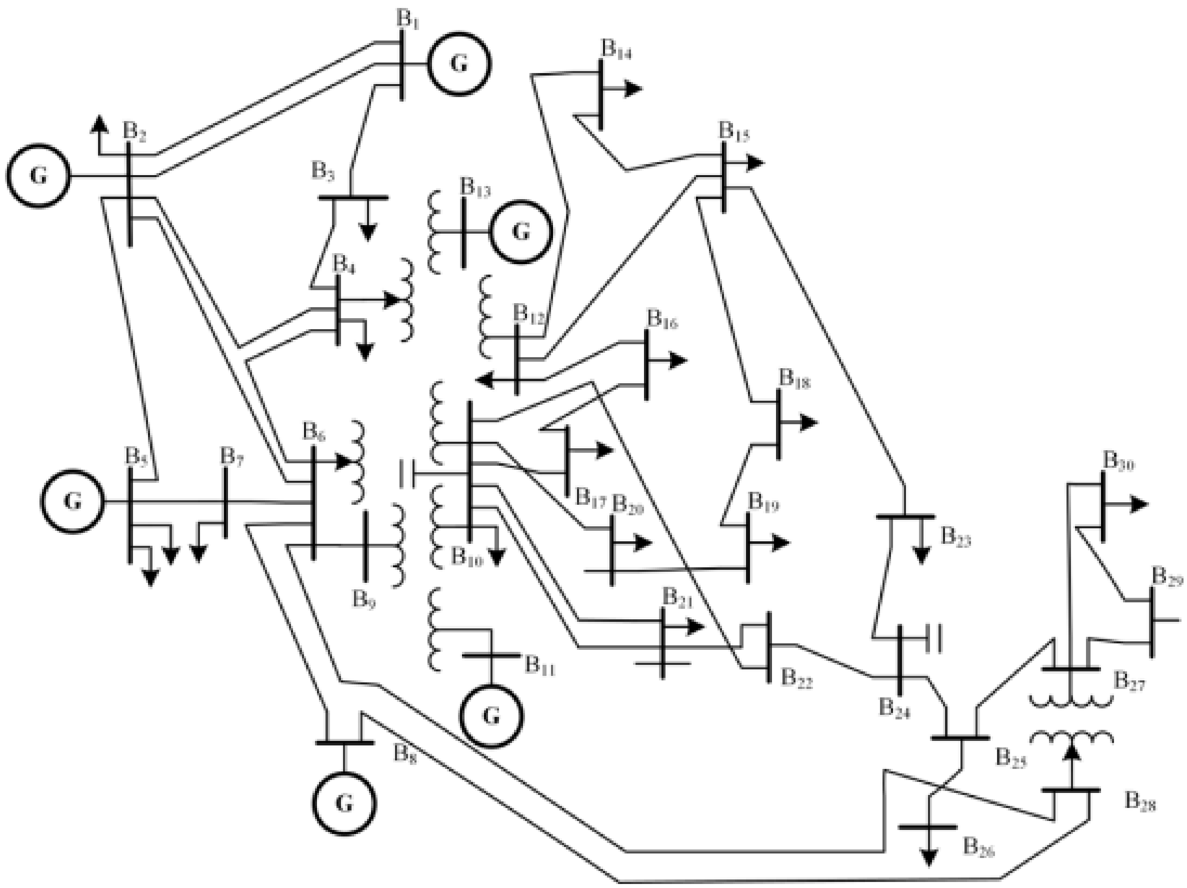

## A. 2 IEEE 30-Bus Test System Bus Data

| **Bus No** | **Type** | **$V_m$** | **Theta** | **$PG_i$** | **$QG_i$** | **$PL_i$** | **$QL_i$** | **$QG_{min}$** | **$QG_{max}$** |
|---|---|---|---|---|---|---|---|---|---|
| | | **P.U** | **rad** | **MW** | **MVAR** | **MW** | **MVAR** | **MVAR** | **MVAR** |
| 1 | 1 | 1.06 | 0 | 0 | 0 | 0 | 0 | 0 | 0 |
| 2 | 2 | 1.043 | 0 | 40 | 50.0 | 21.7 | 12.7 | -40 | 50 |
| 3 | 3 | 1.0 | 0 | 0 | 0 | 2.4 | 1.2 | 0 | 0 |
| 4 | 3 | 1.0 | 0 | 0 | 0 | 7.6 | 1.6 | 0 | 0 |
| 5 | 2 | 1.01 | 0 | 0 | 37.0 | 94.2 | 19.0 | -40 | 40 |
| 6 | 3 | 1.0 | 0 | 0 | 0 | 0.0 | 0.0 | 0 | 0 |
| 7 | 3 | 1.0 | 0 | 0 | 0 | 22.8 | 10.9 | 0 | 0 |
| 8 | 2 | 1.01 | 0 | 0 | 37.3 | 30.0 | 30.0 | -10 | 40 |
| 9 | 3 | 1.0 | 0 | 0 | 0 | 0.0 | 0.0 | 0 | 0 |
| 10 | 3 | 1.0 | 0 | 0 | 0 | 5.8 | 2.0 | 0 | 0 |
| 11 | 2 | 1.082 | 0 | 0 | 16.2 | 0.0 | 0.0 | -6 | 24 |
| 12 | 3 | 1.0 | 0 | 0 | 0 | 11.2 | 7.5 | 0 | 0 |
| 13 | 2 | 1.071 | 0 | 0 | 10.6 | 0.0 | 0.0 | -6 | 24 |
| 14 | 3 | 1.0 | 0 | 0 | 0 | 6.2 | 1.6 | 0 | 0 |
| 15 | 3 | 1.0 | 0 | 0 | 0 | 8.2 | 2.5 | 0 | 0 |
| 16 | 3 | 1.0 | 0 | 0 | 0 | 3.5 | 1.8 | 0 | 0 |
| 17 | 3 | 1.0 | 0 | 0 | 0 | 9.0 | 5.8 | 0 | 0 |
| 18 | 3 | 1.0 | 0 | 0 | 0 | 3.2 | 0.9 | 0 | 0 |
| 19 | 3 | 1.0 | 0 | 0 | 0 | 9.5 | 3.4 | 0 | 0 |
| 20 | 3 | 1.0 | 0 | 0 | 0 | 2.2 | 0.7 | 0 | 0 |
| 21 | 3 | 1.0 | 0 | 0 | 0 | 17.5 | 11.2 | 0 | 0 |
| 22 | 3 | 1.0 | 0 | 0 | 0 | 0.0 | 0.0 | 0 | 0 |
| 23 | 3 | 1.0 | 0 | 0 | 0 | 3.2 | 1.6 | 0 | 0 |
| 24 | 3 | 1.0 | 0 | 0 | 0 | 8.7 | 6.7 | 0 | 0 |
| 25 | 3 | 1.0 | 0 | 0 | 0 | 0.0 | 0.0 | 0 | 0 |
| 26 | 3 | 1.0 | 0 | 0 | 0 | 3.5 | 2.3 | 0 | 0 |
| 27 | 3 | 1.0 | 0 | 0 | 0 | 0.0 | 0.0 | 0 | 0 |
| 28 | 3 | 1.0 | 0 | 0 | 0 | 0.0 | 0.0 | 0 | 0 |
| 29 | 3 | 1.0 | 0 | 0 | 0 | 2.4 | 0.9 | 0 | 0 |
| 30 | 3 | 1.0 | 0 | 0 | 0 | 10.6 | 1.9 | 0 | 0 |

## A. 3 IEEE 30-Bus System Line Data

| Line No | From Bus | To Bus | R [P.U] | X [P.U] | $B_{sh}$[P.U] | Tap Set. |
|---|---|---|---|---|---|---|
| 1 | 1 | 2 | 0.0192 | 0.0575 | 0.0264 | 1 |
| 2 | 1 | 3 | 0.0452 | 0.1652 | 0.0204 | 1 |
| 3 | 2 | 4 | 0.0570 | 0.1737 | 0.0184 | 1 |
| 4 | 3 | 4 | 0.0132 | 0.0379 | 0.0042 | 1 |
| 5 | 2 | 5 | 0.0472 | 0.1983 | 0.0209 | 1 |
| 6 | 2 | 6 | 0.0581 | 0.1763 | 0.0187 | 1 |
| 7 | 4 | 6 | 0.0119 | 0.0414 | 0.0045 | 1 |
| 8 | 5 | 7 | 0.0460 | 0.1160 | 0.0102 | 1 |
| 9 | 6 | 7 | 0.0267 | 0.0820 | 0.0085 | 1 |
| 10 | 6 | 8 | 0.0120 | 0.0420 | 0.0045 | 1 |
| 11 | 6 | 9 | 0.0 | 0.2080 | 0.0 | 1.0155 |
| 12 | 6 | 10 | 0.0 | 0.5560 | 0.0 | 0.9629 |
| 13 | 9 | 11 | 0.0 | 0.2080 | 0.0 | 1 |
| 14 | 9 | 10 | 0.0 | 0.1100 | 0.0 | 1 |
| 15 | 4 | 12 | 0.0 | 0.2560 | 0.0 | 1.0129 |
| 16 | 12 | 13 | 0.0 | 0.1400 | 0.0 | 1 |
| 17 | 12 | 14 | 0.1231 | 0.2559 | 0.0 | 1 |
| 18 | 12 | 15 | 0.0662 | 0.1304 | 0.0 | 1 |
| 19 | 12 | 16 | 0.0945 | 0.1987 | 0.0 | 1 |
| 20 | 14 | 15 | 0.2210 | 0.1997 | 0.0 | 1 |
| 21 | 16 | 17 | 0.0824 | 0.1923 | 0.0 | 1 |
| 22 | 15 | 18 | 0.1073 | 0.2185 | 0.0 | 1 |
| 23 | 18 | 19 | 0.0639 | 0.1292 | 0.0 | 1 |
| 24 | 19 | 20 | 0.0340 | 0.0680 | 0.0 | 1 |
| 25 | 10 | 20 | 0.09360 | 0.2090 | 0.0 | 1 |
| 26 | 10 | 17 | 0.0324 | 0.0845 | 0.0 | 1 |
| 27 | 10 | 21 | 0.0348 | 0.0749 | 0.0 | 1 |
| 28 | 10 | 22 | 0.0727 | 0.1499 | 0.0 | 1 |
| 29 | 21 | 23 | 0.0116 | 0.0236 | 0.0 | 1 |
| 30 | 15 | 23 | 0.1000 | 0.2020 | 0.0 | 1 |
| 31 | 22 | 24 | 0.1150 | 0.1790 | 0.0 | 1 |
| 32 | 23 | 24 | 0.1320 | 0.2700 | 0.0 | 1 |
| 33 | 24 | 25 | 0.1885 | 0.3292 | 0.0 | 1 |

Continued on next page

Continued from previous page

| **Line No** | **From Bus** | **To Bus** | **R [P.U]** | **X [P.U]** | **$B_{sh}$[P.U]** | **Tap Set.** |
|---|---|---|---|---|---|---|
| 34 | 25 | 26 | 0.2544 | 0.3800 | 0.0 | 1 |
| 35 | 25 | 27 | 0.1093 | 0.2087 | 0.0 | 1 |
| 36 | 28 | 27 | 0.0000 | 0.3960 | 0.0 | 0.9581 |
| 37 | 27 | 29 | 0.2198 | 0.4153 | 0.0 | 1 |
| 38 | 27 | 30 | 0.3202 | 0.6027 | 0.0 | 1 |
| 39 | 29 | 30 | 0.2399 | 0.4533 | 0.0 | 1 |
| 40 | 8 | 28 | 0.0636 | 0.2000 | 0.0214 | 1 |
| 41 | 6 | 28 | 0.0169 | 0.0599 | 0.065 | 1 |

## A. 4 Double-fed induction generator data with variable speed wind turbine data

| | |
|---|---|
| Rated power (MVA) | 153 |
| Rated voltage (KV) | 690 |
| Rated frequency (Hz) | 50 |
| Stator Resistance $R_r$ and Reactance $X_r$ (p.u) | [0.01 0.10] |
| Rotor Resistance $R_r$ and Reactance $X_r$ (p.u) | [0.01 0.08] |
| Magnetization Reactance $X_m$ (p.u) | 3 |
| Inertia constants $H_m$ (KWs/KVA) | 3 |
| Gain in pitch control $K_p$ (p.u) | 10 |
| Time constant $T_p$ (s) | 3 |
| Gain in voltage control $K_v$ (p.u) | 10 |
| Time constant for power control $T_e$ (s) | 0.01 |
| Number of poles $P$ | 4 |
| Gear box ratio | [1/89] |
| Blade Length | [75.00 3] |
| $P_{max}$, $P_{min}$ (p.u) | [1.00 0.00] |
| $Q_{max}$, $Q_{min}$ (p.u) | [0.7 -0.7] |
| The number of wind turbines in the park | 102 |

## A. 5 Static Synchronous Compensator (STATCOM) Data

| | |
|---|---|
| Rated Power (MVA) | 100.0 |
| Rated Voltage (kV) | 13.80 |
| Rated Frequency (Hz) | 50.0 |
| Gain kr | 50.0 |
| Current control time constant $T_r$ $(p.u/p.us)$ | 0.10 |
| Max. Current (p.u) | 0.50 |
| Min. Current (p.u) | −0.5 |

## A. 6 IEEE 30-Bus Modified Test System Compensator Data

| **Compensator** | **Comp. 1** | **Comp. 2** | **Comp. 3** | **Comp. 4** | **Comp. 5** |
|---|---|---|---|---|---|
| Power ratings (MVA) | 100.0 | 100.0 | 100.0 | 100.0 | 100.0 |
| Voltage ratings (kV) | 132.0 | 132.0 | 132.0 | 33.0 | 33.0 |
| Magnitude of voltage $(p.u)$ | 1.043 | 1.01 | 1.01 | 1.082 | 1.071 |
| Maximum reactive power $(Q_{max}(p.u))$ | 0.5 | 0.4 | 0.4 | 0.24 | 0.24 |
| Minimum reactive power $(Q_{min}(p.u))$ | -0.4 | -0.4 | -0.1 | -0.06 | -0.06 |
| Maximum Voltage $(V_{max}(p.u))$ | 1.2 | 1.2 | 1.2 | 1.2 | 1.2 |
| Minimum Voltage $(V_{min}(p.u))$ | 0.8 | 0.8 | 0.8 | 0.8 | 0.8 |
| Loss Participation Coefficients | 1 | 1 | 1 | 1 | 1 |

## A. 7 Turbine Governor Data for the IEEE 30-Bus Modified Test System

| **Type** | **BPA-GG** | **BPA-GG** |
|---|---|---|
| **Bus Number** | **1(31)** | **2(32)** |
| Power rating (MVA) | 270.0 | 51.20 |
| Voltage rating (kV) | 18.0 | 13.80 |
| Maximum power output of the turbine $P_{max}$ (p.u) | 0.85180 | 1.0350 |
| Stabilization or droop of the turbine in steady state R (p.u) | 0.01850 | 0.15230 |
| Governor delay (control time constant) $T_1$ (s) | 0.10 | 0.20 |
| Time constant of hydro reset $T_2$ (s) | 0.0 | 0.0 |
| Time constant of servo $T_3$ (s) | 0.2590 | 0.30 |
| Time constant of Steam valve bowl $T_4$ (s) | 0.10 | 0.09 |
| Time constant of steam reheat $T_5$ (s) | 10.0 | 0.0 |
| Output shaft ahead the reheater F | 0.272 | 1.000 |

## A. 8 Synchronous Machine Data for the IEEE 30-Bus Modified Test System

| GENERATOR | G1 | G2 | G3 | G4 |
|---|---|---|---|---|
| **Bus Number** | **1** | **2** | **5,8** | **11,13** |
| Power rating (MVA) | 270 | 51.2 | 40 | 25 |
| Voltage rating (kV) | 18 | 13.8 | 13.8 | 13.8 |
| Power factor rating | 0.85 | 0.8 | 0.0 | 0.0 |
| Inertia constant $H(s)$ | 4.130 | 5.078 | 1.520 | 1.200 |
| Damping coefficient $D$ | 2.000 | 2.000 | 0.000 | 0.000 |
| Armature resistance $r_a$(p.u) | 0.0016 | 0.000 | 0.000 | 0.0025 |
| $d_{axis}$ synchronous reactance $x_d$(p.u) | 1.700 | 1.270 | 2.373 | 1.769 |
| $q_{axis}$ synchronous reactance $x_q$(p.u) | 1.620 | 1.240 | 1.172 | 0.855 |
| $d_{axis}$ transient reactance $x'_d$(p.u) | 0.256 | 0.209 | 0.343 | 0.304 |
| $q_{axis}$ transient reactance $x'_q$(p.u) | 0.245 | 0.850 | 1.172 | 0.5795 |
| $d_{axis}$ subtransient reactance $x''_d$(p.u) | 0.185 | 0.116 | 0.231 | 0.2035 |
| $q_{axis}$ subtransient reactance $x''_q$(p.u) | 0.185 | 0.116 | 0.231 | 0.2035 |
| Leakage reactance $x_l$(p.u) | 0.155 | 0.108 | 0.132 | 0.1045 |
| $d_{axis}$ transient OC time constant $T'_{do}$(s) | 4.800 | 6.600 | 11.600 | 8.000 |
| $q_{axis}$ transient OC time constant $T'_{qo}$(s) | 0.004 | 0.004 | 0.159 | 0.008 |
| $d_{axis}$ subtransient OC time constant $T''_{do}$(s) | 0.004 | 0.004 | 0.058 | 0.0525 |
| $q_{axis}$ subtransient OC time constant $T''_{qo}$(s) | 0.004 | 0.004 | 0.201 | 0.0151 |

## A. 9 Automatic Voltage Regulator Data for IEEE 30-Bus Modified Test System

| Type | IEEET1 | IEEET1 | IEEET1 | IEEET1 |
|---|---|---|---|---|
| **Bus Number** | **1** | **2** | **5, 8** | **11, 13** |
| Power rating (MVA) | 270 | 51.2 | 40 | 25 |
| Voltage rating (kV) | 18 | 13.8 | 13.8 | 13.8 |
| Filter time constant for regulator input $T_r$ (s) | 0.001 | 0.001 | 0.001 | 0.001 |
| Gain for regulators $K_a$ (p.u) | 30 | 400 | 400 | 400 |
| Time constant for regulators (s) | 0.400 | 0.050 | 0.050 | 0.050 |
| Maximum output of the regulator $VR_{max}$(p.u) | 4.590 | 0.613 | 6.630 | 4.407 |
| Minimum output of the regulator $VR_{min}$(p.u) | -4.590 | -0.613 | -6.630 | -4.407 |
| Self-excitation exciter $K_e$ (p.u) | -0.02 | -0.0769 | -0.170 | -0.170 |
| Time constant of exciter $T_e$ (s) | 0.560 | 1.370 | 0.950 | 0.950 |
| Circuit gain stabilizing regulator $K_f$ (p.u) | 0.050 | 0.040 | 0.040 | 0.040 |
| Circuit time constant of regulator stabilizing $T_f$ | 1.300 | 1.000 | 1.000 | 1.000 |
| Field voltage value,1 in p.u. E1 | 2.5875 | 3.0975 | 6.375 | 4.2375 |
| Field voltage value,2 in p.u. E2 | 3.450 | 4.130 | 8.500 | 5.650 |

## A. 10 Results of Power Flow for IEEE 30 bus system for faulty condition in PSAT

| Bus | V [p.u.] | Phase [rad] | P gen [p.u.] | Q gen [p.u.] | P load [p.u.] | Q load [p.u.] |
|---|---|---|---|---|---|---|
| Bus 1 | 1.06000 | 0.00000 | 3.5203 | −0.35115 | 0.00000 | 0.00000 |
| Bus 10 | 1.04936 | −0.27242 | 0.00000 | 0.00000 | 0.05800 | −0.18922 |
| Bus 11 | 1.08200 | −0.24481 | 0.00000 | 0.14390 | 0.00000 | 0.00000 |
| Bus 12 | 1.06196 | −0.25999 | 0.00000 | 0.00000 | 0.11200 | 0.07500 |
| Bus 13 | 1.07100 | −0.25999 | 0.00000 | 0.06914 | 0.00000 | 0.00000 |
| Bus 14 | 1.04711 | −0.27535 | 0.00000 | 0.00000 | 0.06200 | 0.01600 |
| Bus 15 | 1.04247 | −0.27684 | 0.00000 | 0.00000 | 0.08200 | 0.02500 |
| Bus 16 | 1.04903 | −0.26977 | 0.00000 | 0.00000 | 0.03500 | 0.01800 |
| Bus 17 | 1.04428 | −0.27534 | 0.00000 | 0.00000 | 0.09000 | 0.05800 |
| Bus 18 | 1.03281 | −0.28730 | 0.00000 | 0.00000 | 0.03200 | 0.00900 |
| Bus 19 | 1.03021 | −0.29021 | 0.00000 | 0.00000 | 0.09500 | 0.03400 |
| Bus 2 | 1.04500 | −0.09292 | 0.40000 | 0.45404 | 0.21700 | 0.12700 |
| Bus 20 | 1.03422 | −0.28675 | 0.00000 | 0.00000 | 0.02200 | 0.00700 |
| Bus 21 | 1.03705 | −0.28010 | 0.00000 | 0.00000 | 0.17500 | 0.11200 |
| Bus 22 | 1.03760 | −0.27986 | 0.00000 | 0.00000 | 0.00000 | 0.00000 |
| Bus 23 | 1.03188 | −0.28344 | 0.00000 | 0.00000 | 0.03200 | 0.01600 |
| Bus 24 | 1.02613 | −0.28628 | 0.00000 | 0.00000 | 0.08700 | 0.02172 |
| Bus 25 | 1.02185 | −0.27864 | 0.00000 | 0.00000 | 0.00000 | 0.00000 |
| Bus 26 | 1.00425 | −0.28590 | 0.00000 | 0.00000 | 0.03500 | 0.02300 |
| Bus 27 | 1.02769 | −0.26942 | 0.00000 | 0.00000 | 0.00000 | 0.00000 |
| Bus 28 | 1.01085 | −0.20254 | 0.00000 | 0.00000 | 0.00000 | 0.00000 |
| Bus 29 | 1.00795 | −0.29070 | 0.00000 | 0.00000 | 0.02400 | 0.00900 |
| Bus 3 | 1.04500 | −0.13703 | 0.00000 | 0.45862 | 0.02400 | 0.01200 |
| Bus 30 | 0.99653 | −0.30596 | 0.00000 | 0.00000 | 0.10600 | 0.01900 |
| Bus 4 | 1.02499 | −0.16330 | 0.00000 | 0.00000 | 0.07600 | 0.01600 |
| Bus 5 | 1.01000 | −0.24499 | 0.00000 | 0.33141 | 0.94200 | 0.19000 |
| Bus 6 | 1.01544 | −0.19202 | 0.00000 | 0.00000 | 0.00000 | 0.00000 |
| Bus 7 | 1.00547 | −0.22293 | 0.00000 | 0.00000 | 0.22800 | 0.10900 |
| Bus 8 | 1.01000 | −0.20354 | 0.00000 | 0.22600 | 0.30000 | 0.30000 |
| Bus 9 | 1.05434 | −0.24481 | 0.00000 | 0.00000 | 0.00000 | 0.00000 |

## A. 11 Results of Power Flow for IEEE 30 bus system for faulty with PSO-placed STATCOM in PSAT

| Bus | V | Phase | P gen | Q gen | P load | Q load |
|---|---|---|---|---|---|---|
| | [p.u.] | [rad] | [p.u.] | [p.u.] | [p.u.] | [p.u.] |
| Bus 1 | 1.06000 | 0.00000 | 3.5203 | −0.57826 | 0.00000 | 0.00000 |
| Bus 10 | 1.02760 | −0.39716 | 0.00000 | 0.00000 | 0.08120 | −0.17263 |
| Bus 11 | 1.08200 | −0.35763 | 0.00000 | 0.21089 | 0.00000 | 0.00000 |
| Bus 12 | 1.04881 | −0.37982 | 0.00000 | 0.00000 | 0.15680 | 0.10500 |
| Bus 13 | 1.07100 | −0.37982 | 0.00000 | 0.16977 | 0.00000 | 0.00000 |
| Bus 14 | 1.02706 | −0.40191 | 0.00000 | 0.00000 | 0.08680 | 0.02240 |
| Bus 15 | 1.02004 | −0.40379 | 0.00000 | 0.00000 | 0.11480 | 0.03500 |
| Bus 16 | 1.02895 | −0.39356 | 0.00000 | 0.00000 | 0.04900 | 0.02520 |
| Bus 17 | 1.02087 | −0.40155 | 0.00000 | 0.00000 | 0.12600 | 0.08120 |
| Bus 18 | 1.00522 | −0.41911 | 0.00000 | 0.00000 | 0.04480 | 0.01260 |
| Bus 19 | 1.00097 | −0.42337 | 0.00000 | 0.00000 | 0.13300 | 0.04760 |
| Bus 2 | 1.04500 | −0.14318 | 0.40000 | 0.86692 | 0.30380 | 0.17780 |
| Bus 20 | 1.00649 | −0.41824 | 0.00000 | 0.00000 | 0.03080 | 0.00980 |
| Bus 21 | 1.01004 | −0.40813 | 0.00000 | 0.00000 | 0.24500 | 0.15680 |
| Bus 22 | 1.01087 | −0.40767 | 0.00000 | 0.00000 | 0.00000 | 0.00000 |
| Bus 23 | 1.00425 | −0.41275 | 0.00000 | 0.00000 | 0.04480 | 0.02240 |
| Bus 24 | 0.99523 | −0.41595 | 0.00000 | 0.00000 | 0.12180 | 0.05121 |
| Bus 25 | 0.99663 | −0.40495 | 0.00000 | 0.00000 | 0.00000 | 0.00000 |
| Bus 26 | 0.97857 | −0.41259 | 0.00000 | 0.00000 | 0.03500 | 0.02300 |
| Bus 27 | 1.00621 | −0.39336 | 0.00000 | 0.00000 | 0.00000 | 0.00000 |
| Bus 28 | 1.00291 | −0.29799 | 0.00000 | 0.00000 | 0.00000 | 0.00000 |
| Bus 29 | 0.97725 | −0.42474 | 0.00000 | 0.00000 | 0.03360 | 0.01260 |
| Bus 3 | 1.04500 | −0.20193 | 0.00000 | 0.69044 | 0.03360 | 0.01680 |
| Bus 30 | 0.96053 | −0.44760 | 0.00000 | 0.00000 | 0.14840 | 0.02660 |
| Bus 4 | 1.01893 | −0.24094 | 0.00000 | 0.00000 | 0.10640 | 0.02240 |
| Bus 5 | 1.01000 | −0.36191 | 0.00000 | 0.64223 | 1.31880 | 0.26600 |
| Bus 6 | 1.00881 | −0.28310 | 0.00000 | 0.00000 | 0.00000 | 0.00000 |
| Bus 7 | 0.99775 | −0.32828 | 0.00000 | 0.00000 | 0.31920 | 0.15260 |
| Bus 8 | 1.01000 | −0.30188 | 0.00000 | 0.58250 | 0.42000 | 0.42000 |
| Bus 9 | 1.04146 | −0.35763 | 0.00000 | 0.00000 | 0.00000 | 0.00000 |

## A. 12 Results of Line Flow for IEEE 30 bus system for Faulty condition in PSAT

| From bus | To bus | Line | P flow | Q flow | P loss | Q loss |
|---|---|---|---|---|---|---|
| | | | [p.u.] | [p.u.] | [p.u.] | [p.u.] |
| Bus 2 | Bus 1 | 1.00000 | −1.66509 | 0.33766 | 0.05111 | 0.09457 |
| Bus 6 | Bus 8 | 2.00000 | 0.29518 | 0.04415 | 0.00104 | −0.00558 |
| Bus 12 | Bus 14 | 3.00000 | 0.07849 | 0.02440 | 0.00074 | 0.00153 |
| Bus 12 | Bus 15 | 4.00000 | 0.17831 | 0.06941 | 0.00215 | 0.00423 |
| Bus 16 | Bus 12 | 5.00000 | −0.07111 | −0.03418 | 0.00053 | 0.00112 |
| Bus 1 | Bus 3 | 6.00000 | 0.89265 | −0.10806 | 0.03235 | 0.07302 |
| Bus 14 | Bus 15 | 7.00000 | 0.01575 | 0.00687 | 0.00006 | 0.00005 |
| Bus 17 | Bus 16 | 8.00000 | −0.03604 | −0.01590 | 0.00007 | 0.00027 |
| Bus 18 | Bus 15 | 9.00000 | −0.05949 | −0.01621 | 0.00038 | 0.00078 |
| Bus 19 | Bus 18 | 10.00000 | −0.02744 | −0.00711 | 0.00005 | 0.00010 |
| Bus 20 | Bus 19 | 11.00000 | 0.06773 | 0.02723 | 0.00017 | 0.00034 |
| Bus 10 | Bus 20 | 12.00000 | 0.09054 | 0.03603 | 0.00081 | 0.00180 |
| Bus 17 | Bus 10 | 13.00000 | −0.05396 | −0.04210 | 0.00014 | 0.00036 |
| Bus 10 | Bus 21 | 14.00000 | 0.15779 | 0.09958 | 0.00110 | 0.00237 |
| Bus 10 | Bus 22 | 15.00000 | 0.07614 | 0.04566 | 0.00052 | 0.00107 |
| Bus 22 | Bus 21 | 16.00000 | 0.01831 | 0.01480 | 0.00001 | 0.00001 |
| Bus 2 | Bus 4 | 17.00000 | 0.43164 | −0.02611 | 0.00973 | −0.00978 |
| Bus 23 | Bus 15 | 18.00000 | −0.04967 | −0.02938 | 0.00031 | 0.00063 |
| Bus 24 | Bus 22 | 19.00000 | −0.05686 | −0.02908 | 0.00045 | 0.00069 |
| Bus 24 | Bus 23 | 20.00000 | −0.01761 | −0.01325 | 0.00006 | 0.00012 |
| Bus 24 | Bus 25 | 21.00000 | −0.01253 | 0.02061 | 0.00010 | 0.00018 |
| Bus 25 | Bus 26 | 22.00000 | 0.03544 | 0.02366 | 0.00044 | 0.00066 |
| Bus 27 | Bus 25 | 23.00000 | 0.04832 | 0.00369 | 0.00024 | 0.00046 |
| Bus 27 | Bus 29 | 24.00000 | 0.06189 | 0.01667 | 0.00085 | 0.00162 |
| Bus 27 | Bus 30 | 25.00000 | 0.07091 | 0.01660 | 0.00161 | 0.00303 |
| Bus 30 | Bus 29 | 26.00000 | −0.03670 | −0.00542 | 0.00033 | 0.00063 |
| Bus 4 | Bus 3 | 27.00000 | −0.82697 | −0.24773 | 0.00934 | 0.01781 |
| Bus 6 | Bus 28 | 28.00000 | 0.18757 | 0.01909 | 0.00059 | −0.01126 |
| Bus 2 | Bus 5 | 29.00000 | 0.81843 | 0.02824 | 0.02906 | 0.07796 |
| Bus 2 | Bus 6 | 30.00000 | 0.59802 | −0.01275 | 0.01903 | 0.01804 |

Continued on next page

Continued from previous page

| From bus | To bus | Line | P flow | Q flow | P loss | Q loss |
|---|---|---|---|---|---|---|
| | | | [p.u.] | [p.u.] | [p.u.] | [p.u.] |
| Bus 8 | Bus 28 | 31.00000 | −0.00586 | −0.02427 | 0.00000 | −0.04369 |
| Bus 4 | Bus 6 | 32.00000 | 0.73244 | 0.03164 | 0.00609 | 0.01182 |
| Bus 5 | Bus 7 | 33.00000 | −0.15264 | 0.09168 | 0.00152 | −0.01688 |
| Bus 7 | Bus 6 | 34.00000 | −0.38216 | −0.00043 | 0.00386 | −0.00551 |
| Bus 6 | Bus 9 | 35.00000 | 0.27771 | −0.07281 | 0.00000 | 0.01590 |
| Bus 6 | Bus 10 | 36.00000 | 0.15886 | 0.00368 | 0.00000 | 0.01278 |
| Bus 9 | Bus 11 | 37.00000 | 0.00000 | −0.14022 | 0.00000 | 0.00368 |
| Bus 9 | Bus 10 | 38.00000 | 0.27771 | 0.05150 | −0.00000 | 0.00789 |
| Bus 4 | Bus 12 | 39.00000 | 0.44045 | 0.18377 | 0.00000 | 0.04821 |
| Bus 13 | Bus 12 | 40.00000 | 0.00000 | 0.06914 | 0.00000 | 0.00058 |
| Bus 28 | Bus 27 | 41.00000 | 0.18111 | 0.04977 | 0.00000 | 0.01281 |

## A. 13 Results of Line Flow for IEEE 30 bus system for Faulty With PSO-placed STATCOM in PSAT

| From bus | To bus | Line | P flow | Q flow | P loss | Q loss |
|---|---|---|---|---|---|---|
| | | | [p.u.] | [p.u.] | [p.u.] | [p.u.] |
| Bus 1 | Bus 2 | 1.00000 | 2.61532 | −0.42932 | 0.11961 | 0.29971 |
| Bus 8 | Bus 6 | 2.00000 | −0.41247 | 0.14609 | 0.00227 | −0.00123 |
| Bus 14 | Bus 12 | 3.00000 | −0.10921 | −0.03372 | 0.00152 | 0.00317 |
| Bus 15 | Bus 12 | 4.00000 | −0.24627 | −0.09767 | 0.00447 | 0.00880 |
| Bus 12 | Bus 16 | 5.00000 | 0.10175 | 0.05696 | 0.00117 | 0.00246 |
| Bus 3 | Bus 1 | 6.00000 | −1.24064 | 0.35853 | 0.06971 | 0.20958 |
| Bus 15 | Bus 14 | 7.00000 | −0.02228 | −0.01120 | 0.00013 | 0.00012 |
| Bus 16 | Bus 17 | 8.00000 | 0.05158 | 0.02930 | 0.00017 | 0.00064 |
| Bus 15 | Bus 18 | 9.00000 | 0.08549 | 0.02773 | 0.00083 | 0.00170 |
| Bus 18 | Bus 19 | 10.00000 | 0.03985 | 0.01344 | 0.00011 | 0.00023 |
| Bus 19 | Bus 20 | 11.00000 | −0.09326 | −0.03439 | 0.00034 | 0.00067 |
| Bus 20 | Bus 10 | 12.00000 | −0.12439 | −0.04486 | 0.00162 | 0.00361 |

Continued on next page

Continued from previous page

| From bus | To bus | Line | P flow | Q flow | P loss | Q loss |
|---|---|---|---|---|---|---|
| | | | [p.u.] | [p.u.] | [p.u.] | [p.u.] |
| Bus 10 | Bus 17 | 13.00000 | 0.07485 | 0.05321 | 0.00026 | 0.00067 |
| Bus 21 | Bus 10 | 14.00000 | −0.21512 | −0.13596 | 0.00221 | 0.00475 |
| Bus 22 | Bus 10 | 15.00000 | −0.10310 | −0.06240 | 0.00103 | 0.00213 |
| Bus 21 | Bus 22 | 16.00000 | −0.02988 | −0.02084 | 0.00002 | 0.00003 |
| Bus 4 | Bus 2 | 17.00000 | −0.57683 | 0.04655 | 0.01850 | 0.01719 |
| Bus 15 | Bus 23 | 18.00000 | 0.06826 | 0.04614 | 0.00065 | 0.00132 |
| Bus 22 | Bus 24 | 19.00000 | 0.07320 | 0.04153 | 0.00080 | 0.00124 |
| Bus 23 | Bus 24 | 20.00000 | 0.02281 | 0.02242 | 0.00013 | 0.00027 |
| Bus 25 | Bus 24 | 21.00000 | 0.02688 | −0.01095 | 0.00016 | 0.00028 |
| Bus 26 | Bus 25 | 22.00000 | −0.03500 | −0.02300 | 0.00047 | 0.00070 |
| Bus 25 | Bus 27 | 23.00000 | −0.06234 | −0.01275 | 0.00045 | 0.00085 |
| Bus 29 | Bus 27 | 24.00000 | −0.08571 | −0.02161 | 0.00180 | 0.00340 |
| Bus 30 | Bus 27 | 25.00000 | −0.09699 | −0.01892 | 0.00339 | 0.00638 |
| Bus 29 | Bus 30 | 26.00000 | 0.05211 | 0.00901 | 0.00070 | 0.00133 |
| Bus 3 | Bus 4 | 27.00000 | 1.20704 | 0.31511 | 0.01885 | 0.04516 |
| Bus 28 | Bus 8 | 28.00000 | 0.00762 | −0.05946 | 0.00009 | −0.04306 |
| Bus 28 | Bus 6 | 29.00000 | −0.25830 | −0.03061 | 0.00113 | −0.00915 |
| Bus 5 | Bus 2 | 30.00000 | −1.10463 | 0.19016 | 0.05853 | 0.20175 |
| Bus 6 | Bus 2 | 31.00000 | −0.79647 | 0.09482 | 0.03696 | 0.07269 |
| Bus 6 | Bus 4 | 32.00000 | −1.02622 | 0.06583 | 0.01237 | 0.03379 |
| Bus 7 | Bus 5 | 33.00000 | 0.21798 | −0.19702 | 0.00381 | −0.01095 |
| Bus 6 | Bus 7 | 34.00000 | 0.54500 | −0.03753 | 0.00781 | 0.00689 |
| Bus 9 | Bus 6 | 35.00000 | −0.38453 | 0.06417 | 0.00000 | 0.02915 |
| Bus 10 | Bus 6 | 36.00000 | −0.21899 | −0.01242 | 0.00000 | 0.02533 |
| Bus 11 | Bus 9 | 37.00000 | 0.00000 | 0.21089 | 0.00000 | 0.00790 |
| Bus 10 | Bus 9 | 38.00000 | −0.38453 | −0.12187 | 0.00000 | 0.01695 |
| Bus 12 | Bus 4 | 39.00000 | −0.62002 | −0.13906 | 0.00000 | 0.09397 |
| Bus 12 | Bus 13 | 40.00000 | 0.00000 | −0.16626 | 0.00000 | 0.00352 |
| Bus 27 | Bus 28 | 41.00000 | −0.25068 | −0.06390 | 0.00000 | 0.02618 |

## A. 14 Branch impedance of cluster A and distance between each tower

| S/N | Branch | | Distance | R | X | C | Z |
|---|---|---|---|---|---|---|---|
| | From | To | (Km) | (pu/Km) | (pu/Km) | ($\mu$F/Km) | (pu/Km) |
| 1 | S 14 | S 15 | 0.45 | 0.01 | 0.0067 | 0.270 | 0.012 |
| 2 | S 15 | S 16 | 0.29 | 0.0082 | 0.0051 | 0.270 | 0.008 |
| 3 | S 16 | S 17 | 0.33 | 0.009 | 0.055 | 0.270 | 0.009 |
| 4 | S 17 | CCG1 | 0.10 | 0.006 | 0.003 | 0.270 | 0.003 |
| 5 | S 18 | CCG1 | 1.40 | 0.015 | 0.007 | 0.270 | 0.038 |
| 6 | S 19 | S 18 | 0.30 | 0.008 | 0.028 | 0.270 | 0.008 |
| 7 | S 19 | S 20 | 0.23 | 0.008 | 0.005 | 0.440 | 0.006 |
| 8 | S 20 | S 21 | 0.24 | 0.007 | 0.005 | 0.270 | 0.006 |
| 9 | S 21 | S 22 | 1.09 | 0.007 | 0.005 | 0.270 | 0.029 |
| 10 | S 22 | S 23 | 0.23 | 0.007 | 0.005 | 0.270 | 0.006 |
| 11 | S 23 | S 24 | 0.20 | 0.0018 | 0.005 | 0.440 | 0.005 |

## A. 15 MATLAB Code for Particle Swarm Optimization Algorithm

```
%% MATLAB CODE FOR MAIN PSO ALGORITHMS
clc;
clear;
params;
define_constants;
nBus = mpc.bus(end, 1);
% Runs power flow to get initial power losses and voltage
   profile
iniResults = runpf(mpc, mpoption('verbose', 0, 'pf.alg', 'NR'
   , 'out.all', 0));
iniLoss = sum(real(get_losses(iniResults)));
fprintf(" x1 | x2 | y1 | y2 | Losses(MW) | VDI | FO\n");
% Setup PSO parameters
nvars = nStatcom * 2;  % Num of Variables (2 * num STATCOMs)
% nStatcom = 1; % Assuming 1 STATCOMs
lb = [2  0]; % Location: 2-30, Injection: 0-100
```

```
ub = [30 100]; % Location: 2-30, Injection: 0-100
% PSO Settings
options = optimoptions('particleswarm', 'PlotFcn', @pswplotbestf);
obj_func = @(x)objectives(x, mpc, iniLoss, lossWeight, voltageWeight, PD, QD, VM);
rng default  % For reproducibility
[x, fval, exitflag, output] = particleswarm(obj_func, nvars, lb, ub, options);
x(1:nStatcom) = round(x(1:nStatcom));  % Apply integer condition for location
% Place the STATCOMs with optimal locations and reactive power injections
for i = 1:nStatcom
bus = x(i);
qInjection = -x(nStatcom + i);  % Note the negative sign for reactive power injection
% Inject reactive power from STATCOM
mpc.bus(bus, QD) = mpc.bus(bus, QD) - qInjection;
end
% Runs power flow after optimal STATCOM placement
results = runpf(mpc, mpoption('verbose', 0, 'pf.alg', 'PQSUM', 'out.all', 0));
busLossesAfter = real(get_losses(results));
busLossesBefore = real(get_losses(iniResults));
% Display results *******************************************
disp("Optimal results found : ");
disp('Bus No     Q Injection (MVar)');
display([x(1:nStatcom)',        x(nStatcom + 1:nvars)']);
```

```
fprintf("\n Losses before STATCOM placement (MW): %f", iniLoss);
fprintf("\n Losses after STATCOM placement (MW): %f", sum(real(get_losses(results))));
% Plot results ******************************************
figure(2);
plot(iniResults.bus(:,VM), 'red');
hold on;
plot(results.bus(:,VM),'blue');
hold off;
title('Voltage profile of the system');
xlabel('Bus') ;
ylabel('voltage [p.u]') ;
legend('Initial voltage profile','STATCOMs + PSO');
% Plot results ******************************************
figure(3);
losses=[sum(real(get_losses(iniResults))); sum(real(get_losses(results)))];
bar(losses);
legends=categorical({'Initial losses', 'STATCOMs + PSO'});
legends = reordercats(legends,{'Initial losses', 'STATCOMs + PSO'});
bar(legends,losses);
ylabel('Active Power Losses (MW)');
title('Total active power losses (MW)');
% Plot results ******************************************
figure(4);
losses=[sum(imag(get_losses(iniResults))),sum(imag(get_losses(results)))];
legends=categorical({'Initial losses',  'STATCOMs + PSO'});
```

```
legends = reordercats(legends,{'Initial losses', 'STATCOMs +
   PSO'});
bar(legends,losses,'g');
ylabel('Reactive Power Losses (MVAR)');
title('Total reactive power losses (MVAR)');
% Plot results *********************************************
figure(5)
iniLoss= real(get_losses(iniResults));
loss = real(get_losses(results));
losses=[iniLoss,loss];
bar(losses);
title('Active Power losses (MW)');
xlabel('Line') ;
grid on;
ylabel('Real Power loss (MW)') ;
legend("Without STATCOMs", "STATCOMs + PSO");
% Plot results *********************************************
figure(6)
iniLoss= imag(get_losses(iniResults));
loss = imag(get_losses(results));
losses=[iniLoss,loss];
bar(losses);
title('Reactive Power losses (MW)');
xlabel('Line') ;
ylabel('Reactive Power loss (MVAR)') ;
grid on;
legend("Without STATCOMs", "STATCOMs + PSO");
```

```
% % MATLAB CODE FOR OBJECTIVE FUNCTION
function y = objectives(x, mpc, iniLoss, lossWeight,
```

```
voltageWeight, PD, QD, VM)
nStatcom = numel(x) / 2;  % Number of STATCOMs
% Apply integer condition for STATCOM placement
x(1:nStatcom) = round(x(1:nStatcom));
% Place STATCOMs with optimal locations and reactive power injections
for i = 1:nStatcom
bus = x(i);
qInjection = x(nStatcom + i);
% Inject reactive power from STATCOM
mpc.bus(bus, QD) = mpc.bus(bus, QD) - qInjection;
end
%   Run power flow with STATCOMs
results = runpf(mpc, mpoption('verbose', 0, 'pf.alg', 'NR', 'out.all', 0));
% Objective Function
% Calculate mean squared error of voltage magnitudes
vmag = results.bus(:, VM); % Voltage magnitude of all bars
vmag = vmag - 1; % Calculate error for all bars
vmag = vmag.*vmag; % Square the error
vobjective = sum(vmag) / numel(vmag); % Obtain mean squared error (Voltage Deviation Index)
% Calculate active power losses
loss = sum(real(get_losses(results)));
lobjective = loss / iniLoss; % Ratio of losses with STATCOM/Losses without STATCOM (Losses index)

y = lossWeight * lobjective + voltageWeight * vobjective;
fprintf("%f |", x);
fprintf("%f |", lobjective * iniLoss * 1000);
```

```
fprintf("%f |", vobjective);
fprintf("%f\n", y);
end
```

```
% % MATLAB CODE TO SET THE PSO PARAMETERS WANT TO OPTIMIZE.
nStatcom=1; % Num of Statcom to be placed in the system
mpc=loadcase('case30');% matpower 'case 30' file for power flow
statcomMaxQ = 100; % Maximum reactive power of STATCOM (MVar)
statcomMinQ = 0; % Minimum reactive power of STATCOM (MVar)
swarmSize=500; % Num of particles in the swarm; 'SwarmSize'
%Objective Function Parameters
lossWeight=0.6; % Loss weight
voltageWeight=0.4; % Voltage weight (Sum of weight must be 1)
```